Erosion of river banks along the Paraná de las Palmas River

Masterproject, CT4061



Joost den Bieman
Michael van de Koppel BSc
Greta van Velzen BSc
Wilbert Verbruggen BSc

December 2010

TU Delft Delft University of Technology

Challenge the future

General notice to the reader:

In the academic programme for Hydraulic Engineering we have in the 4th year (i.e. in the first year of the Master Programme) the requirement that students should do in a group of four to six persons a so-called "groupwork". It is also called "Master Project". During this groupwork they should make a full design of something. The work should be integral, starting with terms of reference, and ending with the real design. This can be a structure, but also it can be a harbour lay-out, a policy plan design, etc. The total time available for the project is in the order of two months and will provide 10 European Credits. It has to be practical and applied.
It is certainly not an M.Sc. thesis assignment (the thesis work is individual, 6 months and more focussed on research or advanced design work on details). But it is also not an apprenticeship, internship or traineeship where the student has to work together with a group of experienced people. For this groupwork they have to solve the problem on their own (of course with guidance).

This report is the result of such a Master Project. This report has been assessed by staff of TU Delft. It has been provided with a passing mark (i.e. a mark between 6 and 10 on a scale of 10), and consequently considered sufficient for publication.

However, this work has not been fully corrected by TU Delft staff and therefore should be considered as a product made in the framework of education, and not as a consultancy report made by TU Delft.

The opinions presented in this report are neither the opinions of TU Delft, neither of the other sponsoring organisations.

Department of Hydraulic Engineering
Delft University of Technology

Erosion of river banks along the Paraná de Las Palmas River

Masterproject, Faculty of Civil Engineering and Geosciences, TU Delft

Commitee of recommendation

- Prof. ir. L. de Quelerij, Dean faculty of Civil Engineering and Geosciences, TU Delft
- Prof. drs. ir. J.K. Vrijling, Professor Hydraulic structures, TU Delft
- Prof. dr. ir. H.J. de Vriend, Professor River Engineering, TU Delft
- Prof. dr. ir. M.J.F. Stive, Professor Coastal Engineering, TU Delft
- Prof. ir. H. Ligteringen, Professor Ports and Waterways, TU Delft
- Prof. dr. ir. H.H.G. Savenije, Professor Hydrology, TU Delft

Supervisors

TU Delft, Delft University of Technology

- Dr. ir. C.J. Sloff, River Engineering
- Ir. H.J. Verhagen, Coastal Engineering

UNSAM, Universidad Nacional de San Martin

- C.M. Schwerdtfeger MSc

Students

- Joost den Bieman *1303783*
- Michael van de Koppel BSc *1310208*
- Greta van Velzen BSc *1319523*
- Wilbert Verbruggen BSc *1304305*

Disclaimer

This report, which is part of the studies at the Faculty of Civil Engineering and Geosciences and has been prepared with great care under the guidance of staff of Delft University of Technology. However, one should realize that this report has been prepared for educational purposes and will be primarily judged on educational criteria. Delft University of Technology and their students cannot accept liability for all contents of this report.

Primary sponsors





Secondary sponsors





In cooperation with









Index

Preface vii
Summary ix
Samenvatting xiii
List of figures xvii
List of tables xix
List of symbols xx
1 Introduction 1
2 System Analysis 3
2.1 Borders 3
2.1.1 Positioning along the river 3
2.1.2 Reference levels 3
2.1.3 Slope of the river 4
2.2 Ship characteristics 4
2.3 Hydraulic Characteristics 5
2.3.1 Bathymetry 5
2.3.2 Tidal influence 7
2.3.3 Wind setup 9
2.3.4 Discharge 9
2.3.5 Velocity 11
2.3.6 Water level 12
2.4 Morphological characteristics 13
2.4.1 Composition of transported sediment 13
2.4.2 Composition river bed 15
2.4.3 Composition river bank 15
2.5 Dredging activities 19
3 Problem analysis 21
3.1 Analysis of erosion rates 21
3.1.1 Satellite images 21
3.1.2 Bathymetry data 23
3.2 Erosion model 25
3.2.1 Bank Erosion Model 26
3.3 Erosion agents, quantitative description 30
3.3.1 Rapid drawdown after a flood 30
3.3.2 River flow 33
3.3.3 Ship waves 37
3.4 Conclusion of problem analysis 45
4 Computational modelling 47
4.1 General modelling considerations 47
4.1.1 Modelling goal 47
4.1.2 Important physical processes 47
4.2 Delft3D model 47
4.2.1 Model characteristics 47
4.2.2 Computational grid 47
4.2.3 Delft3D-FLOW input 49
4.3 Modelling results 51

4.3.1 Water level 51
4.3.2 Flow field 52
4.3.3 Erosion 56
4.4 Conclusion 58
5 Preventive measures 59
5.1 Introduction 59
5.1.1 Damping of incoming waves 59
5.1.2 Armouring of the river banks 60
5.1.3 Reduction of wave generation 60
5.1.4 Relocating of land use 61
5.2 Vegetation 61
5.2.1 Load reduction by vegetation 61
5.2.2 Soil conservation by root systems 62
5.2.3 Suitable plants 63
5.3 Foreshore 65
5.3.1 Wave damping 66
5.3.2 Stability 67
5.3.3 Conclusion 67
5.4 Pile screens, longitudinal dams and groynes 68
5.4.1 Pile screen as longitudinal dam 70
5.4.2 Pile screen as groyne 70
5.5 Floating wave absorbing constructions 72
5.6 Limitations to vessel velocities 75
5.6.1 Model 75
5.6.2 Results 76
5.7 Revetment 78
5.7.1 Observed revetments 78
5.7.2 Closed and open granular filters 79
5.7.3 Design of a granular filter 80
5.7.4 Conclusion revetment 84
5.8 Geotextile 84
5.9 Combined solutions 85
5.9.1 Longitudinal pile dam with vegetation 85
5.9.2 Groynes with vegetation 87
5.10 Evaluation 91
5.11 Conclusion of preventive measures 92
6 Conclusions and recommendations 95
6.1 Conclusions 95
6.2 Recommendations 96
Literature list 98
Appendices 103
A. Pictures of the erosion 105
B. Erosion Theory 109
C. Measurements of ship waves 121
D. Analysis of ship waves and movement 125
E. Sensitivity analysis BEM 139
F. Delft3D input 145

Preface

This report has been written as the final product of the course CT4061 Multidisciplinary Project, which is part of the Master of Science (MSc) education at the Faculty of Civil Engineering and Geosciences of the Delft University of Technology in Delft, the Netherlands. All project participants are currently in the final stages of their MSc in Civil Engineering, specialisation Hydraulic Engineering. The course CT4061 Multidisciplinary Project has the goal to engage a group of students in a real life practical engineering problem, possibly in a different environment or culture than their own. Most of the work on this report has been conducted during a period of ten weeks on different locations in Argentina. The finalization of the report took place in the Netherlands during a period of approximately two weeks.

The project group wants to express its gratitude towards both the supervisor in Argentina, Maximiliano Schwerdtfeger, for all his help during the project, and the supervisors in the Netherlands, Kees Sloff and Henk-Jan Verhagen, for their useful commentary on the report.
Furthermore, thanks go out to FUNDAR, especially Fransisco Cachaza Iramont and Lorenzo R. Stewart for providing lots of useful data and information and to the University of San Martin (UNSAM), Buenos Aires.
Last but not least, the project group wants to thank the project sponsors; both our primary sponsors, Damen Dredging Equipment and Royal Boskalis Westminster, as well as our sponsors Royal BAM Group and Van Oord.

Joost den Bieman
Michael van de Koppel
Greta van Velzen
Wilbert Verbruggen

December, 2010

Summary

The Paraná River is the second longest river in South America and of great importance for Brazil, Bolivia, Paraguay and Argentina which contain large parts of the river basin. Besides that, the river is of great economic interest due to the shipping traffic on the river. The lower reaches of the river form a delta which flows out into the Rio de la Plate.

One of the branches of the Paraná delta is the Paraná de las Palmas River. This branch doesn't have the biggest discharge but has the most navigation. The situation in the Paraná de las Palmas isn't without problems though; the river banks show erosion over the whole length of the branch. This erosion has been investigated by the following research questions:

- What are the contributions of the different erosion agents to the total erosion rate of the river banks along the Paraná de las Palmas River?
- What kind of measures can be taken to decrease the erosion rate, and what are the effects of the different measures?

Although the bank erosion occurs in the whole river branch, in answering the research questions, a smaller study area is defined between km 81 and km 90 of the river branch (measured from Buenos Aires), close to the city of Campana. This study area contains one bend and one straight river section.

The Paraná de las Palmas River is rich in sediment and the banks have cohesive properties. For the amount of transport of non-cohesive material the Shields expression is often used. Such an expression isn't available for the transport of cohesive material.
Three physical mechanisms contribute to the failure of cohesive river banks: particle entrainment, mass failure and the undermining of deeper layers (in the case of stratified soil). Since the total erosion rate depends on the contributions of these mechanisms and there is no widespread formula to calculate the erosion of cohesive material, the erosion rate has to be determined using a empirical model. In an erosion rate model, both discontinuous processes (like mass failure) and particle entrainment are modeled as continuous processes. The erosion rate model results in an erosion rate when the hydraulic load exceeds the erosion resistance (critical shear stress) of the river banks. In this report, the Bank Erosion Model (BEM), developed by the research institute Deltares, is used.

The bank erosion can be influenced by a number of phenomena that occur in the river. The Paraná de las Palmas River hasn't been deepened by dredging during the last fifteen years. The depth in the middle of the river in the straight section of the study area corresponds well with the theoretical equilibrium depth, which makes it unlikely that past dredging operations contribute significantly to the problem, so they will not be investigated any further.

The occurrence of a large increase in water levels (flooding) followed by a rapid lowering of the water level could cause an unstable river bank. There are two failure methods for an unstable river bank; planar failure and rotational failure. Planar failure in this case only occurs if the water level abruptly drops by 2,35 m of more. Such a large drop in water level doesn't occur in the available water level data, so this failure mechanism is assumed to have

negligible contribution to the bank erosion rate. Rotational failure has been regarded for the known maximum abrupt drawdown during a period of 61 years, which is 2,14 m. Rotational failure due to drawdown has been tested with the computer program Slope. The results give a safety factor of F = 1,14 so on those grounds rotational failure is also disregarded as important contribution to the bank erosion rate.

A further influence on the bank erosion rate is the load of ship waves on the river banks. The study area experiences heavy shipping traffic with ship varying from inland navigation vessels with lengths in between 60 m and 100 m (42% of the shipping traffic), to Panamax type ships with a maximum draught of 12,8 m and a length up to 220 m (9% of the shipping traffic). Ships generate primary and secondary waves of which the interference cusps are the most important load on the river bank. The height of these cusps can be determined with an empirical expression, which has been developed by Rijkswaterstaat and Deltares. During a period of two days, the wave heights of all ship waves have been measured, in addition to other information like sailing speed, length, draught, etc. These measurements compared well to theoretical values for the cusp heights. Consequently, a representative wave was determined for all the separate ship classes in both the inner bend, outer bend and the straight river section. Then, the Bank Erosion Model was used to calculate the contribution of each ship class to the ship wave induced erosion. This ship wave induced erosion amounts to 0,97 m per year in the outer bend and 0,93 m per year in the inner bend and on the straight river section (the erosion rate in the inner bend is probably overestimated, due to disregarding wave damping by shallow bottom profile in the inner bend). The sensitivity of these calculations has been investigated using a Monte Carlo simulation and shows that the erosion rate ranges from 0,2 to 2,5 m per year.

Besides ship wave, also river flow influences the bank erosion rate. This river flow consists of the meandering effects in river bends and the seasonal discharge variations. The flow pattern in river bends causes erosion of the outer bend and accretion in the inner bend, and high river discharge causes erosion of the toe of the river bank. The amount of erosion caused by meandering has been determined using the Bank Erosion Model. However, the results are extremely sensitive to slight variations in the critical shear stress of the soil and flow velocities. From the analysis of satellite pictures an erosion rate of 1,25 m per year can be observed in the outer bend. Besides the effect of ship waves, river flow has the largest contribution to the erosion rate in the outer bend, so the erosion rate due to river flow is estimated at an order of magnitude of 0,3 m per year. Regarding these results, it can be stated that the erosion rate of the river banks of the Paraná de las Palmas is significant and is caused, for the most part, by ship waves.

To reduce the bank erosion rate, a number of mitigating measures has been developed that either reduces the height of the generated waves, or damps the incoming waves or increases the resistance of the river banks against wave load.

The first measure under investigation was the use of vegetation planted in the water in front of the river bank or planted directly on the river bank. Vegetation planted in front of the river bank helps in two ways; it reduces the incoming wave height by the stem drag and movement of the stems which reduces wave energy, also it strengthens the soil by the consolidating properties of the root systems of the vegetation. The wave damping effect of

the vegetation is dependent on the season and can annually reduce the wave induced erosion by an average of 34%. For this application, common reed is probably the most suitable plant, and vetiver grass is better suited for planting directly on the river bank.

A second solution to reduce the bank erosion rate is the construction of a foreshore. In some situations, a foreshore is created naturally, mainly when the erosion due to river flow is small compared to the erosion around the water line. A foreshore can also be constructed and the wave height is effectively reduced in the small water depth on the foreshore (dependant on the size of the foreshore, wave transmission can be as low as 14%). However, a constructed foreshore is expected to be unstable, so this creates the need for protection of the foreshore itself. This is deemed unwanted due to the additional costs involved and isn't investigated any further.

Construction of pile rows is a third possible solution to decrease the erosion rate. The incoming wave energy is partly reflected, partly dissipated and partly transmitted by the pile row. The effectiveness of the pile row is dependent on the shape of the piles and the centre-to-centre distance between the piles. A square pile has the most efficient shape and a small centre-to-centre distance contributes to a small transmission of waves. Pile rows can be constructed as both a longitudinal dam and a groyne field. The use of a pile row longitudinal dam reduces the erosion by 62%. Application of pile groynes is somewhat more complex and is less effective in reducing the wave induced erosion. The pile groynes do have a positive effect on reducing the erosion rate due to river flow.

Also, floating structures are investigated as a measure to reduce the erosion rate. The effectiveness of floating structures is heavily dependent on the ratio wave length to width of the floating structure. In the Paraná de las Palmas branch, a floating plate is regarded as the most suitable floating structure.

The reduction of the height of the ship waves is also a possible strategy. This can be accomplished by reducing the maximum allowed ship speed; this reduces the wave height and thus the wave induced erosion. However, a stricter maximum sailing speed has economic consequences that can't be investigated within this report, but these consequences should certainly be investigated further regarding the feasibility of a stricter speed limit. As an illustration the effect of a new speed limit of 4 kts has been determined (the current speed limit is 5 kts). In this case, the erosion due to ship waves is reduced by 64%.

Currently, the river banks are protected locally by improvised hard revetments. The stones used for these revetments are mostly larger than strictly necessary for stability and, due to the lack of filter layers, increase turbulence that actually increases the erosion locally. As in improvement to the current situation, a hard revetment including filter layers has been designed. However, this revetment is mainly useful in the straight sections of the river, because the meandering would, given enough time, undermine the revetment if it isn't constructed up to great depths. Another possibility is the application of a geotextile instead of a granular filter to stabilize the soil particles. In this case, stones are also needed to fixate the geotextile.

It's also possible to combine different solutions. The combinations of a pile groyne with vegetation and a longitudinal pile dam with vegetation have been elaborated and give erosion reductions of respectively 71% and 75%. The application of these combined solutions is regarded as promising.

In this research, the ship waves have been measured during a two day measuring campaign. It is recommended to measure during a longer period in subsequent investigation and to determine the wave length and wave period with greater accuracy. Regarding morphology, the following additional data has to be collected: a depth profile close to the river banks, bottom stratigraphy close to the river and critical shear stress of the river banks (using laboratory tests). Using these data, a more detailed analysis can be made of the reduction of wave height in shallow parts and of the strength of the river banks. Furthermore, calibrating and validating the BEM would improve the accuracy of the resulting erosion rate. To do this, a straight river section, without meander movement, would have to be used.
The designed measures in this report are preliminary designs. If one of these measures is to be implemented, the design of this measure has to be finalized in greater detail.

Samenvatting

De Paraná is de op één na langste rivier van Zuid Amerika en van groot belang voor de landen Brazilië, Bolivia, Paraguay en Argentinië welke grootte delen van het stroomgebied van de Paraná rivier bevatten. Tevens is de rivier van groot economisch belang vanwege de beroepsscheepvaart op de rivier. De benedenloop van de rivier bestaat uit een delta welke uitmondt in de Rio de la Plata.

Eén van de riviertakken van de Paraná delta is de Paraná de las Palmas. Deze tak is qua afvoer niet de grootste riviertak maar het is wel de drukst bevaren rivier tak. De situatie in de Paraná de las Palmas is echter niet probleemloos; de oevers vertonen over de gehele lengte erosie. Deze erosie is onderzocht aan de hand van de volgende twee onderzoeksvragen:

- Wat zijn de bijdragen van de verschillende erosiemechanismen aan de totale erosiesnelheid van de oevers in de Paraná de las Palmas?
- Welke maatregelen kunnen de erosiesnelheid van de oevers beperken en hoe groot is het effect van de verschillende maatregelen?

Hoewel de oevererosie in de gehele Paraná de las Palmas voorkomt is voor de beantwoording van de onderzoeksvragen enkel een studie gebied tussen km 81 en km 90 (gemeten vanaf Buenos Aires) beschouwd, in de buurt van de stad Campana. Dit studiegebied bevat een bocht en een recht stuk.

De Paraná de las Palmas is rijk aan sediment en heeft oevers met cohesieve eigenschappen. Voor de grootte van het transport van niet-cohesief materiaal wordt de uitdrukking van Shields gebruikt. Voor cohesief materiaal is een dergelijke relatie niet beschikbaar. Er dragen drie mechanismen bij aan het bezwijken van cohesieve oevers: meevoering van deeltjes, bezwijken van een grondmassa en ondermijning (in geval van gelaagde grond). Aangezien de totale erosiesnelheid afhankelijk is van deze verschillende mechanismen en een goede transportformule voor cohesief materiaal ontbreekt, moet de erosiesnelheid met een empirisch model worden bepaald. In een erosiesnelheidsmodel worden zowel de discontinue processen (bezwijken van grondmassa) als de meevoering van deeltjes, als continu gemodelleerd. Het erosiesnelheidsmodel geeft een erosiesnelheid op het moment dat de hydraulische belasting groter is dan de weerstand van de oever tegen erosie. In dit onderzoek is gebruik gemaakt van het Bank Erosion Model (BEM) wat is ontwikkeld door het kennisinstituut Deltares.

De erosie van de oevers kan worden beïnvloed door een aantal verschijnselen dat in de rivier optreedt. De Paraná de las Palmas is gedurende de laatste vijftien jaar niet uitgediept door middel van baggeren. De diepte in het midden van de rivier op rechte stukken komt overeen met de theoretische evenwichtsdiepte, waardoor oevererosie ten gevolge van baggeren niet verder wordt beschouwd.

Het optreden van een grote waterstandsverhoging (overstroming) gevolgd door een sterke daling van de waterspiegel na de hoogwaterperiode kan een mogelijke instabiliteit van de oever veroorzaken. Er zijn twee mogelijkheden voor het bezwijken van instabiel geworden

grond; wigvormig bezwijken en roterend bezwijken. Wigvormig bezwijken komt in dit geval voor bij een abrupte waterstandsdaling van meer dan 2,35 meter. Een dergelijk grote waterstandsdaling komt niet voor in de gegevens van het waterstandsverloop, waardoor wigvormig bezwijken wordt uitgesloten als belangrijke factor in de erosie van de oevers. Roterend bezwijken is getoetst voor een weerstandsdaling van 2,14 meter wat de maximale abrupte waterstandsdaling in 61 jaar is. Roterend bezwijken als gevolg van een abrupte waterstandsverlaging is getoetst met het programma Slope. Uit de resultaten blijkt een veiligheidsfactor van F=1,14 en daarom kan het roterend bezwijken van grond uit worden gesloten als belangrijke factor voor de erosie van oevers.

Een volgende invloed op de erosie van de oevers is de belasting van scheepsgolven op de oevers. De Paraná de las Palmas wordt in het gekozen studiegebied intensief bevaren door schepen variërend van binnenvaartschepen met lengtes van 60 tot 100 meter (42% van de totale scheepvaart), tot schepen van het Panamax type met een maximale diepgang van 12,80 meter en lengte tot 220 meter (9% van de totale scheepvaart). Schepen genereren primaire en secondaire golven waarvan de interferentiepieken in het secondaire golfpatroon de belangrijkste belasting op de oevers vormen. Voor de hoogte van deze interferentiepieken is een empirische uitdrukking beschikbaar, welke is ontwikkeld door Rijkswaterstaat in combinatie met Deltares. Gedurende een periode van twee dagen zijn van alle passerende schepen in het studiegebied de golfhoogtes genoteerd in combinatie met de overige scheepsinformatie zoals snelheid van het schip, lengte, diepte etc. Deze metingen zijn vergeleken met de theoretische uitdrukking voor de hoogte van de interferentiepieken, wat goed met elkaar overeenkwam. Vervolgens is per scheepsklasse een representatieve golf voor de binnenbocht, buitenbocht en rechte riviersectie bepaald. Uit het Bank Erosion Model volgt vervolgens het aandeel van elke scheepsklasse in de over erosie als gevolg van scheepsgolven. De totale erosie, ten gevolge van scheepsgolven, van de buitenbocht is 0,97 meter per jaar. In de binnenbocht en op het rechte stuk is de erosiesnelheid 0,93 meter per jaar, waarbij de erosie in de binnenbocht wordt overschat, aangezien de dempende werking van het ondiepe bodemprofiel in de binnenbocht niet is meegenomen. De gevoeligheid van deze berekening is onderzocht met een Monte Carlo analyse welke laat zien dat de range van de erosie snelheid tussen 0,2 en 2,5 meter per jaar ligt.

Daarnaast heeft de rivierstroming ook invloed op de erosie van de rivieroevers. Deze rivierstroming bestaat uit het meanderen in bochten en de jaarlijkse variatie in afvoer. Door het stromingspatroon in de bochten ondervind de buitenbocht erosie en de binnenbocht accretie en bij hoge afvoeren vindt uitschuring van de teen van de oever plaats. De grootte van de erosie als gevolg van meanderen is bepaald met het Bank Erosion Model. De oplossing is echter zeer gevoelig voor wijzigingen in de kritieke schuifspanning van de grond en kleine verschillen van de stromingssnelheden. Uit de analyse van satellietfoto's van verschillende jaren blijkt een totale erosie van de buitenbocht van 1,25 meter per jaar. Buiten de scheepsgolven is rivierstroming de belangrijkste oorzaak van erosie van de buitenbocht, daarom wordt de erosie als gevolg hiervan op een ordegrootte van 0,3 meter per jaar geschat. Op basis van deze uitkomsten kan worden gesteld dat de erosiesnelheid van de oevers in de Paraná de las Palmas significant is en voor het voornaamste deel wordt veroorzaakt door scheepsgolven.

Om de erosie van de oever te beperken is er een aantal maatregelen ontwikkeld dat ofwel de hoogte van de gegenereerde golven beperkt, ofwel de binnenkomende golven dempt of de oever versterkt ten aanzien van het opvangen van scheepsgolven.

De eerste maatregel die is onderzocht is het toepassen van vegetatie in het water voor de oever of als begroeiing op de oever. Vegetatie die wordt geplant voor de oever heeft een tweeledige werking; de inkomende golven worden gedempt door weerstand van de stengels op de watermassa en door het meebewegen van de stengels in de golven waardoor de golfenergie afneemt, tevens wordt het effect van de golven op het eroderen van de grond beperkt door de grondverbeterende eigenschappen van de wortelstelsels van de vegetatie. Het effect van golfdempende vegetatie is seizoensafhankelijk en kan op jaarbasis een erosiereductie van ongeveer 34% realiseren. Voor de toepassing in het water is riet de meest geschikte plantsoort en voor de versterking van de oever door beplanting op het droge deel van de oever is vetiver gras het meest geschikt.

Een tweede mogelijkheid om de erosie van de oevers te beperken is de aanleg van een vooroever. In sommige situaties ontstaat een vooroever op natuurlijke wijze als de erosie als gevolg van stroming beperkt is ten opzichte van erosie rond de waterspiegel. Een vooroever kan echter ook aangelegd worden en dempt door de geringe waterdiepte op de vooroever de golven op een effectieve manier (afhankelijk van de dimensionering is de golftransmissie slechts 14%). Een aangelegde vooroever is echter vermoedelijk niet stabiel waardoor deze door middel van een vooroeverbescherming verdedigd zou moeten worden. Deze situatie wordt niet wenselijk geacht door de bijkomende kosten en is verder niet beschouwd.

Palenrijen zijn een derde mogelijkheid om erosie te voorkomen. De inkomende golven worden door een palenrij deels gereflecteerd en gedissipeerd. De transmissie van de golven vormt het overgebleven deel van de inkomende golfenergie. De werking van een palenrij is afhankelijk van de vorm van de palen en de hart-op-hart afstand van de palen. Een vierkante paal is het meest efficiënt gebleken en een kleine hart-op-hart afstand draagt eveneens bij aan een lagere transmissie. Palenrijen kunnen worden toegepast als strekdam of als krib. Bij gebruik als strekdam is een erosiereductie van 62% mogelijk. Een palenrij, toegepast als krib, heeft een enigszins gecompliceerdere werking en een lagere reductie van de oevererosie ten gevolge van scheepsgolven. Wel heeft het toepassen van palenrijen als kribben een positief effect op het beperken van de erosie ten gevolge van rivierstroming.

Drijvende constructies zijn tevens onderzocht als maatregel om oevererosie tegen te gaan. De werking van drijvende constructie is sterk afhankelijk van de verhouding van de golflengte ten opzichte van de breedte van de drijvende golfdempende constructie. In de situatie van de Paraná de las Palmas is een drijvende plaat de best toepasbare drijvende constructie.

Het beperken van de hoogte van de door schepen gegenereerde golven is eveneens een mogelijkheid. Door het beperken van de maximale snelheid van de schepen neemt de golfhoogte van de scheepsgolven af en daarmee de door scheepsgolven veroorzaakte erosie. Het beperken van de maximale snelheid heeft economische consequenties die niet verder worden beschouwd in dit onderzoek en waarvan de gevolgen op maatschappelijke wenselijkheid moeten worden getoetst. Ter illustratie is het gevolg van een

snelheidsverlaging naar 4 knopen (de huidige maximumsnelheid bedraagt 5 knopen) bepaald. De erosie neemt in dit geval met ongeveer 64% af.

Lokaal wordt de oever op enkele plaatsen beschermd door een zeer eenvoudige harde oeverbescherming. De stenen die ter plaatse gebruikt worden zijn groter dan noodzakelijk om stabiel te blijven in de stroming en veroorzaken door de directe plaatsing op de onderlaag turbulentie, die de erosie versterkt. Ter verbetering van de huidige situatie is er een oeververdediging voorzien van filterlagen ontworpen. Deze is echter voornamelijk van nut op rechte delen van de rivier aangezien in de bochten door meanderen de oeverbescherming naar verloop van tijd wordt ondermijnd indien deze niet tot op grote diepte wordt uitgevoerd. In plaats van een granulair filter is het ook mogelijk om een geotextiel te gebruiken voor het vasthouden van de gronddeeltjes. Hierbij zijn ook stenen nodig om het geotextiel te fixeren.

Het is ook mogelijk om een combinatie van de verschillende maatregelen te maken. Een combinatie van kribben met vegetatie en een strekdam met vegetatie is uitgewerkt en geeft een grotere erosiereductie, namelijk respectievelijk 71% en 75%. De toepassing van deze gecombineerde maatregelen wordt als de meest veelbelovende ingreep gezien.

In het kader van dit onderzoek zijn de golven van passerende schepen gemeten tijdens een tweedaagse meetreeks. Voor vervolgonderzoek is het aan te raden deze meetserie uit te breiden en in het bijzonder de golflengte en golfperiode nauwkeurig te bepalen. In morfologisch opzicht dient de volgende data verzameld te worden: een bodemprofiel vlak voor de oever, de bodemopbouw dichtbij de rivier en de kritieke schuifspanning van de oever (door middel van experimenten in een laboratorium). Met behulp van deze data kan meer gezegd worden over de golfdemping ten gevolge van de bodem en de sterkte van de oever. IJking en validatie van het Bank Erosion Model zou ook tot betrouwbaardere waarden voor de erosiesnelheid moeten leiden. Hiervoor zou een rechte riviersectie, zonder meanderende invloeden, beschouwd moeten worden.
De ontwerpen in dit rapport zijn ontworpen met behulp van basisregels. Indien besloten wordt om één van deze maatregelen toe te passen dient het desbetreffende ontwerp verder uitwerkt te worden.

List of figures

Figure 1-1: Paraná Delta and study area....1
Figure 1-2 Bank erosion between 1964 and 2001 (indicated by the light grey areas) 2
Figure 2-1: Study area, highlighted....3
Figure 2-2: Different reference levels in Argentina 4
Figure 2-3: Observation points km 80-92 5
Figure 2-4: Bathymetry River bend in front of INTA 6
Figure 2-5: Cross-sections along the bend....6
Figure 2-6: Bathymetry bend seen from SE direction....7
Figure 2-7: Overview Rio de la Plata 8
Figure 2-8: Simulation and predicted tidal movement for Montevideo (a), Torre Oyarvide (b), Colonia (c) and Buenos Aires (d)....8
Figure 2-9: JPD of tidal and surge water level elevations 9
Figure 2-10: Discharges at Zárate 10
Figure 2-11: a) Normal state, b) El Niño, c) La Niña 11
Figure 2-12: Maximum velocities (surface and bottom) at Zárate 11
Figure 2-13: Sediment output of Paraná river in Rio de la Plata [Piedra-Cueva, 2007]....13
Figure 2-14: Classification of the 'American Geographical Union....13
Figure 2-15: Sieve curve river bottom material 15
Figure 2-16: Location of Standard Penetration Tests 16
Figure 2-17: Composition of the soil near Paraná de las Palmas....16
Figure 2-18: N-values 17
Figure 3-1: River banks 2003 (red) and river banks 2010 (green). Satellite image 2010 (background)....21
Figure 3-2: Transgression/regression river bank between 2003 and 2010 22
Figure 3-3: Erosion hole 1 (between x=500 m and x=1750 m) 22
Figure 3-4: Erosion hole 2 (between x=4000 m and x=4500 m) 23
Figure 3-5: Sedimentation erosion plot of 2008-2010 added to the river bank locations at 2003 and 2010 23
Figure 3-6: Sedimentation (+) and erosion (-) plot 2008-2010 24
Figure 3-7 Two expressions for c_E as function of u_c 29
Figure 3-8: Mohr circle for undrained, unconsolidated cohesive soil....31
Figure 3-9: Schematisation soil structure 31
Figure 3-10: Rotational failure of the river bank for a water level at -0,23 m RD 32
Figure 3-11: Comparison of formulae of Verheij and Mosselman....34
Figure 3-12: Histogram of measured ship wave height 34
Figure 3-13: Sensitivity of delta y for u 35
Figure 3-14: Sensitivity of delta y for tau critical 35
Figure 3-15: Location A, where bank erosion due to high flow velocities is expected (velocities that are given are the flow velocities during a summer discharge)....37
Figure 3-16: Calibration of ζ for Class A1, draft > 8 m....39
Figure 3-17: Reduced wave height at the inner bank in case of a foreshore 44
Figure 3-18: Reduced erosion rate at the inner bank in case of a foreshore 44
Figure 3-19: Cumulative distribution erosion rate, straight river section....45
Figure 4-1: The computational grid used for the simulation 48
Figure 4-2: The river bathymetry used in the simulation 49

Figure 4-3: Water level with summer discharge 51
Figure 4-4: Water level with winter discharge 52
Figure 4-5: Depth averaged velocity with summer discharge 53
Figure 4-6: Depth averaged velocity with winter discharge 53
Figure 4-7: First bend, summer (both length and colour of the arrows are proportional to the velocity) 54
Figure 4-8: First bend, winter (both length and colour of the arrows are proportional to the velocity) 54
Figure 4-9: Second bend, summer (both length and colour of the arrows are proportional to the velocity) 55
Figure 4-10: Second bend, winter (both length and colour of the arrows are proportional to the velocity) 55
Figure 4-11: Cumulative erosion (negative) sedimentation (positive) at the end of the simulation 56
Figure 4-12: Initial bed level (before simulation) 56
Figure 4-13: Eventual bed level (after simulation) 57
Figure 4-14: Sedimentation 'hotspots' (sedimentation is positive, erosion is negative) 58
Figure 5-1: Roots as armour against sliding [Schiereck, 2004] 62
Figure 5-2: Different parts of the P. australis [Kortlever, 1994] 63
Figure 5-3: Spartina alterniflora [University of Florida, 1998] 64
Figure 5-4: Vetiver grass [Truong et al., 2008a] 65
Figure 5-5: Foreshore in a waterway [Verheij,2000] 65
Figure 5-6: Breaker depth as function of ξ [Schiereck, 2004] 66
Figure 5-7: Wave transmission as function of the length of the foreshore for different slopes. Expressions are invalid under the horizontal line (Transmission = 0,1353) 67
Figure 5-8: Jet behind the piles 68
Figure 5-9: A wave approaching the pile screen under an angle β 69
Figure 5-10: C_T from the formulae of Hartmann 70
Figure 5-11: Diffraction and reflection in a groyne field (groynes are in red) 71
Figure 5-12: Flow patterns and mixing layer in groyne field 71
Figure 5-13: C_T for different floating structures 73
Figure 5-14: Wave attack on an angle 74
Figure 5-15: Pile anchorage 75
Figure 5-16: Wave height reduction in case of limitations to vessel speed (relative to the ground) 76
Figure 5-17: Cause of discontinuity in previous plot 77
Figure 5-18: Bank protection with stone rubble 78
Figure 5-19: Design criteria for granular filters 79
Figure 5-20: Composition of granular revetment 80
Figure 5-21: Run-up and run-down 81
Figure 5-22: Schematic design of a protection consisting of a longitudinal pile dam and a reed bed 85
Figure 5-23: Monte Carlo simulation (N = 100.000) of the percentage of reduction of wave induced erosion for a longitudinal dam in combination with a reed bed 87
Figure 5-24: Schematic design of a protection consisting of a pile groyne and a reed bed 88
Figure 5-25: Monte Carlo simulation (N = 100.000) of the percentage of reduction of wave induced erosion for a groyne field in combination with a reed bed 90

List of tables

Table 2-1: Ship classes on the Paraná de las Palmas 5
Table 2-2: Discharges Paraná de las Palmas and Paraná Guazú 10
Table 2-3: Surface velocity measurements near Campana.....12
Table 2-4: Water levels at the Paraná de las Palmas for 1976-1980 [FUNDAR].....12
Table 2-5: Composition of transported sediment in the Paraná River 14
Table 2-6: Composition of suspended transport in the Paraná River.....14
Table 2-7: Composition of suspended transport in the Paraná de las Palmas 14
Table 2-8: Soil hatchings in Figure 2-17 16
Table 2-9: Soil parameters location 18 17
Table 2-10: Classification soil location 18 18
Table 2-11: Soil parameters for BEM 18
Table 3-1: Limit, max. economic speed and minimum speed of the different ship classes 37
Table 3-2: ζ-values for different classes.....39
Table 3-3: Representative and significant wave heights for all classes 40
Table 3-4: Wave lengths and periods of all classes.....41
Table 3-5: Yearly ship movement along the Paraná de las Palmas.....41
Table 3-6: Erosion rate due to ship waves.....42
Table 4-1: Discharge at the upstream boundary (the increase between different discharges is linear).....51
Table 5-1: Erosion reduction for a reed bed with B_{veg} = 5, N = 100 and β = 55°.....62
Table 5-2: Erosion reduction for different values of W/L 74
Table 5-3: Results of Revetment calculations with MATLAB 83
Table 5-4: Combined effect of a longitudinal pile dam and reed in wave induced erosion reduction.....85
Table 5-5: Combined effect of a pile groyne and reed in wave induced erosion reduction.....89
Table 5-6: Evaluation of protective measures 91

List of symbols

a	wave amplitude	[m]
A	spiral flow factor	[-]
A_c	river cross-section	[m^2]
A_s	wet ship cross-section	[m^2]
b	pile width	[m]
B	river width at water level	[m]
B_{eff}	effective width of the vegetation zone	[m]
B_{veg}	width of the vegetation zone	[m]
c	wave celerity	[ms^{-1}]
C	Chézy coefficient	[$m^{1/2}s^{-1}$]
C_b	block coefficient	[-]
C_E	soil strength coefficient	[$m^{-1}s^{-1}$]
c_f	roughness coefficient	[-]
C_R	reflection coefficient	[-]
C_T	transmission coefficient	[-]
c’	effective cohesion	[kPa]
d	grain diameter	[m]
d_{n50}	nominal median grain diameter	[m]
e	centre to centre distance between piles	[m]
E	erodibility coefficient	[-]
E_θ	equivalent wave energy on floating structures	[J]
F_{centr}	centripetal force	[N]
Fr	Froude number	[-]
F_s	safety factor	[-]
F_{wind}	wind force	[N]
g	gravitational acceleration	[ms^{-2}]
h	average water depth	[m]
H	wave height	[m]
h_e	equilibrium water depth	[m]
H_i	incident wave height	[m]
i	pressure gradient	[-]
i_b	bottom slope	[-]
K_s	slope factor	[-]
k_{sn}	spiral flow factor	[-]
K_v	velocity/turbulence factor	[-]
L_s	length of the ship	[m]
L_θ	wave length exerted on floating structure	[m]
m	mass	[kg]
n	Manning coefficient	[$sm^{-1/3}$]
N_0	number of passing ships per unit of time	[s^{-1}]
p	seasonal state of vegetation coefficient	[-]
q	specific discharge	[m^2s^{-1}]
Q	discharge	[m^3s^{-1}]
r	radius	[m]
R	hydraulic radius	[m]
R_d	wave run-down	[m]
Re	Reynolds number	[-]

Re_*	particle Reynolds number	[-]
R_u	wave run-up	[m]
s	distance between river bank and ship	[m]
S	damage parameter	[-]
S_r	shear strength	[kPa]
s_q	specific sediment transport	[m^2y^{-1}]
S_{tot}	total sediment transport	[m^3y^{-1}]
$S_{ShipAboveWaterline}$	ship surface above waterline	[m^2]
$S_{ShipBelowWaterline}$	ship surface below waterline	[m^2]
S_u	undrained shear strength	[kPa]
T	wave period	[s]
t_p	duration of loading by return current	[s]
Δt	time step	[s]
u	average flow velocity	[ms^{-1}]
u_c	critical flow velocity	[ms^{-1}]
u_{*c}	critical shear stress velocity	[ms^{-1}]
$\bar{u}_p$	mean pore velocity	[ms^{-1}]
u_{return}	return current velocity	[ms^{-1}]
v_{drift}	drift velocity	[ms^{-1}]
v_{lim}	ship limit velocity	[ms^{-1}]
v_s	ship velocity	[ms^{-1}]
v_{wind}	wind velocity	[ms^{-1}]
v_0	amplitude of wave run-up velocity	[ms^{-1}]
W	ratio: pile width/centre-to-centre distance	[-]
w_s	unhindered sediment settling velocity	[ms^{-1}]
W_{50}	median weight	[N]
Δx	grid cell size	[m]
Δy	grid cell size	[m]
dy	bank displacement	[m]
z	water level depression	[m]
β	angle of wave incidence	[°]
γ	specific weight	[gcm^{-3}]
γ_b	wave breaking coefficient	[-]
Δ	specific density	[-]
ζ	ship geometry parameter	[-]
η	dynamic viscosity of water	[$kgms^{-1}$]
κ	Von Karmann constant	[-]
μ	damping coefficient	[m^{-1}]
ν	kinematic viscosity of water	[m^2s^{-1}]
ξ	Iribarren number	[-]
ρ_{air}	air density	[kgm^{-3}]
ρ_s	soil density	[kgm^{-3}]
ρ_w	water density	[kgm^{-3}]
τ	shear stress	[Pa]
τ_b	bed shear stress	[Pa]
τ_{bank}	bank shear stress	[Pa]
τ_c	critical shear stress	[Pa]
ϕ	angle of internal friction	[°]
Ψ_c	mobility parameter	[-]
ω	angular wave frequency	[$rads^{-1}$]
ω_m	moisture content	[%]



HOE VER GA JIJ?

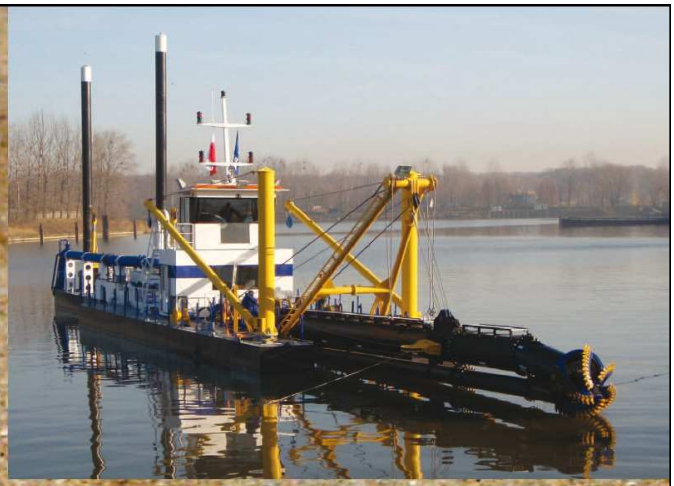
Je weet waar je vandaag staat in je carrière (studie). Maar waar ben je volgend jaar? Of in 2020?

Bij Boskalis misschien wel veel verder dan je voor mogelijk houdt.

Koninklijke Boskalis Westminster nv

BOSKALIS.NL/TRAINEE









DAMEN DREDGING EQUIPMENT

YOUR JOB, OUR TOOLS

- LARGE RANGE OF STANDARD EQUIPMENT
- DREDGING TOOLS – FIT FOR PURPOSE
- DELIVERY FROM STOCK

CLOCKWISE, FROM TOP LEFT

TRAILING SUCTION PIPE SYSTEMS
DAMEN CUTTER SUCTION DREDGER 450
DAMEN TRAILING SUCTION HOPPER DREDGER 2300
DOP® 1815 SUBMERSIBLE DREDGE PUMP

DAMEN

DAMEN DREDGING EQUIPMENT

Member of the DAMEN SHIPYARDS GROUP

Edisonstraat 32
3861 NE Nijkerk

P.O. Box 1021
3860 BA Nijkerk
The Netherlands

phone +31 (0)33 247 40 40
fax +31 (0)33 247 40 60

info@damendredging.com
www.damendredging.com

1 Introduction

The second longest river in Southern America, Rio Paraná (Paraná River), bifurcates in many rivers, thus creating a large delta, before it flows into the Rio de la Plata. One of the main rivers in the delta is the Paraná de las Palmas, which is the main waterway for navigation up to northern Argentina and even Paraguay (see Figure 1-1).
The Paraná de las Palmas river branch experiences a lot of bank erosion (see Figure 1-2). Some structures near the river are about to collapse by this bank erosion. The hypothesis of local experts is that the erosion is caused by waves which are generated by passing ships, because the erosion rate has drastically increased with the increase of size and frequency of the passing ships.



Figure 1-1: Paraná Delta and study area

The first objective of this project is to determine the cause of the bank erosion. The following erosion agents will be investigated: floods, natural meander movement, ship waves and dredging. The second objective of this research is the design of protective measures against the river bank erosion and to quantify the effects of the different measures.

The research questions are the following:

- *What are the contributions of the different erosion agents to the total erosion rate of the riverbanks along the Paraná de las Palmas?*
- *What kind of measures can be taken to decrease the erosion rate, and what are the effects of the different measures?*

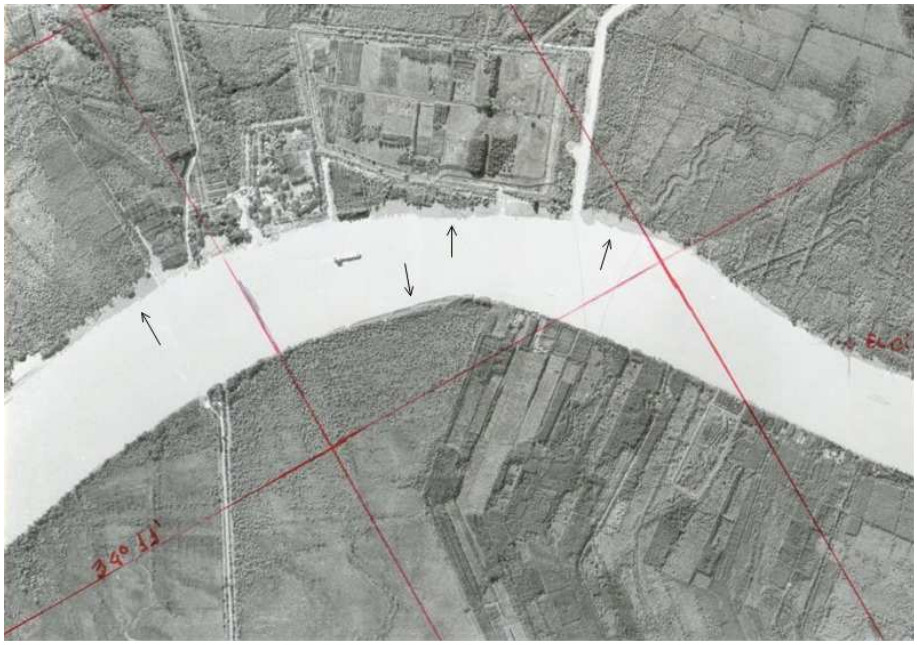


Figure 1-2 Bank erosion between 1964 and 2001 (indicated by the light grey areas)

In chapter 2 the total river system is analyzed. This chapter contains: the description of the system borders, hydraulic, morphological and ship characteristics of the river and the dredging activities.
Chapter 3 is focussed on the first research question. This chapter contains: the theoretical background of the erosion mechanisms, including an erosion rate model for cohesive river banks; the problem analysis, in which the contribution of different erosion agents is quantified; the computational modelling of the river flow.
Chapter 4 is focussed on the second research question. In this chapter several preventive measures are presented.
Chapter 5 gives the conclusions of the research and some recommendations for further research.

2 System Analysis

2.1 Borders

In this research the focus is on the erosion problems near the banks of the Paraná de las Palmas. These erosion problems can be seen along the whole the river. It is expected that the mechanisms for erosion are the same along the entire river.

Because of both time and computational constraints, it is impossible to take the whole river into account. Therefore only a part of the river is contemplated for measuring and modelling. This section can be seen in Figure 2-1. This section contains km 81 up to 90 of the Paraná de las Palmas river (calculated from Buenos Aires). The reason for this choice is that this section contains a bend and a straight part of the river and both parts will have their own dynamics.



Figure 2-1: Study area, highlighted

2.1.1 Positioning along the river

The positions on the river are measured in kilometre [km] upstream from the “end” of the river at Buenos Aires. Buenos Aires is taken as 0 km and the origin of the river is at 4.880 km.

2.1.2 Reference levels

In Argentina a number of reference levels are common as can be seen in Figure 2-2.
The blue line is the ‘Nivel de aguas medias (L.I.M.B.) Mar del Plata’ reference level which is the mean sea level at the city Mar del Plata, which stands directly in contact with the sea. From this the national used reference level is obtained, which is the grey line in Figure 2-2; ‘the Nivel de la estrella central del peristilo de la Catredral Metrolitana’, the base of one of the pillars of the main cathedral of Buenos Aires. From this zero another zero is obtained (the green line) which is the ‘cero del Riachuelo’. This reverence level is the most commonly used in the sources about the Paraná river.



Figure 2-2: Different reference levels in Argentina

Another zero level that is commonly used with respect to the Paraná de las Palmas river is the 95% water level. This is the water level of the river that is guaranteed 95% of the time. From the yearly water level curve a level is chosen that is exceeded 95% of the time. This means that this level depends on the location and is not absolute. The bathymetry data that is given in paragraph 2.3.1 is relative to the 95% water level.

2.1.3 Slope of the river

The slope of the river is 1:100.000 (10^{-5}) [FUNDAR, 2010]. Since the bathymetry data is given with respect to the 95% water level this slope is important for determining the position of the reference level for each data point. The depths of the river are taken relative to the 95% water level line, which was held constant for 5 km and then raised to the next level for practical reasons. So for determining the position of the zero for a random data point one has to know the distance between this point and Campana, calculate the number of 5 km steps between Campana and the point of interest, multiply the number of steps with the vertical difference per step and subtract it from the zero level at Campana.

A complicating factor is the absence of information of the position of the steps. Because of this and also for practical reasons the bathymetry data is not matched based on the stepwise system but by a constant slope. The maximum deviation is now 2,5 cm which is considerable smaller than the water depth.

2.2 Ship characteristics

The Paraná de las Palmas river branch of the Paraná river is used as main entrance channel for the ports of Rosario and Santa Fé since the first deepening of the river in 1976. The river is used by large ocean going vessels but the major part of the ship movements consists of inland waterway vessels.
The ships which are able to sail the Paraná de las Palmas river can be subdivided in different classes a shown in Table 2-1 [FUNDAR,2010], the maximum size of the ships in the Paraná de las Palmas river is of the Panamax type. For further information about the table one is referred to appendix D.

Class	Type	Draft	C_b
A1	Tankers & Dry Bulk carriers	> 8 m	0,82
A2	Tankers & Dry Bulk carriers	< 8 m	0,82
B	Container ships & Ro Ro	> 0 m	0,61-0,63
C1	Inland Waterway vessels	> 2,5 m	0,80
C2	Inland Waterway vessels	< 2,5 m	0,80
D	Recreational vessels		0,60

Table 2-1: Ship classes on the Paraná de las Palmas

2.3 Hydraulic Characteristics

For researching and simulating bank erosion problems in the Paraná de las Palmas it is necessary to obtain some information of the waterway. A high water level for instance can give a totally different erosion/sedimentation pattern, because of the difference in flow patterns during high and low water. In the next paragraphs the following hydraulic characteristics are described:

- Bathymetry
- Tidal influence
- Wind setup
- Discharges
- Velocities
- Width, area and perimeter

To describe these characteristics a lot of data of a measuring station at Zárate is used. Zárate is a city 10km upstream of the area of interest (Figure 1-1). These data are gathered over a period of 5 years, this is quite a short period to find the probability density of a random event. Therefore also other information (generally stations which are hundreds of kilometres upstream) is used to get an idea of the characteristics of the Paraná de las Palmas.

2.3.1 Bathymetry

The bathymetry of the Paraná de las Palmas is gathered for the section 80 up to 92 km (calculated from Buenos Aires). Only in the bends detailed depth information is available [Hydrovía, 2010a]. The pattern of observation points can be seen in Figure 2-3. All the measured cross-sections (in 2010) of the river are numbered. The x- and y-axis show the location, given in Gauss-Krüger coordinates (POSGAR94 (WGS'84) – zone 5).

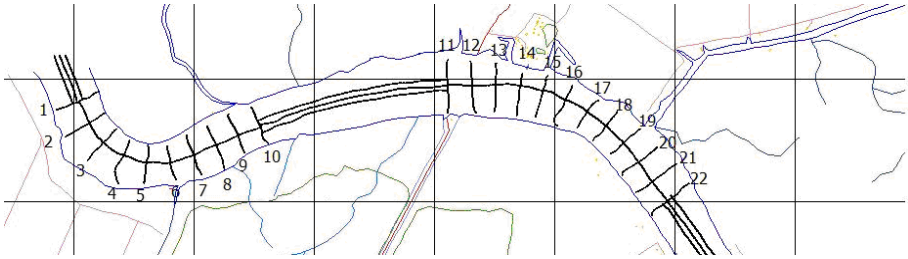


Figure 2-3: Observation points km 80-92

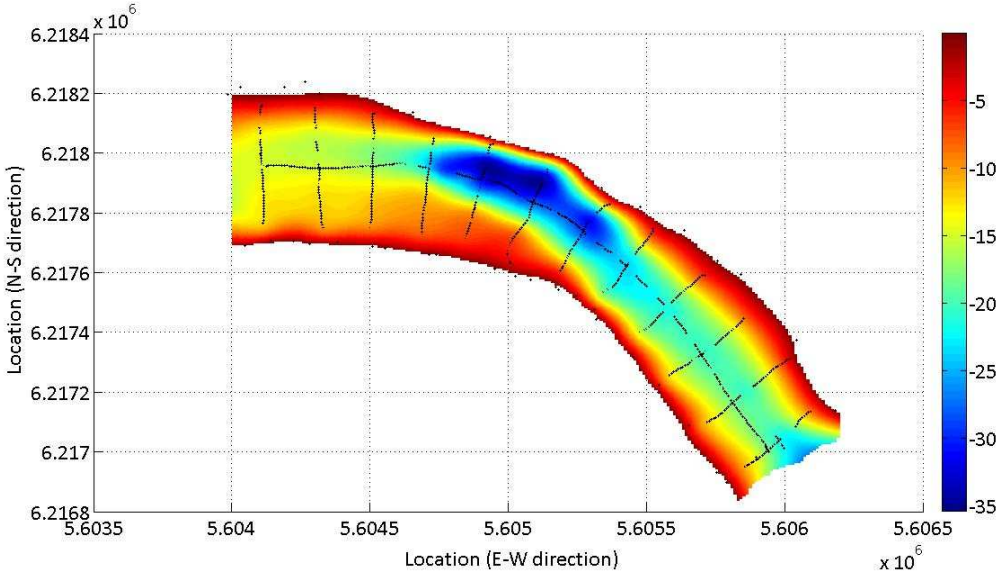


Figure 2-4: Bathymetry River bend in front of INTA

In Figure 2-4 the bathymetry of the river bend (cross-section 11-22) is shown. The x- and y-axis show the location, given in Gauss-Krüger coordinates. It can be seen that the deepest spots are located in the outer bend and the lower spots in the inner bend. This is quite a normal observation for river bends. The black dots are the observation spots. The other data is interpolated with the program MATLAB [2008b, version 7.7.0.471, September 2008, MathWorks]. The depth values are taken in reference to the zero water level which can be guaranteed in 95% of the time as is mentioned in 2.1.2. The deepest spots in this river are located 37 m under this reference level.

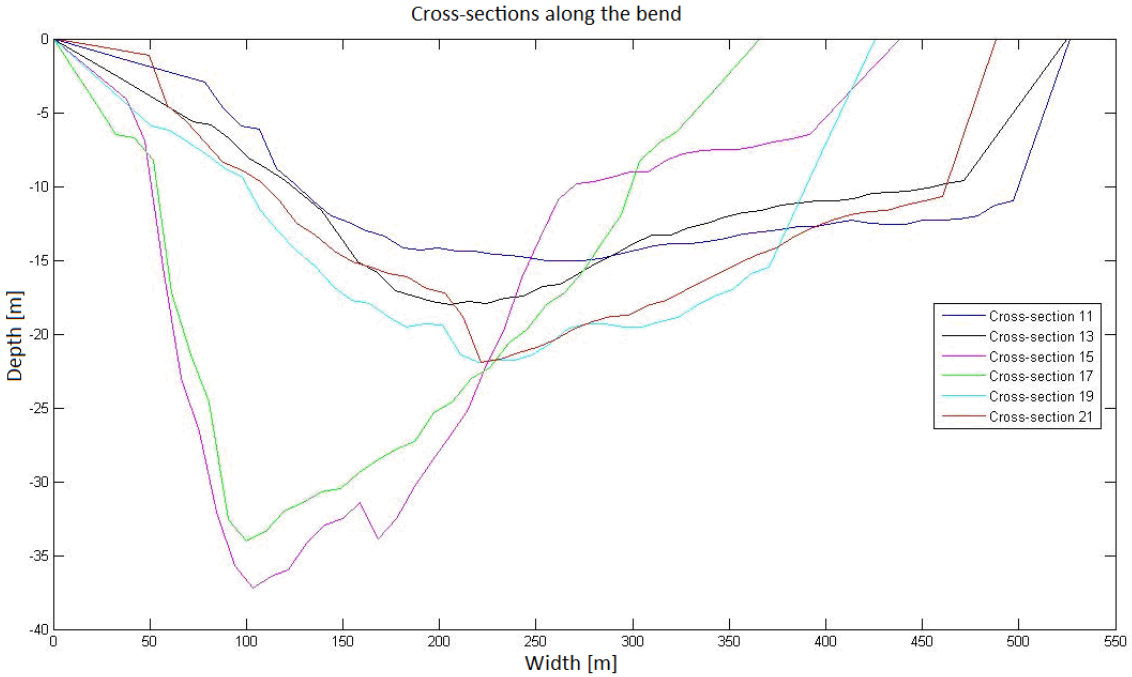


Figure 2-5: Cross-sections along the bend

In Figure 2-5 the cross-sections along the bend are plotted. The value 0 m width corresponds with the outer bend and the value 550 m width corresponds with the inner bend. In the middle of the bend (cross-sections 13-17) the outer bend has much greater depths than the inner bend. Before and after this middle part the cross-section has a more symmetric shape. Another difference between the middle of the bend (cross-sections 13-17) and the outer cross-sections is the width of the river. In the middle of the bend the width of the river is significantly smaller than in the outer cross-sections.
In cross-section 15 the outer bend is very deep (35 m below zero reference water level), but the inner bend is only 10 m deep. For the larger ships it is therefore necessary to sail near the outer bend.
Figure 2-6 shows a 3D simulation of the bathymetry in the river bend.

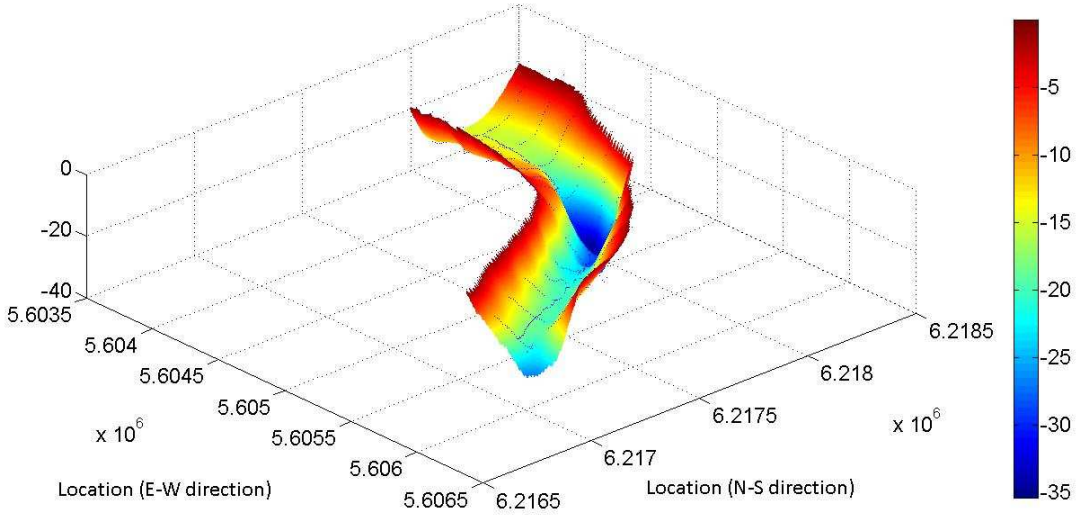


Figure 2-6: Bathymetry bend seen from SE direction

2.3.2 Tidal influence

The Paraná de las Palmas river flows into the Rio de la Plata, one of the largest estuaries of the world. The Rio de la Plata is a northwest to southeast orientated funnel shaped river, it has a length of 300 km and a width that varies from 220 km at the mouth to 40 km at the upper end.
The Rio de la Plata has a total mean runoff of 22.000 m^3/s, contributed by three main rivers. The Uruguay river has a mean discharge of 6.000 m^3/s, the Paraná Guazú-Bravo 12.000 m^3/s and the Paraná de las Palmas 4.000 m^3/s. Because the Uruguay river and the Paraná rivers drain from different basin, their high discharges don't necessary occur simultaneously. With the occurrence of El Niño or La Niña the runoff of the Rio de la Plata can be as high as 75.000 m^3/s and as low as 8.000 m^3/s.



Figure 2-7: Overview Rio de la Plata

The Rio de la Plata river behaves as an estuary, because the currents are controlled by the tide. With only 0,60 m between high and low tide the amplitude is small, but the large area of the estuary, 35.000 km^2 , makes the tidal prism dominant, despite the large discharge of the main tributaries.
The dominant tidal component is the M_2 tide, at Montevideo the amplitude of this component is 0,135 m. Other tidal components are S_2=0,03 m, K_1= 0,02 m, O_1= 0,07 m and N_2= 0,05 m, all measured at Montevideo.

The funnel shape of the estuary amplifies the tidal amplitude, as can be seen from the series of Montevideo compared to the series of the other three series: Torre Oyarvide, Colonia and Buenos Aires, see Figure 2-8.

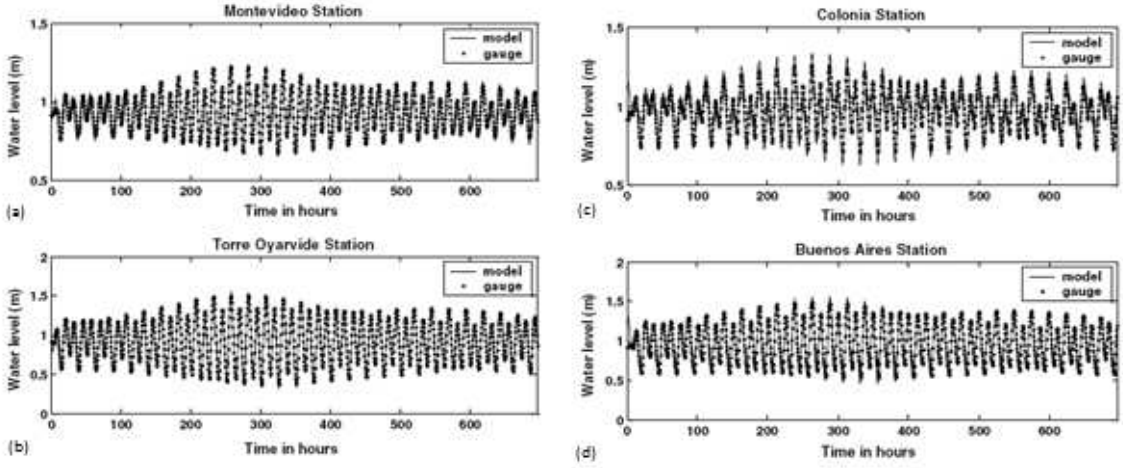


Figure 2-8: Simulation and predicted tidal movement for Montevideo (a), Torre Oyarvide (b), Colonia (c) and Buenos Aires (d)

The amplification of the amplitude is much stronger in Buenos Aires and Torre Oyarvide than it is for Colonia. This can be explained by the fact that in the deep ocean, off the shelf break, the M_2 tidal amplitude varies from 20 cm south of the estuary to 5 cm north of it, due to the occurrence of several amphidromic points. This will result in higher tides near the Argentinean coast than that near the Uruguayan coast. The Coriolis force, which deflects the tidal motion to the left in the Southern Hemisphere will also contribute to this difference in tidal amplitude between both coasts [Piedra-Cueva, 2003].

2.3.3 Wind setup

Besides the tide another important driving force is the wind. South-easterly winds, 'Sudestadas', can cause a setup of the water level near the mouth of the Paraná de las Palmas. These Sudestadas can reach wind speeds of 85 km/h when a cyclogenesis, the development of a cyclonic circulation, passes the Rio de la Plata. The typical duration of the Sudestadas is 48 hours, the first 36 hours the wind speed increases, the last 12 hours the wind speed rapidly decreases [Simionato, 2009].

When a cold front passes the Rio de la Plata south-westerly winds, 'Pamperos', can occur. These Pamperos can cause a setup at the northern part of the Rio the la Plata, the Uruguayan coast. The typical duration of the Pamperos differs from that of the Sudestadas; the duration of the Pamperos is 24 hours.

The combined probability density function of the tidal and surge levels is given in Figure 2-9. Mind that the surge levels are given referred to Riachuelo Datum and mean water level at the Rio de la Plata is +0,80 m RD. The return period is the time that elapses between the occurrences of two similar events.

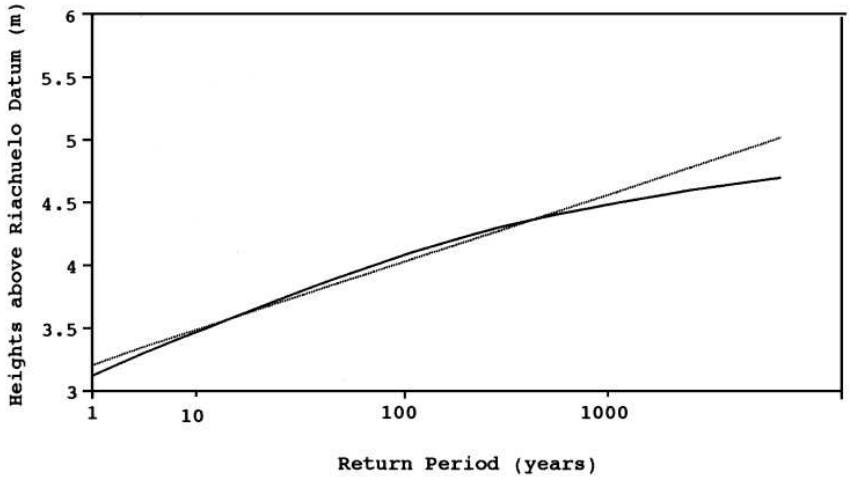


Figure 2-9: JPD of tidal and surge water level elevations

2.3.4 Discharge

In the Paraná Delta the Paraná river splits into two main tributaries: Paraná de las Palmas and Paraná Guazú. Before the river enters the delta it has an average discharge of about 16.000 m^3/s. The extremes of the Paraná are 65.000 m^3/s and 2.450 m^3/s.

In the delta, the Paraná Guazú collects the largest part of the discharge. The values for the discharges in the Paraná de las Palmas and the Paraná Guazú can be seen in Table 2-2 [Simionato, 2009].

Q (m^3/s)	Mean		Extreme	
	Summer	Winter	Low	High
Paraná de las Palmas	4.400	3.700	3.000	6.800
Paraná Guazú	14.800	12.400	10.200	22.800

Table 2-2: Discharges Paraná de las Palmas and Paraná Guazú

To verify this data also some hydraulic data from a station in Zárate is gathered. Zárate is located 5 km upstream of Campana. Once every two months a lot of data is gathered. In Figure 2-10 the discharge is plotted against the time.

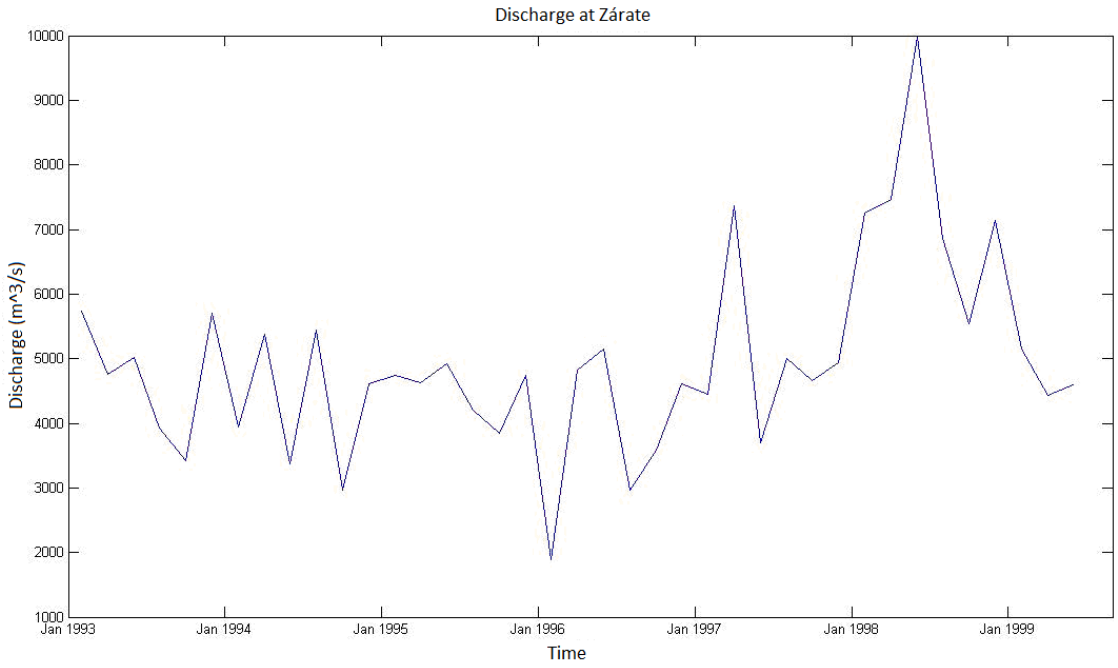


Figure 2-10: Discharges at Zárate

The mean discharge, calculated with the plotted data, is 4.950 m^3/s. So it is slightly different compared to the data presented inTable 2-2. That can be explained by a period of wet years. Although the data are not exactly the same, they are of the same order and therefore it can be assumed that the data of Table 2-2 is reliable.

Extreme high or low discharges are triggered by the occurrence of the ENSO, El Niño/ La Niña- Southern Oscillation. The ENSO is a disruption in the equatorial air-sea state that occurs in the tropical Pacific Ocean [Stewart, 2003]. This disruption had a period that varies from three to seven years. The rising of the temperature in the tropical eastern Pacific Ocean, El Niño, is accompanied by a high air surface pressure in the west Pacific and a negative state of the southern oscillation where trade winds are small. The falling of the temperature in the tropical eastern Pacific Ocean, La Niña, is accompanied by a low air surface pressure in the west Pacific and a positive state of the Southern Oscillation where trade winds are strong, as can be seen in Figure 2-11, [PMEL, 2010].

The occurrence of El Niño means a rising of sea water temperature at the west coast of the South American continent, because it hinders the upwelling of cold nutrient-rich water.

It also leads to an increase in rainfall, especially because El Niño is in phase with the normal high water period [Depetris, 2007], the December-February months. La Niña has the opposite effect of El Niño; La Niña causes a drought at the west coast of the South American continent.

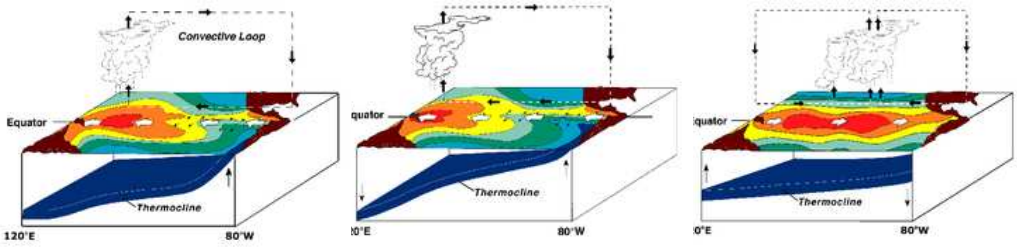


Figure 2-11: a) Normal state, b) El Niño, c) La Niña

This increase in rainfall during the El Niño can lead to severe floods along the Paraná river. In the Paraná watershed, the ENSO-triggered floods of 1982-1983 summed 547.000 hm^3 in a period from October to March. In the same period the ENSO floods accumulated 390.000 hm^3 in 1992-1993. Another 431.000 hm^3 was accumulated by the ENSO-floods of 1997-1998.

2.3.5 Velocity

At the Zárate station the maximum velocities in the middle of the river are measured. A distinction is made between the surface velocity and the bottom velocity. In Figure 2-12 the maximum surface and bottom velocities are plotted in one figure. It is easy to see that there is a clear relationship between the maximum velocity at the surface and the one at the bottom. Also it can be seen that there is a clear relationship between the velocities and the discharges (see Figure 2-10). The width of the river near Zárate is smaller than the width near Campana, which could cause a bit higher velocity at Zárate, compared to Campana.

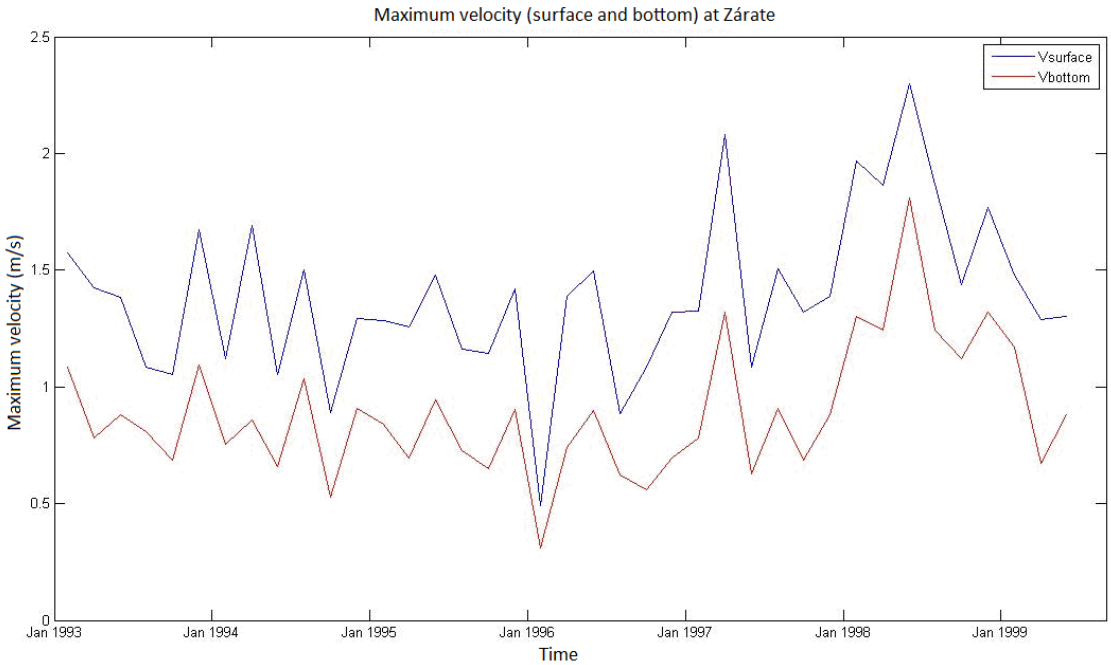


Figure 2-12: Maximum velocities (surface and bottom) at Zárate

To extend this data several surface velocity measurements are performed in the outer bend near Campana, see Table 2-3. These measurements, done by the project group, were performed near the bank, which explains why the values of the measurement are lower than those shown in Figure 2-12, which shows the maximum surface velocity near Zárate.

Nr.	Velocity [m/s]
1	0,54 m/s
2	0,67 m/s
3	0,62 m/s

Table 2-3: Surface velocity measurements near Campana

2.3.6 Water level

Detailed water level information is available in a period from 1976 to 1980, see Table 2-4. Furthermore the extremes between 1919 and 1980 are known. The maximum water level that was recorded in a period between 1919 and 1980 is +4,110 RD, during the El Niño of 1959. The absolute minimum in that period was recorded in 1925, during La Niña conditions. In the period 1976-1980 no extreme conditions like the El Niño and La Niña events are recorded [Depetris, 2007], thus these data will represent average conditions and can be used in further research. The further research will be concentrated on the data shown in Table 2-4 and not on the El Niño and La Niña events, because the aim of this research is to get a good overview of the bank erosion under normal conditions.

Years	Mean [m]	Maximum [m]	Minimum [m]
1976	+1,285 *	+2,775	+0,525
1977	+1,555	+2,915	+0,585
1978	+1,375	+2,915	-0,025
1979	+1,405	+2,625	+0,415
1980	+1,575	+2,875	+0,695
Average	+1,439	+2,821	+ 0,439

Table 2-4: Water levels at the Paraná de las Palmas for 1976-1980 [FUNDAR]

* all data are with respect to Riachuelo Datum, RD.

2.4 Morphological characteristics



Figure 2-13: Sediment output of Paraná river in Rio de la Plata [Piedra-Cueva, 2007]

In this paragraph the type of sediment in the Paraná de las Palmas is described. A distinction is made between:

- The sediment composition of the sediment in suspension
- The soil composition of the river bed
- The soil composition of the eroded soil at the bank

This is done because all these classes are related to different compositions. For all sediments in this report the classification of the 'American Geographical Union' is used, see Figure 2-14 [De Vriend, 2010]. If this report, for example, refers to silt, this means particles with a grain size of 4-62 µm.

Class name	Grain size in micrometers (µm)	Grain size in Φ-values
Boulders	> 256000	< -8
Cobbles	256000 - 64000	-8 to -6
Gravel	64000 - 2000	-6 to -1
Very coarse sand	2000 - 1000	-1 to 0
Coarse sand	1000 - 500	0 to +1
Medium sand	500 - 250	+1 to +2
Fine sand	250 - 125	+2 to +3
Very fine sand	125 - 62	+3 to +4
Coarse silt	62 - 31	+4 to +5
Medium silt	31 - 16	+5 to +6
Fine silt	16 - 8	+6 to +7
Very fine silt	8 - 4	+7 to +8
Coarse clay	4 - 2	+8 to +9
Medium clay	2 - 1	+9 to +10
Fine clay	1 - 0.5	+10 to +11
Very fine clay	0.5 - 0.25	+11 to +12
Colloids	< 0.25	> +12

Figure 2-14: Classification of the 'American Geographical Union

2.4.1 Composition of transported sediment

To simulate and predict the growth of the Paraná river mouth the INA (Instutio Nacional del Agua) determined the amounts and compositions of the transported sediment in the Paraná [Sarubbi, 2004]. They found that the Paraná river carries about 160 million tons of sediment a year. This was measured at the mouth of the Paraná river, so it's the sediment that is carried by all the branches in the delta (Paraná de las Palmas, Guazú, Bravo, Suace, Braca Grande and Mini). The composition of the transported sediments is given in Table 2-5.

Type of soil	Volume	Volumetric Percentage
Clay	$45 \cdot 10^6$ tons/year	25%
Silt	$90 \cdot 10^6$ tons/year	60%
Sand	$25 \cdot 10^6$ tons/year	15%
Total	**$160 \cdot 10^6$ tons/year**	**100%**

Table 2-5: Composition of transported sediment in the Paraná River

The transported sediment consists of wash load and bed material load. Wash load is only carried in suspension and does not contribute to morphological changes. Bed material load can be carried in suspension or in the bed load transport, and contributes to morphological changes. Wash load consists mainly of very small particles and has its origin generally far upstream. Bed material load consists generally of the bigger particles (sand, silt, etc.).

The composition of the suspended transport can be seen in Table 2-6.

Type of soil	Volume	Volumetric Percentage
Clay	$45 \cdot 10^6$ tons/year	31%
Silt	$90 \cdot 10^6$ tons/year	62%
Sand	$10 \cdot 10^6$ tons/year	7%
Total	**$145 \cdot 10^6$ tons/year**	**100%**

Table 2-6: Composition of suspended transport in the Paraná River

The total amount of bed load transport is $15 \cdot 10^6$ tons/year ($160 \cdot 10^6$ - $145 \cdot 10^6$). The composition of this bed load transport is assumed to be 100% sand, according to Table 2-5 and Table 2-6.

The Paraná de las Palmas carries about 21% of total Paraná discharge. Therefore it is assumed that the Paraná de las Palmas also carries 21% of the total sediment transport. Therefore the relative values for the suspended transport of the Paraná de las Palmas are more or less like Table 2-7.

Type of soil	Volume	Volumetric Percentage
Clay	$9{,}45 \cdot 10^6$ tons/year	31%
Silt	$18{,}9 \cdot 10^6$ tons/year	62%
Sand	$2{,}1 \cdot 10^6$ tons/year	7%
Total	**$30{,}45 \cdot 10^6$ tons/year**	**100%**

Table 2-7: Composition of suspended transport in the Paraná de las Palmas

The total amount of transported sediment by the Paraná de las Palmas is about $33{,}6 \cdot 10^6$ tons/year.

The average sediment concentration in the Paraná de las Palmas depends on many factors, like: storms, ship movement, dredging, tide, etc.). Generally it can be said that the concentration varies between 100 and 250 milligrams/litre.

2.4.2 Composition river bed

The composition of the river bed is researched by Halcrow [2008]. The sieve curve can be seen in Figure 2-15. It shows that the D_{50} of the bed material is 0,37 mm, which can be classified as medium sand.

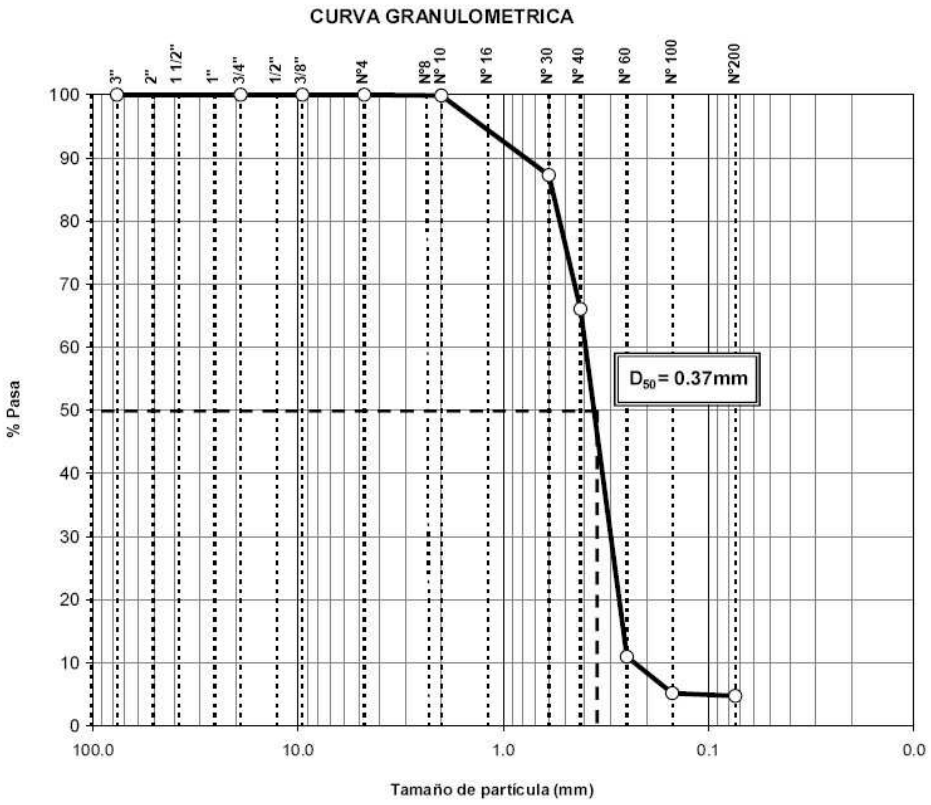


Figure 2-15: Sieve curve river bottom material

2.4.3 Composition river bank

In a soil study, obtained from the Argentinean government database, several standard penetration tests (SPT) are done in the area near Campana. The standard penetration test is a common used in situ testing method for soil characteristics. The test consists of a tick walled sample tube, which will be driven into the ground with a hammer with standard weight and falling height. The sample tube is driven 150 mm into the ground before starting with the test. Then the numbers of blows needed for every 150 mm of penetration is recorded. The number of hits, required for the last 300 mm of penetration, is commonly termed 'standard penetration resistance' or the 'N-value'. The 'N-value' provides an indication of the relative density of the soil and can also be used in several empirical formulations to estimate properties like cohesion, shear strength, etc.

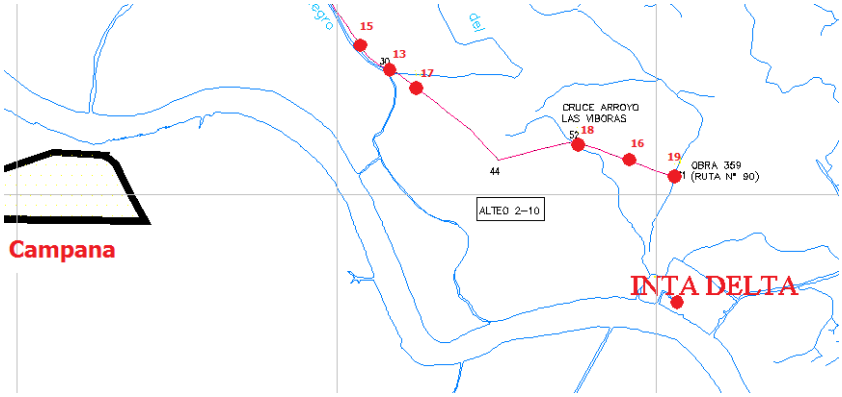


Figure 2-16: Location of Standard Penetration Tests

In Figure 2-16 a few locations can be seen where soil penetration tests are done. The nearest locations for the area of interest of this research are number 18, 16 and 19 (2 km from the river bank). Because number 18 is close to a small waterway which is connected with the Paraná de las Palmas this test is used to determine the soil characteristics. The other measurements give almost the same results so the results of test 18 can be used for a reliable analysis of the soil parameters. This assumption of reliability is supported by a paper of [Rinaldi, -], who investigated the composition of the soil on a large scale. Figure 2-17 is taken from this paper to show the uniformity of the soil composition near the Paraná de las Palmas. The upper layer on both sides of the Paraná de las Palmas stands for 'silt and loosened sand'.

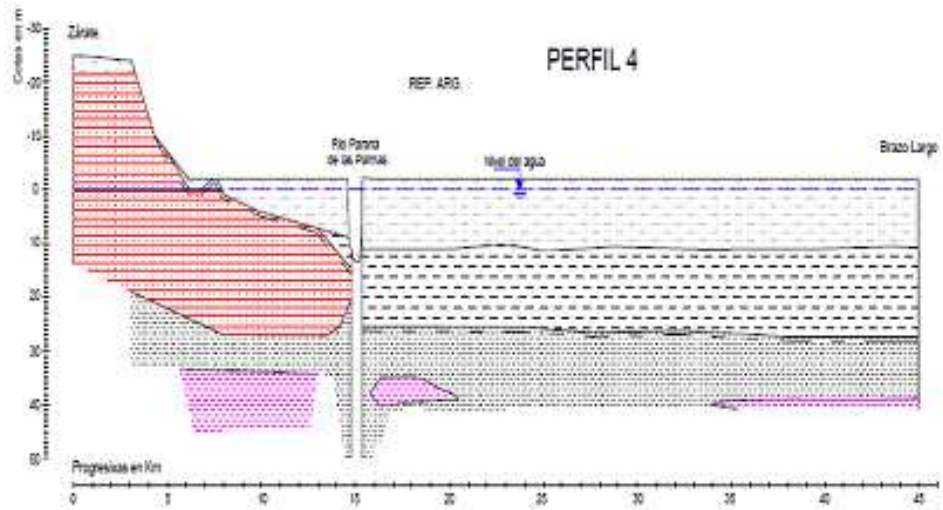


Figure 2-17: Composition of the soil near Paraná de las Palmas

Hatching	Soil Class
	Silty sand
	Soft clay
	Silty clay
	Fine sand
	Compact clay

Table 2-8: Soil hatchings in Figure 2-17

In Figure 2-18 the N-values over depth at location 18 are given. It can be seen that the soil consists of several layers. The first 1,5 m consist of a weak material (N is about 3). The second layer has an N of about 7, which represents a stronger layer. Below that stronger, sandy, layer again a weaker layer, with N is about 3, is present which compares well with Figure 2-17.

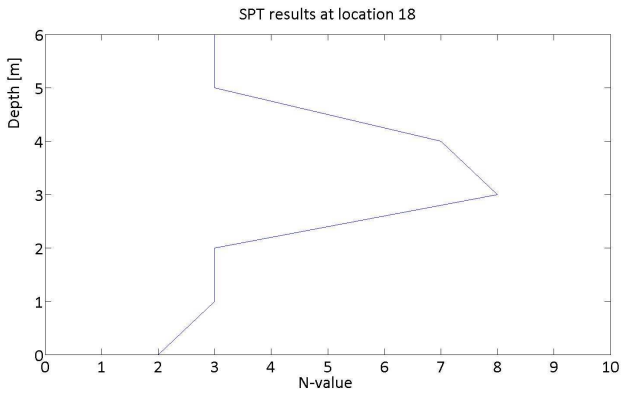


Figure 2-18: N-values

During the soil test also the liquid limit (LL), plastic limit (PL), plasticity index (PI), moisture content (ω_m), and specific weight (γ) of the soil are determined. These parameters are given in Table 2-9.

Depth [m]	LL [%]	PL [%]	PI [%]	ω [%]	γ [g/cm^3]	S_u *[kPa]*	*φ [°]*
1	31	26	5	34,8	1,86	*12*	
2	31	26	5	32,5	1,89	*28*	
3	NP	NP	NP	30,6		*NP*	*<29*
4	NP	NP	NP	33,8	1,87	*NP*	*29-30*
5	38	23	15	43,2	1,77	*11,1*	
6	38	23	15	41,9		*7,4*	

Table 2-9: Soil parameters location 18

Sivrikaya [2006] studied the relation between the N-value and the undrained shear strength. In the past a lot of formulations are derived for this relation. The differences between all these formulation show that it is not well understood. Sivrikaya determined that for fine-grained soils (silty soils) with a Plasticity Index of 5% the relation between the N-value and S_u can best be fitted as: $S_u = 4N$.
For low plasticity clay the ratio S_u/N is about 3,7. The results for S_u of the different layers can be found in Table 2-9.

For non-cohesive (sandy) soils a relation can be given between the N-values and the angle of internal friction [Peck et al., 1974]. For N-values lower than 4 the angle of internal friction (ϕ) is smaller than 29°. For N-values between 4 and 10, ϕ is in the order of 29-30°. The soil at a depth of 3 m and 4 m can be classified as a non-cohesive sandy soil, although some silt particles are present. The values for ϕ can be found in Table 2-9.

For soil classification several methods can be used. In Table 2-10 the classification of the soil can be found according to the Unified Soil Classification System (USCS) and the American Association of State Highway and Transport Officials (AASHTO) classification. For more information about these classification systems ASTM D2487-10 respectively AASHTO M 145 should be consulted.

Depth [m]	Classification USCS		Classification AASHTO	
1	ML	low plasticity silt	A-4 (3-8)	low plasticity silt
2	ML	low plasticity silt	A-4 (8)	low plasticity silt
3	ML	low plasticity silt	A-3 (8)	fine sand
4	ML	low plasticity silt	A-3 (8)	fine sand
5	CL	low plasticity clay	A-6 (10)	low plasticity clay
6	CL	low plasticity clay	A-6 (5-10)	low plasticity clay

Table 2-10: Classification soil location 18

Only for the soil at a depth of 3 m and 4 m there is a difference between the USCS and AASHTO classification methods. In the USCS method it is classified as silt, because more than 50% passes a 0,075 mm sieve. And because the liquid limit is below 50% it is classified as low plasticity silt. The AASHTO method classifies it as fine sand, because there is no plasticity index (apparently too small to measure). For this research the qualification of the AASHTO method is less accurate, because the large part of small particles (less than 0,075 mm) can't be ignored for the erosion process. Therefore the qualification according to the USCS is used in this research. But it can be said that the low plasticity silt of the upper two meters contains less sand than the low plasticity silt of the soil at a depth of 3 m and 4 m, which also has a lower (negligible) plasticity.

The magnitude of the erosion of cohesive soils is strongly dependent on the critical shear stress of the soil. In Table 2-11, a few typical values for this critical shear stress for several soil types are given.

Soil	C_E [$m^{-1}s^{-1}$]	U_c [m/s]	τ_c [Pa]
Very good clay	$0{,}5 \cdot 10^{-4}$	1,00	4
Clay with 60% sand (solid)	$0{,}6 \cdot 10^{-4}$	0,80	2,5
Good clay with little structure	$0{,}75 \cdot 10^{-4}$	0,70	2
Strongly structured good clay (moderate clay)	$1{,}5 \cdot 10^{-4}$	0,60	1,5
Poor clay (weak)	$3{,}5 \cdot 10^{-4}$	0,40	0,65
Sand with 17% silt	$10 \cdot 10^{-4}$	0,23	0,2
Sand with 10% silt	$12{,}5 \cdot 10^{-4}$	0,20	0,15
Sand with 0% silt	$15 \cdot 10^{-4}$	0,16	0,1

Table 2-11: Soil parameters for BEM

2.5 Dredging activities

The first dredging activities in the Paraná date back to the year 1976, when the Paraná River was made ready for ocean going ships. In time and especially at the end of the eighties, when Argentina was in a long recession, the dredging activities in the Paraná River decreased, which caused the minimal depth of the river to decrease from 9,75 m till 7,32 m [Lievens, 1997].

In 1995 a dredging assignment offered by the Argentine government was accepted by Hydrovia (a concession company of Jan de Nul and Emepa). The river was dredged in two phases. In the first phase the river was dredged from 7,32 m to a depth of 8,53 m [Lievens, 1997].
During the second phase the bed level was lowered to a depth of 9,75 m. The last phase was a maintenance phase during which the bed level remains the same till the end of the contract in 2005 [Lievens, 1997]. In 2005 the contract between the Argentinean government and Hydrovia was extended until 2013 and involved a deepening of the channel to 10,36 m. In 2010 the contract was again renewed until 2021, this contract includes the dredging to 10,97 m.

The lowering of the bed level in the Parana river was not necessary at every location since at some locations the depth was already sufficient. The Paraná de las Palmas had already a sufficient depth and is never dredged during this period from 1995 till the present [Hydrovía, 2010b].

However it could be possible that dredging works upstream has some influence on the bathymetry of the study area. In order to verify or the bathymetry of the river is significantly influenced by the dredging activities upstream the measured depth of the river in the study area is compared with the equilibrium depth corresponding to the discharge and the width of the river. The equilibrium depth can be calculated with the following expression:

$$q = \frac{Q}{B}$$
$$h_e = \sqrt[3]{\frac{q^2}{C^2 i_b}} \qquad (2\text{-}1)$$

With the mean discharge Q=4000 m^3/s, an average width of B_{gem}=441 m (averaged over the 22 cross sections, see Figure 2-5), a Chézy-coefficient of 44.6 $m^{½}/s$ (see 4.2.3.2) and a bottom slope of $i_b=10^{-5}$ the equilibrium depth is 16,1 m. This is comparable to the measured depths in the straight sections of the river. Since the actual depth corresponds to the equilibrium depth there is no reason to assume that dredging has influenced the bathymetry of the river.

Furthermore it is possible to calculate the velocity of morphological changes upstream traveling in downstream direction. This can be calculated by the following equations:

$$s_q = \frac{S_{tot}}{B} = \frac{33{,}6 \cdot 10^6}{441} = 7{,}62 \cdot 10^4 \text{ [m}^2\text{/year]}$$
$$\Psi = b\frac{s_q}{Q} = 441\frac{7{,}62 \cdot 10^4}{4000} = 8400 \text{ [-]}$$
$$Fr = \frac{u}{\sqrt{g \cdot h}} = \frac{0{,}565}{\sqrt{9{,}81 \cdot 16{,}1}} 0{,}045 \text{ [-]} \qquad \text{(2-2)}$$
$$C_b = \frac{u \cdot \Psi}{1 - Fr^2} = 4{,}8 \text{ [km/year]}$$

The first equation is the sediment transport per unit with ($S_{q)}$. The second equation is the average sediment transport per cubic meter of discharge (Ψ). The third equation is the Froude number (Fr) and the last equation gives the velocity of the morphological change (like a dredging pit) travelling downstream.

The length of the Paraná de las Palmas between the study area and the bifurcation of the Paraná in the Paraná de las Palmas and Paraná Guazu is 95 km. With a velocity of 4,8 km per year a dredging pit travels this distance in about 20 years. This means that the present bathymetry is not influenced by dredging works upstream of the bifurcation which date from 1990 and later. The dredging works of the late seventies and beginning of the eighties could have some influence but since they were not so extensive as the present dredging works (maintenance dredging) it is suspected that they don't influence the present bathymetry.

3 Problem analysis

3.1 Analysis of erosion rates

The analysis of the erosion rate consists of an analysis of satellite images and an analysis based on bathymetry data over three years (2008, 2009 and 2010) [Hydrovía, 2010a].

3.1.1 Satellite images

To indicate the regression/transgression rate of the banks satellite images are analysed. Satellite images with a high resolution could only be obtained from 2003 and 2010 (Google Earth). The locations of the river bank in 2003 and 2010 are transformed into two polygons (respective polygon 1 and polygon 2). These locations can be seen in Figure 3-1.

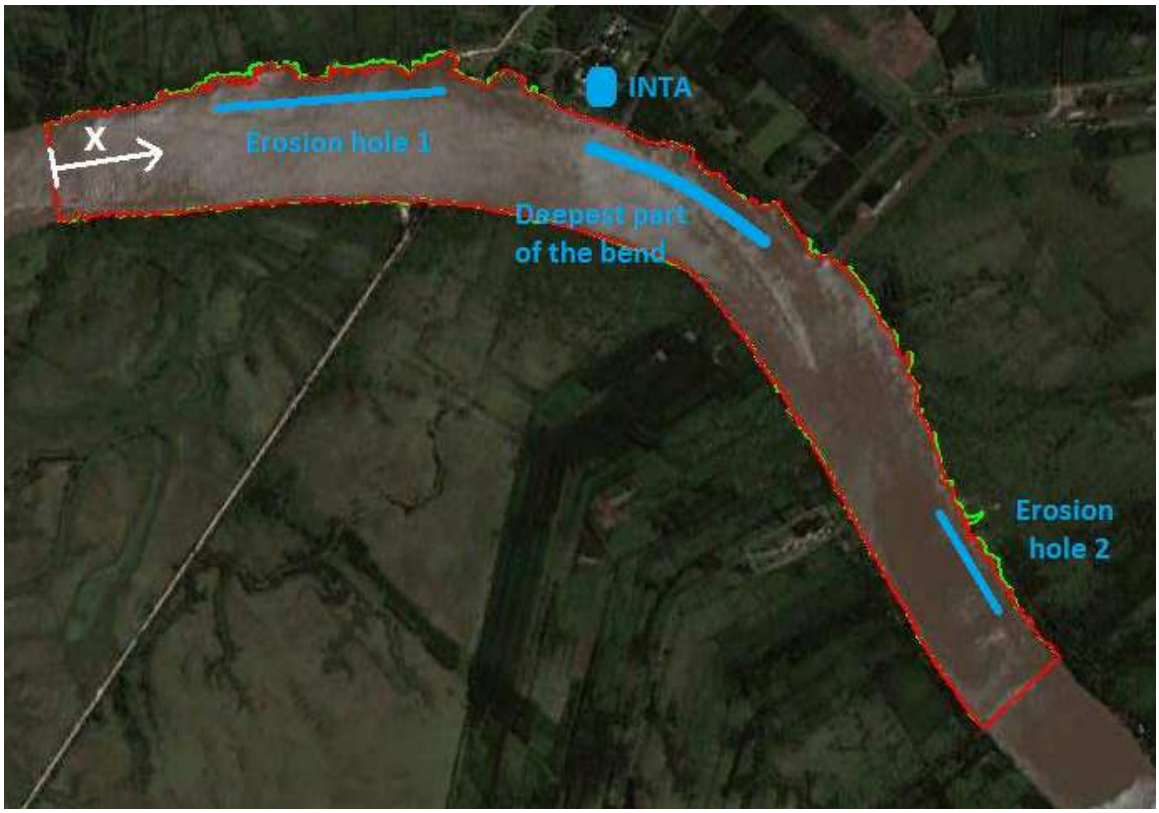


Figure 3-1: River banks 2003 (red) and river banks 2010 (green). Satellite image 2010 (background)

Polygon 1 has an area of 2.175.666 m^2 while polygon 2 has an area of 2.219.925 m^2. In 6,5 years an amount of 44.259 m^2 land area is lost. The length of this river section is about 5 km, because this includes the total bend and a small straight part. The mean regression of the river bank is therefore 4,4 m in 6,5 years (0,68 m/year).

In Figure 3-1 it can be seen that the regression of the river bank has mainly occurred at the outer bank, while the inner bank doesn't show a large regression or transgression. There are some locations where a serious amount of erosion can be seen. This can be seen in Figure

3-2 (x=0 corresponds with the left boundary of the river section in Figure 3-1). The transgression is measured with intervals of 250 m.

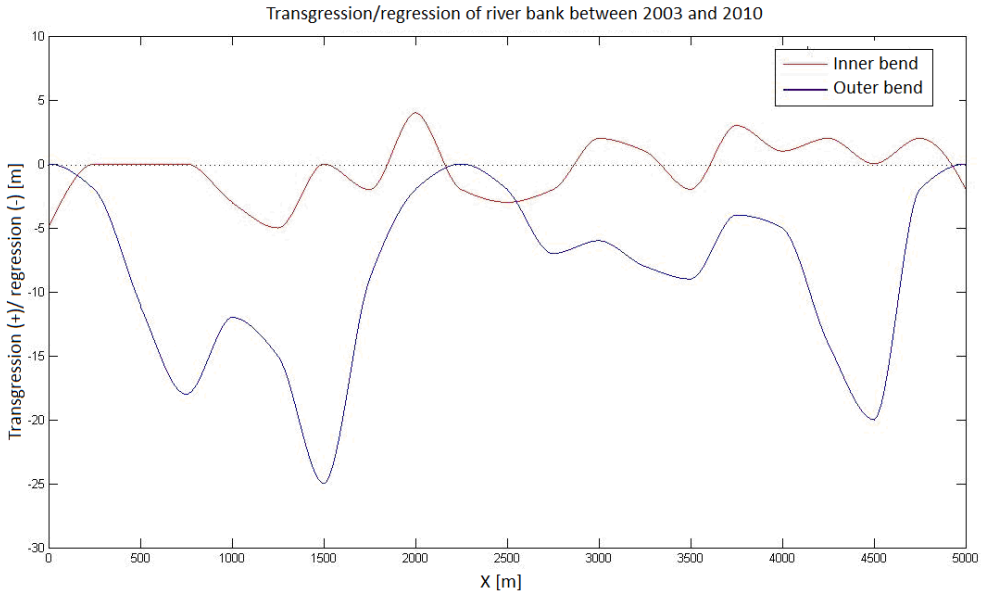


Figure 3-2: Transgression/regression river bank between 2003 and 2010

In the outer bend the mean regression is 8,14 m in 6,5 years (1,25 m/year). At the outer bend two serious erosion holes can be seen. The first erosion hole, between x = 500 m and x = 1750 m, has a mean regression of 15 m in 6,5 years (2,31 m/year), see Figure 3-3. At this section a lot of trees are present, which apparently couldn't stop the erosion process.



Figure 3-3: Erosion hole 1 (between x=500 m and x=1750 m)

The second erosion hole, between x=4000 m and x=4500 m, has a mean regression of 13 m in 6,5 years (2,00 m/year), see Figure 3-4. The extensive erosion in the upper part of Figure 3-4 is not included in the mean regression of 2,00 m/year. In this area fewer trees can be found. The river bank in this section is very steep.

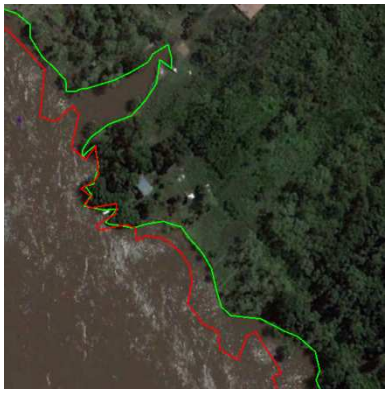


Figure 3-4: Erosion hole 2 (between x=4000 m and x=4500 m)

Between those erosion holes the regression rate is reduced to zero. The reason for this is the presence of a concrete wall. The concrete wall, build in the fifties, is presently partly undermined. Behind the concrete wall some soil is eroded, but the erosion rate is considered to be much smaller than at an unprotected river section. Also a forested area can be noticed at this section, which could have reduced the erosion rate, because the roots of the dense forest will strengthen the soil.

In the inner bend the mean regression is 0,33 m in 6,5 years (0,05 m/year). In the second half of the river section even a small amount of transgression can be seen, the maximum transgression rate is 5 m in 6,5 year (0,77 m/year).

3.1.2 Bathymetry data

The bathymetry of section km 80-92 of the Paraná de las Palmas is obtained for the years 2008, 2009 and 2010. In paragraph 2.3.1 images of the bathymetry in 2010 are given. Only at a part of the bend a high resolution of depth measures is taken. An analysis of bed level change is done for this section.

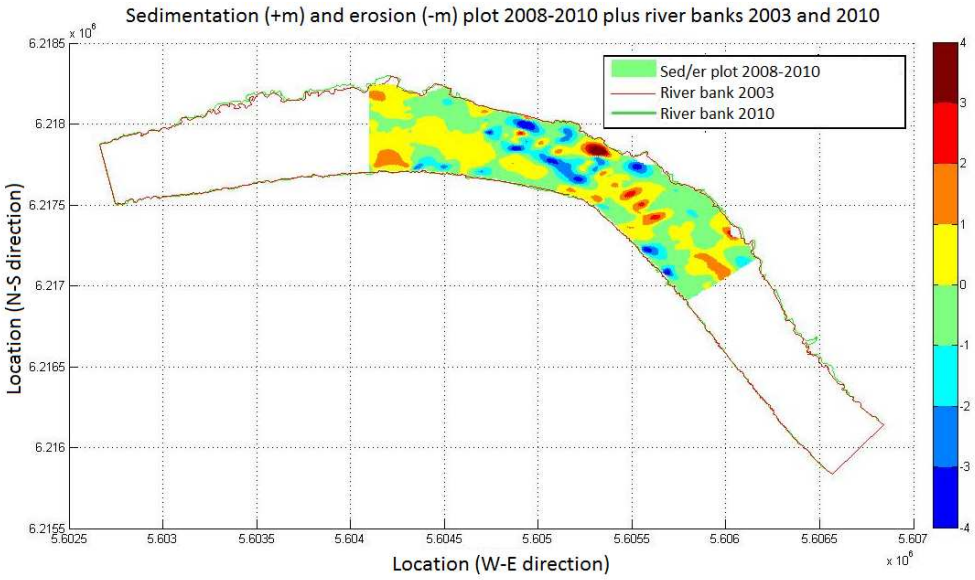


Figure 3-5: Sedimentation erosion plot of 2008-2010 added to the river bank locations at 2003 and 2010

In Figure 3-5 this area is added to a plot of the river bank locations at 2003 and 2010. The period of 2008 to 2010 is quite short to extract an erosion pattern, but it can be used to give an idea of the erosion patterns.

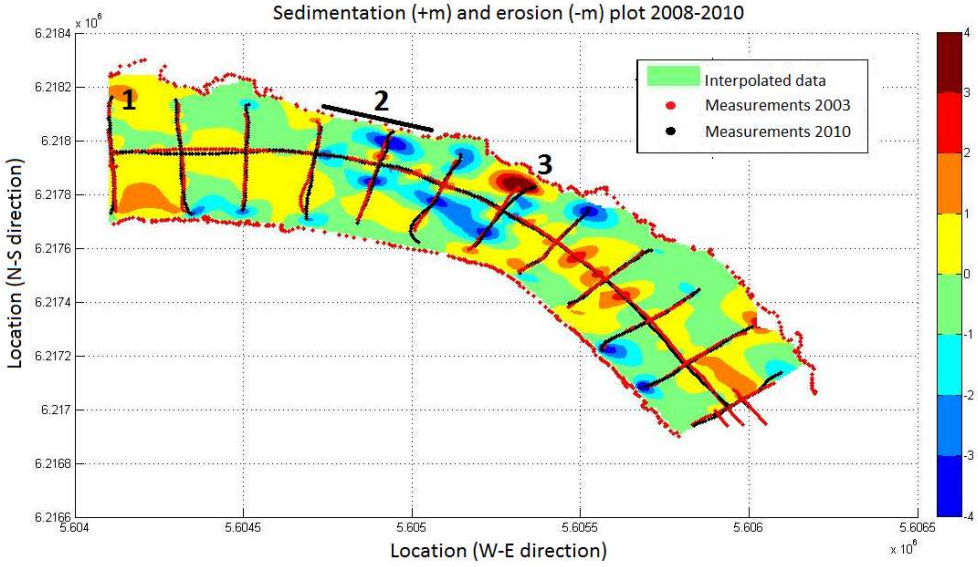


Figure 3-6: Sedimentation (+) and erosion (-) plot 2008-2010

Figure 3-6 shows the cumulative sedimentation and erosion plot from 2008 up to 2010 (erosion is negative and sedimentation positive). At first sight it might be difficult to make some conclusions based on this plot. In the plot a lot of numerical noise can be seen, which is caused by the interpolation between the observation points (red for 2008 and black for 2010). The biggest erosion/sedimentation spots are located under observation points and are therefore reliable. On average the interpolation underestimates the erosion/sedimentation and creates a smoother surface than in reality occurs. The analysis of the bathymetry data is only done for the spots which are located under the observation points.

Generally it can be seen that the outer bend is mainly eroding. This pattern can be systematic, but can also be induced by temporal conditions, like an extreme flood.
There are two significant accretion spots (1 and 3 in Figure 3-6). Near number 1 the banks have retreated over a large distance between 2003 and 2010, which could have added sediment to the system.
In front of the concrete wall (number 2) a lot of erosion can be seen. In front of this wall also the deeper parts of the river can be found (see paragraph 2.3.1). This deeper part can be explained by local scour in front of the concrete wall, which is a common effect near hard structures in the outer bend of a river. If the concrete wall is not founded deep enough it will fail one time.
At spot 3 a significant amount of sedimentation can be seen (3 to 4 meters in two years). In Figure 2-4 it can be seen that the water depth at this spot is still very large. A few meters downstream of this spot the bottom level is getting higher. It is assumed that sedimentation occurs at this spot because the suspended sediment will settle faster because of the reduced water velocity (caused by a rapid enlarging of the water depth). The deeper part of the bend already starts in front of the concrete wall, but sedimentation doesn't occur immediately. This is explained because the sediment needs some travel distance before it will hit the

bottom, the sinking sediment particle has a downward velocity, but also a forward velocity. As stated before, downstream of spot 3 the bottom level is getting higher, and therefore the water depth smaller. This results in an increase of the velocity and therefore in erosion, as can be seen in Figure 3-6.

The inner bend is mainly accreting, although direct next to the river banks some erosion occurs. The accreting of the inner bend can be caused by a secondary bend flow. Sediment from the outer bend is transported to the inner bend, where it is deposited.

The river section has exported $1{,}21 \cdot 10^5$ m^3 sediment between 2008 and 2010. Because of the interpolation this amount of sediment might not be very accurate. But it shows that the river section is losing sediment.

Conclusion
It is obvious that the erosion is significantly more at the outer bend than at the inner bend. Figure 3-6 shows that there is some bed level change in the inner bend, which could be caused by a meander movement. Nevertheless, the absence of a large transgression at the inner bend would suggest that the meander movement is not very strong. Erosion by flooding is not very self-evident, because that would normally act on both sides of the river. It was observed in situ that the ship wave attack is significantly larger at the outer bend. After analyzing the satellite images it looks like ship waves are the main cause of erosion. But it could be that there is a combination between several mechanisms. For example at the inner bend erosion caused by floods can be compensated by a meander movement.

3.2 Erosion model

Due to the lack of good transport formulae for cohesive soils, empirical formulae must be consulted to get a prediction of the erosion of cohesive banks, such as the erosion rate model [Mosselman, 1989].

In an erosion rate model, the speed with which the bank retreats, the erosion rate, is related to surface erosion. This surface erosion is given by the difference between the shear stress exerted on the bank by flow and/or waves and the critical shear stress [Mosselman, 1989].
To account for mass failure the time averaged mass failure is modelled as a continue process that is a response of the toe erosion, even though mass failure is a discrete process, that only occurs when a stability condition is exceeded.

$$Q = \begin{cases} E\left(\frac{\tau_{bank}}{\tau_c} - 1\right), & \tau_{bank} \geq \tau_c \\ 0, & \tau_{bank} < \tau_c \end{cases} \qquad (3\text{-}1)$$

In which Q is the erosion rate, E is the erodibility coefficient, τ_{bank} is the shear stress and τ_c is the critical shear stress.

3.2.1 Bank Erosion Model

The Bank Erosion Model is able to calculate the effect of three different loads on the river bank; hydraulic load due to the discharge in the channel, hydraulic loads due to return currents generated by ships and hydraulic loads due to waves generated by ships [Mosselman, 1996] what makes it a good model to calculate the quantitative effects and to compare the effects of the different loads with each other.

The basis of the BEM is the same as all other erosion models.

$$dy_l = \frac{E_l}{\rho g}\left(\frac{u_l^2}{u_{c,l}^2} - 1\right)\Delta t \qquad \text{Left bank} \qquad (3\text{-}2)$$

$$dy_r = \frac{E_r}{\rho g}\left(\frac{u_r^2}{u_{c,r}^2} - 1\right)\Delta t \qquad \text{Right bank} \qquad (3\text{-}3)$$

One calculates a hydraulic load on the river bank (water velocity at the river bank u_l, u_r) and compares this to the calculated critical velocity for which the bank becomes unstable ($u_{c,l}$, $u_{c,r}$). The outcome of this threshold of motion calculation is weighted by an erosion coefficient (E_l, E_r), in order to produce the correct erosion rate, and multiplied by the considered time span to get a final outcome for the erosion of the river bank measured in horizontal distance of bank retreat (dy).

The erosion coefficient is a function of the soil parameters.

$$E_l = \alpha_1 \tau_{c,l} \exp(-\alpha_2 \tau_{c,l}) \qquad (3\text{-}4)$$

$$E_r = \alpha_1 \tau_{c,r} \exp(-\alpha_2 \tau_{c,r}) \qquad (3\text{-}5)$$

The alphas in the formulae are empiric parameters. $\tau_{c,l}$ and $\tau_{c,r}$ are the critical shear stresses for both banks.

The water velocity for which the bank becomes unstable is a function of the soil parameters ($\tau_{c,l}$, $\tau_{c,}$) and the properties of the channel what is included in het Chézy coefficient (C).

$$u_{c,l} = \sqrt{\frac{\tau_{c,l}}{\rho}\frac{C^2}{g}}$$

$$u_{c,r} = \sqrt{\frac{\tau_{c,r}}{\rho}\frac{C^2}{g}} \qquad (3\text{-}6)$$

3.2.1.1 Hydraulic loads

For each hydraulic phenomenon, a hydraulic load has to be calculated in order to calculate the bank retreat with the BEM. With these loads, one can calculate a bank retreat for each phenomenon separately and add them together to get a total bank retreat. It is not possible to add the hydraulic loads together and then calculate the total bank retreat. Erosion due to the different phenomena takes place on different heights on the river bank (erosion due to flow takes place below the water line while erosion due to ship waves creates erosion at the water

line), which has a different effect on the horizontal bank retreat at ground level (erosion at a lower level has a bigger effect).

One can calculate the hydraulic load of the flow with the following formulae:

$$A = \frac{2}{\kappa^2}\left(1 - \frac{\sqrt{g}}{\kappa C}\right)$$

$$f(\theta_0) = 9\left(\frac{D_{50}}{h}\right)^{0.3}\left(\frac{u^2}{C^2\,\Delta\,D_{50}}\right)^{0.5}$$

$$u_l = \frac{u}{\alpha_3\,B^{1/6}}\left[1 - \frac{1}{4}\left(A\,f(\theta_0) - 1 + 8\,k_{sn}\frac{C^2}{g}\left(\frac{h}{B}\right)^2\right)\frac{B}{R}\right] \qquad (3\text{-}7)$$

$$u_r = \frac{u}{\alpha_3\,B^{1/6}}\left[1 + \frac{1}{4}\left(A\,f(\theta_0) - 1 + 8\,k_{sn}\frac{C^2}{g}\left(\frac{h}{B}\right)^2\right)\frac{B}{R}\right]$$

$$dy_l = \frac{E_l}{\rho g}\left(\frac{u_l^2}{u_{c,l}^2} - 1\right)\Delta t$$

$$dy_r = \frac{E_r}{\rho g}\left(\frac{u_r^2}{u_{c,r}^2} - 1\right)\Delta t$$

The first formula contains a factor (A) which accounts for the effect of spiral flow in river bends on the riverbed. This factor is a function of the river properties (the Von Karman constant κ, and the Chézy coefficient C). The second formula gives a factor f(Θ_0) which gives the effect of gravity on transverse bed slopes in river bends. This factor is a function of the river properties and the soil properties (the median grain size D_{50}[m], the average water depth (h), the Chézy coefficient, the relative weight of submerged soil Δ and the depth average flow velocity (u)).
The third and fourth formulae calculate the hydraulic load from the depth averaged flow velocity, the factors A and f(Θ_0), an empiric coefficient α_3 (which gives the relation between the velocity at the bank and the average velocity in a straight river) the width of the river at water level B, a correction factor for the confection of the main stream due to the spiral flow k_{sn}, the Chézy constant C and the hydraulic radius of the river R.

When the BEM gives a negative result, which should be interpreted as accretion, one should not subscribe a quantitative meaning to it. The BEM only takes the erodibility coefficient for erosion into account, but the erodibility coefficient for the accretion process can be different than the erodibility coefficient for erosion, see Figure B- in appendix B. Another reason why a negative result of the BEM has only qualitative meaning is that the critical shear stress for accretion is different than that of erosion: when the flow velocity is smaller than the critical velocity there will be no erosion, but that doesn't mean that there is accretion. For a certain range of the bank shear stress the bank is stable and the migration rate is zero, see Figure B- in appendix B.

One can calculate the erosion due to return currents with the following formulae:

$$t_p = \frac{L_s}{v_s - u}$$

$$dy_l = \frac{E_l}{\rho g}\left(\frac{(u_l + u_{retour})^2}{u_{c,l}^2} - 1\right) t_p\ N_g\ \Delta t \qquad (3\text{-}8)$$

$$dy_r = \frac{E_r}{\rho g}\left(\frac{(u_r + u_{retour})^2}{u_{c,r}^2} - 1\right) t_p\ N_g\ \Delta t$$

The first expression calculates the time of the load of the return current on the bank (t_p) by dividing the length of the ship (L_s) by the difference between the velocity of the ship (v_s) and the average river velocity (u). The last terms are analogue to the basis erosion rate expression with as difference that the hydraulic load is the river velocity next to the bank plus the return current.

One can calculate the erosion due to ship waves with the following formulae:

$$H = H(h)$$

$$T = T(h)$$

$$v_0 = 1{,}25\sqrt{2\ g\ H\ \cos\beta}$$

$$dy_l = \frac{E_l}{\rho g}\left(\frac{\left(\frac{v_0}{\sqrt{2}}\right)^2}{u_{c,l}^2} - 1\right) n\ T\ N_o\ \Delta t \qquad (3\text{-}9)$$

$$dy_r = \frac{E_r}{\rho g}\left(\frac{\left(\frac{v_0}{\sqrt{2}}\right)^2}{u_{c,r}^2} - 1\right) n\ T\ N_o\ \Delta t$$

The first two expressions indicate that the wave height as generated by ships are influenced by the depth of the river while propagating to the bank. Furthermore the wave height is influenced by the distance between the ship and the bank. One is referred to Appendix B for further reading. The third expression is an expression for the amplitude of the wave run up velocity (v_0) which is a function of the wave height at the bank (H), the angle of the incoming waves with the bank (β) and the gravitational acceleration (g). The erosion rate expressions are analogue to the structure of the previously described erosion rate expressions.

3.2.1.2 Improved expression for erosion due to ship waves

Since the introduction of the BEM of Mosselman, 1996 some research has been done at Deltares (then WL / Delft Hydraulics) in order to improve the expression for erosion rate due to ship waves. Extensive research in the Delta flume lead to a new basic expression for the erosion rate (dy/dt) as function of the squared wave height [Verheij, 2000]:

$$\frac{dy}{dt} = c_E \cdot H^2$$

$$C_E = \frac{1{,}85 \cdot 10^{-4}}{\tau_{cr}} \qquad (3\text{-}10)$$

In which c_E is a strength coefficient comparable to the E of the BEM formulae of [Mosselman, 1996].
C_E is a function of τ_c as described in equation (3-10). There is not a good analytical expression for both of the parameters and it is favourable to conduct a laboratory test to set the values of these parameters [Parchure, 2001]. As illustration the given formula for c_E in [Verheij , 2000] and [Verheij , 2001] are plotted against the data clouds from which these formulae are obtained:

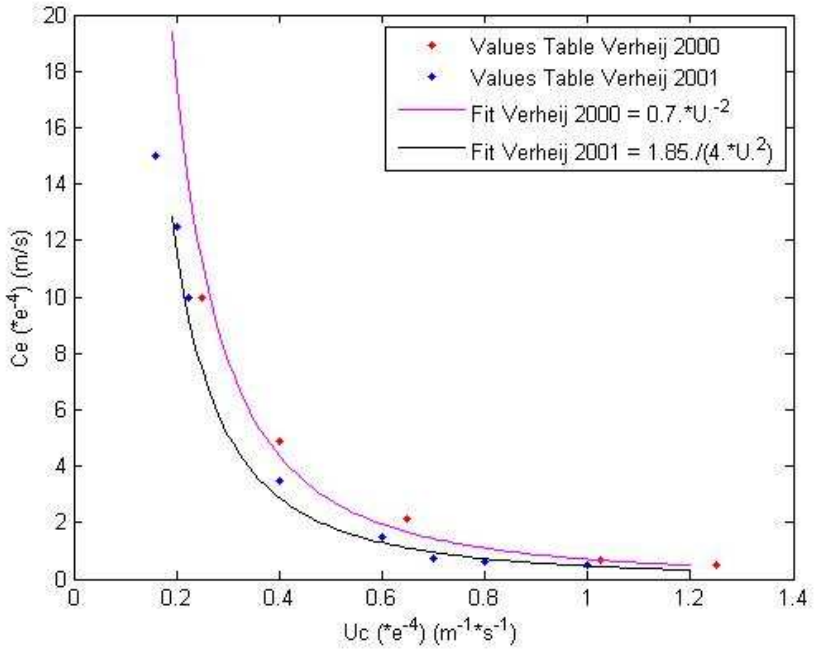


Figure 3-7 Two expressions for c_E as function of u_c

Both expressions show some deviation from the measured values what is an illustration of the uncertainties attached to the expressions. From [Verheij, 2010] is taken that the values of [Verheij, 2001] are more exact than the values of [Verheij, 2000]. The expression of [Verheij, 2001] is therefore the best fit and is used for all modelling.

The basic expression for erosion rate (equation (3-10)) of a river bank as function for the original wave height can be adjusted in order to cope with wave height reduction due to various causes. The original wave height (H) is multiplied with a transmission coefficient C_{tr} in order to calculate the wave height at the bank (H_0). The expression for wave height reduction due to partially transmission reads [Verheij, 2000]:

$$H = H_0 e^{-\mu \cdot y} \qquad (3\text{-}11)$$

The term $e^{-\mu y}$ equals the transmission coefficient C_{tr}. Substitution of this expression in the general erosion rate expression gives a differential equation with as general solution [Verheij, 2000]:

$$y = \frac{1}{2\mu} ln(2\mu \cdot c_E \cdot H_0^{\,2} t + 1) \qquad (3\text{-}12)$$

For $\mu \rightarrow 0$ equation (3-12) gives the same results as (3-10) equation.

3.3 Erosion agents, quantitative description

3.3.1 Rapid drawdown after a flood

Failure of the bank caused by floods can occur due to a mass failure in case of a rapid drawdown and due to the increased velocities near the bank, especially toe erosion can occur. In case of low discharges the hydraulic load (wave attack) on deeper layer can be increased, which can also lead to a failure of the upper layers. Especially the sand layer that is situated 2,5 m below the bank level should be tested on particle entrainment when the hydraulic load is increased.
For the bank failure due to the increased velocities one is referred to paragraph 3.3.2, where the BEM is used to calculate erosion of the bank due to river flow.

3.3.1.1 Failure due to a rapid drawdown

Failure due to a rapid drawdown that can occur after flood, should be tested for a mass failure: a planar and rotational failure mechanism. When the safety factors given in formula (3-13) and formula (3-15) are greater than 1 the plane is stable and no failure due to a rapid draw down is expected.

Planar failure
For planar failure the following equations are given:

$$
\begin{aligned}
&F_s = \frac{S_r}{S_d}, \qquad \begin{cases} F_s > 1 \rightarrow \textit{stable plane} \\ F_s < 1 \rightarrow \textit{unstable plane} \end{cases} \\
&S_r = c' + (\sigma - \mu_a)\tan\varphi' + (\mu_a - \mu_w)\tan\varphi^b = c_a + (\sigma - \mu_a)\tan\varphi' \\
&S_d = W\sin\beta - F_{con}\sin\alpha \\
&\sigma = W\cos\beta + F_{con}\cos\alpha \\
&W = \frac{A\gamma}{L}
\end{aligned}
\qquad (3\text{-}13)
$$

The dominant/most unstable situation occurs when the flood reaches at least the ground level and the drawdown after the flood is maximal. In this situation the soil will still be fully saturated (undrained situation), due to the low permeability of the cohesive soil. The confining pressure from the water isn't present anymore and the matric suction (low water pressure) is changed in to a high pore water pressure in this situation.
In this undrained situation the effective angle of repose, ϕ', is zero, as is the angle ϕ_b and the cohesion is equal to the undrained shear stress, S_u, see the representation in Figure 3-8.

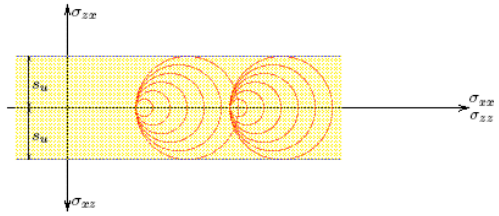


Figure 3-8: Mohr circle for undrained, unconsolidated cohesive soil

Planar failure will occur in steep banks, see appendix B. This means that a planar failure will occur in the cohesive upper layers of the soil, because the bank is not expected to be steep for more than 2,5 m, see Figure 3-9. Because the first layer has significantly less cohesion than the second a planar failure is expected to occur in the first layer.

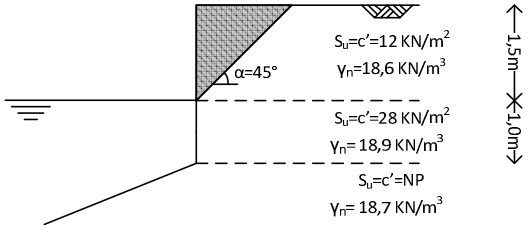


Figure 3-9: Schematisation soil structure

Verruijt gives an upper and lower limit given for the critical height, h_c (the maximum height of a vertical bank that is still stable) when considering straight failure planes. This h_c is minimal when the failure plane makes an angle with the horizontal plane of 45°.

$$\frac{3{,}64c}{\gamma} \leq h_c \leq \frac{4c}{\gamma} \qquad (3\text{-}14)$$

The minimum critical height of the upper layer is 2,35 m, because the layer is only 1,5 m thick planar failure is not expected to occur with this soil structure.
When in some locations the soil structure differs from the schematisation given in Figure 3-9 and the first layer is more than 2,35 m thick a planar failure can occur.

The bank level is situated on +1,93 m RD and the lowest recorded water level in 5 years (1976-1980) is -0,025 m RD, which means that the maximum drawdown that can be reached 1,96 m is. This is lower than the required 2,35 m, so no failure will occur even when the soil structure differs from Figure 3-9 and the upper layer is thicker than 2,35 m. The lowest water level between 1919 and 1980 is -0,23 m RD, this is also not sufficient to lead to erosion.
These low levels are due to the occurrence of an La Niña low discharge and not because of a set down at the Rio de la Plata. The changes in water level due to changes in discharges will not be as rapid as the changes in water level due to the set up and set down at the Rio de la Plata. The given minima will thus not be reached in a very short time span. This means that the cohesive soil will have time to be drained and it will not be fully saturated as is assumed in the calculations, so the stability will even be higher.

Rotational failure

Failure of the river bank due to a rapid water level drawdown should also be tested for a rotational failure mechanism. The formula of Bishop, expression (3-15) is used in this perspective. The background of the formula is outlined in appendix B.

$$F_s = \frac{\sum \frac{c + (\gamma h - u)\tan\varphi}{\cos\alpha\left(1 + \tan\alpha\tan\varphi / FS\right)}}{\sum \gamma h \sin\alpha} \qquad (3\text{-}15)$$

Because a computation of the safety factor with the formula of Bishop uses a lot of iteration loops, the computer program 'Slope' is used. The dominant situation for a rotational failure is the same as for a planar failure: undrained soil after a rapid drawdown. In this situation the cohesion is equal to the undrained shear stress (S_u) and ϕ =0, as is explained above.

The minimum water level between 1919 and 1980 was at -0,23 RD, which is 2,14 m below bank level. The stability of the river bank is computed with 'Slope' for a drawdown of 2,14 m. The banks are assumed to be saturated. The slope is assumed to be 1:4, but this is likely to be an overestimation, so the outcome will be conservative. In Figure 3-10 the result of the computation can be seen. The safety factor for the weakest failure circle is still 1,144. Even with this low water level the river bank is stable (F>0). The failure circle crosses the sand layer because this layer has no cohesion and gives therefore the least resistance.

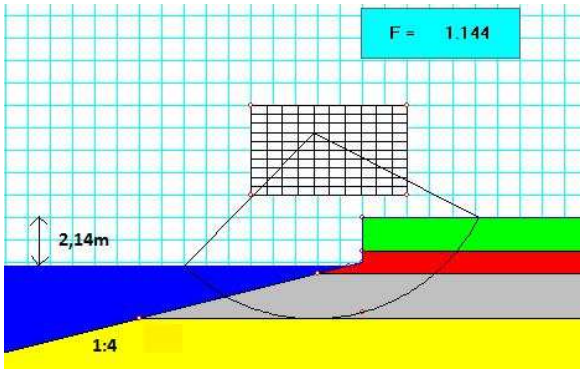


Figure 3-10: Rotational failure of the river bank for a water level at -0,23 m RD

3.3.1.2 Failure of the deeper (sand) layer

In paragraph 2.4.3 the soil stratification is given. It can be seen that on a depth of 2,5 m below surface level a sand layer is present. The sand layer forms a weak point in case of rotation failure, as stated before, but it is shown that rotation failure doesn't occur. The lowest measured water level between 1919 and 1980 is -0,23 m RD, which is 2,14 m below bank level. So it can be assumed that the sand layer is always submerged. Although it is submerged, it can cause bank failure if the sand layer is eroded for a certain distance. In that case the cohesive soil layer with a thickness of 2,5 m is not supported anymore and will fail. Erosion of the sand layer can be caused by:

- Wave attack during extreme low water
- Washing out of sand particles due to a rapid drawdown

Wave attack mainly causes erosion near the actual water level. The wave causes a load on the river bank in a range of two times the wave height below and above water level. If for example a wave of 0,5 m (highest measured wave) approaches the river bank, the increased load can be expected up to 1 m below the water level. The water level which occurs once in five years, see paragraph 2.3.6, is equal to -0,025 m RD, which is 1,96 m below bank level. Even with such a low water level, only the bigger waves can lead to an increased load on the sand layer. Since this condition is only valid once in five years it can be assumed that that erosion of the sand layer by wave attack can be ignored.

The sand layer is more permeable than the top layers, which consists of silty soils. The permeability of sand is in the range of 10^{-2} – 10^{-5} m/s, while the permeability of silt is about 10^{-5} – 10^{-8} m/s. The pressure in the sand layer (as in the silty soils) is related to the water level in the river. Because of the larger permeability, the water pressure in the sand layer follows the water level much faster than the water pressure in the silty soils. If the water level drops it will cause a flow out of the sand layer. This is caused by pressure gradients in the sand layer. The water pressure in the sand at the river bank will immediately follow the water level drop, while the water pressure more landwards needs some time to adjust to the new circumstances. Because maximum water level drops are in the order of 0,15 m/hour (see paragraph 2.3.3) it can be assumed that the pressure build up is not large enough to cause a flow which is able to wash out the sand particles.

It is important to keep in mind that above assumptions are based upon the SPT, as outlined in paragraph 2.4.3 The SPT was done on a distance of a few kilometres from the river. Therefore it is possible that the soil stratigraphy near the river differs from the assumed stratigraphy. If the sand layer, for example, is located at 1 m below bank level it will probably cause bank failure because of wave attack.

3.3.2 River flow

For a calculation of the erosion due to river flow (containing both meander movement and discharge variations) both particle entrainment and mass failure should be accounted for and the BEM can be used, see paragraph 3.2.1 for the equations of the BEM for flow. In these equations several parameters are given to include the typical flow patterns in a bend. Because the Delft3D model (see 4.2) simulates the river flow, the velocities near the bank can be read from the results of the model simulation. In this way the problem of determining the empirical parameter α_3 is eliminated. The empirical coefficients α_1 and α_2 are difficult to determine, but a first approximation of the erodibility coefficient (E) which includes both α_1 and α_2 , can be made by comparing the formulae for the erosion due to waves given by Mosselman [1996] and the formula given by Verheij [2000].

$$dy_l = \frac{E_l}{\rho g}\left(\frac{\left(\frac{v_0}{\sqrt{2}}\right)^2}{u_{c,l}^2} - 1\right) n\, T\, N_o\, \Delta t, \quad v_0 = 1{,}25\sqrt{2\, g\, H\, \cos\beta} \qquad \textit{Mosselman} \qquad (3\text{-}16)$$

$$\frac{dy}{dt} = c_E \cdot H^2, \qquad c_E = \frac{1{,}85 \cdot 10^{-4}}{\tau_c} \qquad \textit{Verheij} \qquad (3\text{-}17)$$

One of the problems of this comparison is that Mosselman gives a linear relation between the erosion rate and the wave height and Verheij gives a quadratic relation. In Figure 3-11 the relation between the erosion rate and the wave height is given for Verheij (black) and for Mosselman (green, purple and red). With the green line the value for E is determined by levelling both formulae for H=0,244 m (Table 3-3), the representative wave height for the outer bend. With the red line the same is done, only for H=0,5 m, the highest measured value. For the purple line the average value of both calculated E values is taken. As can be seen in Figure 3-12 most ships have a wave height between 0,05 m and 0,3 m, appendix C. The function with E=0,0122 N/m^{2}s (green) will give a good approximation for the erosion rate for that range of wave heights, but for the higher measured wave heights the green line underestimates the erosion rate significantly. Because these higher wave height will have a relative big contribution to the erosion rate ($\Delta y \sim H^2$), the green line isn't a good approximation. The function with E=0,0229 N/m^{2}s (red) will overestimate the erosion rate of the bank significantly for all measured values of H. The best approximation of E will thus be an averaged value of those two: E=0,017 N/m^{2}s (purple line).

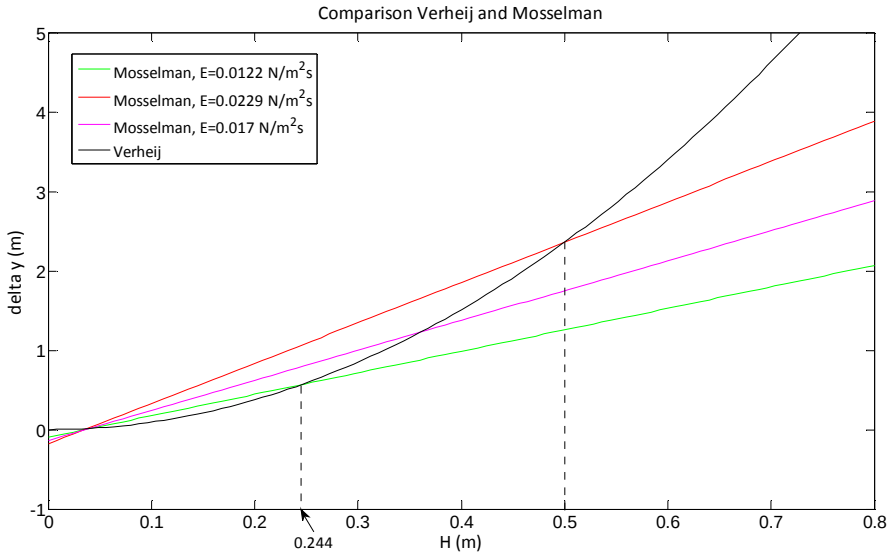


Figure 3-11: Comparison of formulae of Verheij and Mosselman

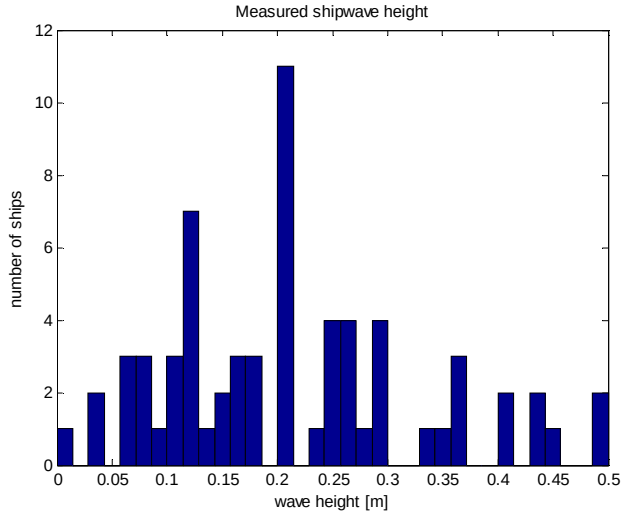


Figure 3-12: Histogram of measured ship wave height

The determined empirical coefficient (E = 0,017 N/m^{2}s) and the computed flow velocity in the outer bend (u = 0,65 m/s), paragraph 2.3.5 and 4.2, lead to an unrealistic high value of the bank erosion rate (21,26 m/year) when the critical shear stress is 1,5 N/m^2, following from equation (3-6). This unrealistic result is partly due to a lack of good experiments to determine the coefficients and partly due to the high sensitivity of the bank erosion rate to both the flow velocity (Figure 3-13) and the critical shear stress (Figure 3-14).

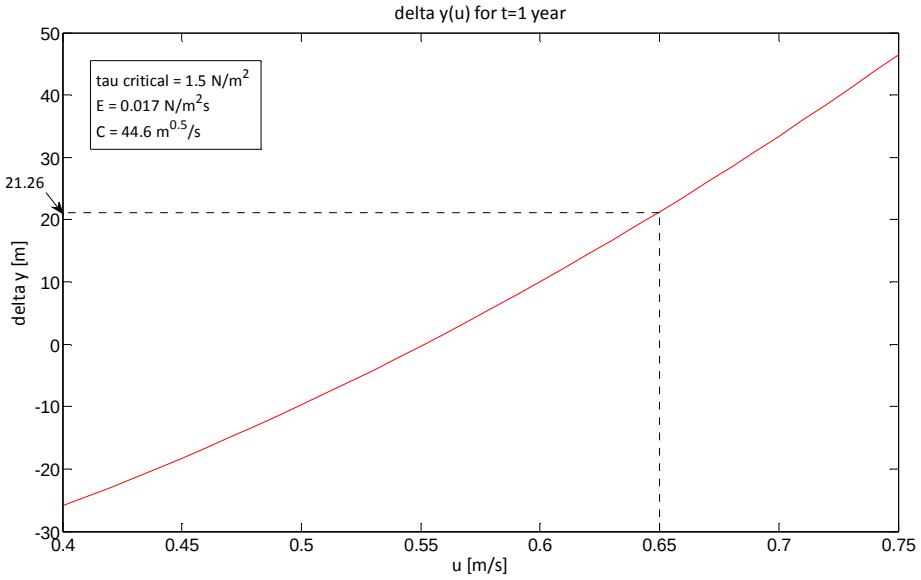


Figure 3-13: Sensitivity of delta y for u

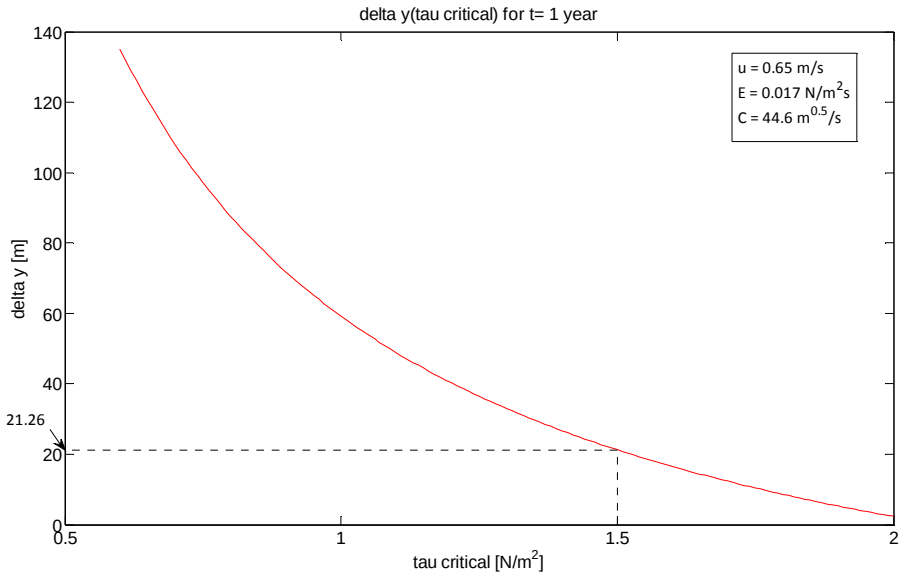


Figure 3-14: Sensitivity of delta y for tau critical

The above method and results can't be used in the further study, because of the high sensitivity of both the critical shear stress and the flow velocity. Especially the sensitivity of the critical shear stress leads to unusable results, because this parameter can't be determined with a high accuracy. A determination of the critical shear stress with a high accuracy can only be achieved with laboratory experiments, which can't be performed due

to time constraints. In this study the value of the critical shear stress is solely based on Table 2-11 and some Standard Penetration Test results.
To give an example of the accuracy: When the value of tau critical is 2 N/m^2 instead of 1,5 N/m^2 and the flow velocity isn't 0,65 m/s but 0,64 m/s, the erosion rate is just 0,55 m/year.

Another way to get an indication of the amount of erosion due to river flow is to use the satellite images (paragraph 3.1) and the results of the BEM for the erosion due to waves (paragraph 3.3.3). The calculated erosion rate due to ship waves for the outer bend is 0,97 m/year, but the average erosion rate in the outer bend that follows from the satellite images is 1,25 m/year. This difference can be subscribed to different factors: accuracy of the parameters used in the calculation (paragraph 3.3.3.5), accuracy of the satellite image measurements and the existence of other erosion agents. In the inner bend the calculated erosion due to ship waves is 0,93 m/year, but due to the existence of a shallow part in the inner bend (which isn't taken into account in the calculations) this value is an overestimation (paragraph 3.3.3.5). Concluding from these calculations and measurements a first indication of the amount of erosion in the outer bend due to river flow, which included both the meander movement and erosion due discharge variations, is in the order of 0,25 m/year. The transgression of the inner bend will be less than 0,25 m per year, because the meander movement causes accretion in the inner bend, but discharge variations cause erosion in the inner bend. This transgression is totally opposed by the erosion due to the ship waves.

Apart from the erosion at the outer bend some other locations can be pointed out where erosion can occur due to high flow velocities. Especially when dealing with a summer discharge (see Figure 3-15) the flow velocities near the bank are on many locations higher than the critical velocity: u_c=0,55 m/s, see equation (3-6). One should however take a critical look at the outcome shown in this figure for several reasons. The bathymetry data which is used as model input doesn't provide detailed information near the bank and the depth information near the bank is thus extrapolated from depth information near the centre of the river. Especially on the straight parts not much information was available and extrapolation can lead to large errors. In these straight parts the depth doesn't change a lot in the cross direction (see Figure 4-2), even though it is expected that the bathymetry shows a deeper part in the centre of the river and a shallower part near the banks. Because the flow will be concentrated in the deeper part the flow velocity on the shallower parts, near the bank, is expected to be less than is shown in Figure 4-5. Furthermore the spatial scale of a grid cell in the cross direction of the bank is around 50 m. This large spatial also introduces inaccuracies of the flow near the bank.
Taking this criticism in consideration, there is still a location where high flow velocities are expected, this location is encircled in Figure 3-15. The high velocities in this location are the result of meander movement in the bend upstream. The curved motion of the outer bend is still present after the bend due to the inertia, which leads to high velocities at the opposite bank somewhat downstream of the bend. For this location the same solution for the erosion problems as in the outer bend can be proposed. For the part downstream of location A the high velocities near the bank are assumed to be an overestimation due to the above mentioned inaccuracies. Bank erosion in this part is thus not expected to be caused by high flow velocities.

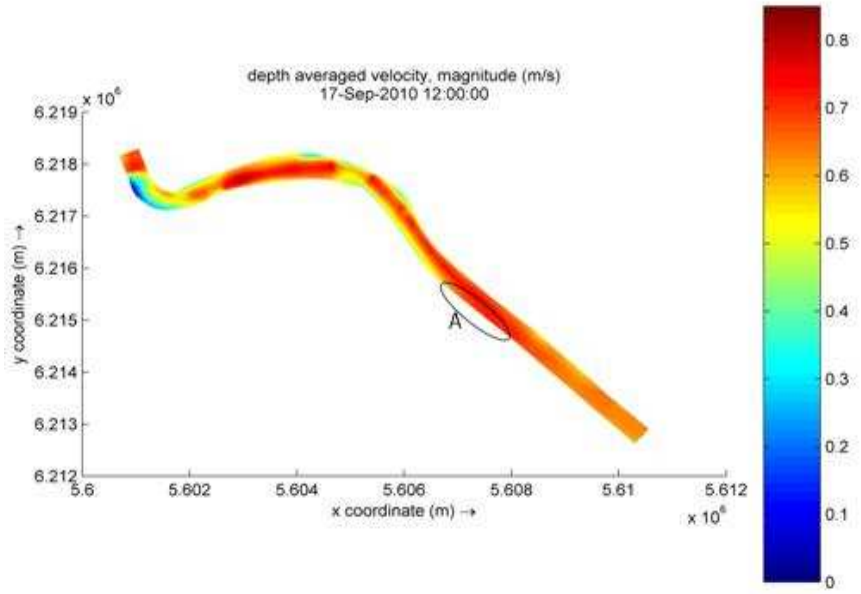


Figure 3-15: Location A, where bank erosion due to high flow velocities is expected (velocities that are given are the flow velocities during a summer discharge)

3.3.3 Ship waves

In order to calculate the erosion, caused by ship waves, a measurement of the ship waves took place. In this paragraph, a brief description is given of the measurements. After that the results of the measurement will be discussed. These results are used for the calculation of the erosion rate, with the BEM, as described in paragraph 3.2.1.

3.3.3.1 Theoretical speed limits

Every vessel has a minimum speed, in order to maintain rudder control. Also each vessel has a limit speed. The limit speed is the minimum of the hull speed and the limit speed related to the return current. The results can be found in Table 3-1. The background of the computations can be found in appendix B.

Class	A1	A2	B	C1	C2	D
Limit speed [m/s]	7,74	8,76	8,83	8,98	8,98	4,33
Max. economic speed [m/s]	6,19	7	7,06	7,19	7,19	3,46
Min speed [m/s]	1,11	2,37	5,29	1,35	2,19	3,5

Table 3-1: Limit, max. economic speed and minimum speed of the different ship classes

3.3.3.2 Measurements

During a two day measurement campaign, the waves of passing vessels are measured. The wave cusps are measured visually with use of a gauge rod. The rod was placed in front of a concrete revetment in the outer bend of the Paraná de las Palmas at km 87. During measurement also the following is measured: vessel speed, wave length, wave period, draught and water level. A full description of the measurements can be read in appendix C.

The objective of the measurements was twofold: firstly they have been conducted in order to verify whether the calculated cusp height, see expression (3-18) and appendix B, corresponds to the measured cusp height.

$$\frac{H}{h} = \zeta \left(\frac{s}{h} \right)^{\frac{-1}{3}} Fr^4 \qquad (3\text{-}18)$$

The second objective was to characterize the wave generation of different classes of vessels with which the representative wave can be calculated. This representative wave height is needed for erosion rate computations.

The measured ships are divided into six classes, as stated in Table 2-1. The ships are divided in these classes to compare the influence of the C_b (block coefficient) and the draft on the value of ζ.

For the computations only the ships are used of which the following parameters were measured:

- Type of ship
- Vessel velocity (relative to the ground)
- Wave height
- Distance to the bank
- Water level

All the measured data can be found in appendix B.

3.3.3.3 Analysis of measurements

In this section a lot of computations are presented to analyse the measurements. Only the used method and expressions are given together with the results. In appendix D.5 a calculation example is given for class A2. For a better understanding of this section it might be convenient to check this calculation example.

ζ-values

The measurements of the wave heights is only done for two days, but the measurement of ship velocities can be done for a much longer period (via the Automatic Identification System). Therefore the zeta values are calibrated in such a way that if the measured velocities are put into equation (3-18), the calculated wave heights can be used in expression (3-19) to calculate the representative wave height.

Erosion ~ H^2

$H(1,2,..,n)$ (set of wave heights)

$$Hrepr = \sqrt{\frac{\sum_{j=1}^{n} H_j^2}{n}} \qquad (3\text{-}19)$$

The contribution of the higher waves to the erosion is higher and therefore also to the determination of the zeta value.

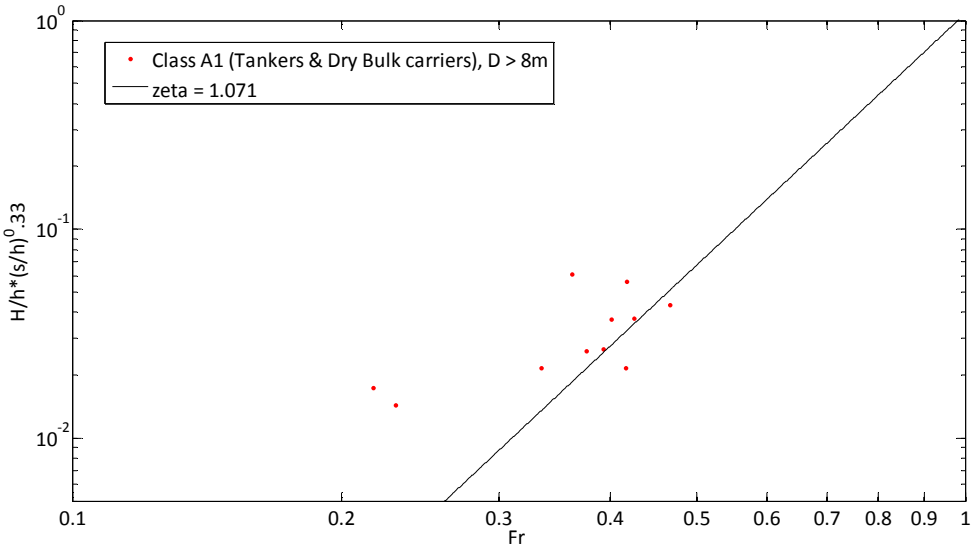


Figure 3-16: Calibration of ζ for Class A1, draft > 8 m

Only for Class A1 the plot with observed vessels and the determined zeta value is given. In Figure 3-16 it can be seen that the graph with ζ=1,071 fits the major part of the measurements. Only two data points are badly correlated with this ζ. As is stated before, the higher wave heights contribute more to the erosion, which causes the line to be directed more to the right of the figure (lower zeta).

For the background of the determination of zeta values is referred to appendix D.

Class	ζ	$H/h*(s/h)^{0.33}$
A1	1,07	Var
A2	0,68	Var
B	1,34	Var
C1	1,11	Var
C2	1,36	Var
D	-	0,04

Table 3-2 gives the ζ values for all the classes. For class D no ζ value could be estimated, because it consisted mainly of speed boats, which were above Fr = 0,75 (so expression (3-18) was not valid anymore).

Class	ζ	$H/h*(s/h)^{0.33}$
A1	1,07	Var
A2	0,68	Var
B	1,34	Var
C1	1,11	Var
C2	1,36	Var
D	-	0,04

Table 3-2: ζ-values for different classes

Representative wave height

In paragraph 3.2.1 it is stated that the erosion rate is proportional to H^2 if no damping is assumed by a foreshore or structure. If there is damping (μ), the erosion rate is proportional to $\ln(c_E \cdot \mu \cdot H^2 + 1)$. For small μ (which is often the case) this proportionality is almost the same as to H^2. Therefore the representative wave height is based on the following proportionality: Erosion rate ~ H^2.

The representative wave heights are determined for the following locations:

- Outer bend
- Inner bend
- Along straight river sections

Mind the difference between the representative and the significant wave height. The representative wave height is the wave height that leads to the same erosion rate as the whole wave spectrum. The significant wave height is the mean height of the highest third of all the measured waves. The results are summarized in Table 3-3.

Class	Outer bank		Inner bank		Straight section	
	H_{repr} [m]	$H_{1/3}$ [m]	H_{repr} [m]	$H_{1/3}$ [m]	H_{repr} [m]	$H_{1/3}$ [m]
A1	0,25	-	0,18	-	0,20	-
A2	0,29	-	0,20	-	0,23	-
B	0,32	-	0,21	-	0,24	-
C1	0,17	-	0,21	-	0,18	-
C2	0,23	-	0,27	-	0,24	-
D	0,20	-	0,21	-	0,21	-
Overall	0,24	0,34	0,24	0,27	0,23	0,28

Table 3-3: Representative and significant wave heights for all classes

Wave length and period

For estimation of the period and length of secondary ship waves a reliable expression is developed [Schiereck, 2004]:

$$T = \cos(\theta) \cdot v_s \frac{2\pi}{g}$$

$$L = \frac{gT^2}{2\pi} \qquad (3\text{-}20)$$

These expressions are valid in deep water (h/L > 0,5), when Fr < 0,75.

The measured wave lengths and periods do not correspond well with the calculated wave lengths and periods. Because of the reliability of the theoretical approach it is decided to use the theoretical wave lengths and periods. For all classes the mean, representative and significant length and periods are calculated. The representative values correspond with the H_{repr} and have to be used for erosion rate computations, with the BEM. The significant values

are the mean values for the highest one-third of all the measured waves. The results are summarized in Table 3-4.

Class	L_{mean} [m]	T_{mean} [s]	L_{repr} [m]	T_{repr} [s]	$L_{1/3}$ [m]	$T_{1/3}$ [s]
A1	9,1	2,4	9,6	2,5	-	-
A2	9,8	2,3	13,3	2,7	-	-
B	8,9	2,3	10,0	2,5	-	-
C1	8,4	2,3	8,4	2,3	-	-
C2	9,3	2,4	9,1	2,4	-	-
D*	10,2	2,4	15,2	3,1	-	-
overall	9,1	2,3	10,2	2,5	10,3	2,5

Table 3-4: Wave lengths and periods of all classes

3.3.3.4 Ship movement

Based on a database of a 24 day ship track, the yearly ship movement is estimated [Prefectura Naval, 2010].

Class	Number of ships per year at km 87 (extrapolated)	Percentage [%]
A1	2.367	9
A2	4.457	17
B	1.813	7
C1	2.567	10
C2	11.372	41
D	1.374	5
Remaining	2.798	11
Total	26.739	100

Table 3-5: Yearly ship movement along the Paraná de las Palmas

3.3.3.5 Erosion caused by ship waves

As explained in paragraph 3.2.1 the erosion rate of the river bank can be modeled with a Bank Erosion Model (BEM). Depending on the presence of a foreshore the following formulae can best be used:

$$dy = c_{\varepsilon} \cdot H^2 \cdot n \cdot T \cdot N$$
$$dy = \frac{1}{2\mu} \ln(2\mu \cdot c_E \cdot H_0^2 \cdot n \cdot T \cdot N + 1) \qquad (3\text{-}21)$$

The first formula is the same as the second one if the damping is assumed to be zero. Because of a lack of exact information about the bathymetry near the banks it is first assumed that there are no shallow parts in the river which introduce wave damping. After

the calculation of the erosion without the presence of shallow parts the results will be compared to the observation, as described in paragraph 3.1.1.

The erosion is calculated according to a Monte Carlo simulation [Vrijling, 2006], a full probabilistic method. For this simulation the probability distributions of all present parameters are used to calculate the erosion rate. The erosion rate, first of expression (3-21), is calculated 30.000 times, each time with random chosen variables. The advantage of a full probabilistic method is that it gives an idea of the reliability of the computation. The assumed distribution functions for all the used variables are given and explained in appendix D.

Erosion rate without damping

In Table 3-6 the computed erosion rate for three different locations is given. The analyzed locations are the outer bend, the inner bend and a straight river section. At all the locations an erosion rate in the order of 0,9 m/year is computed. This might look strange, but can be explained by the fact that a lot of smaller vessels take the inner bend. The erosion at the inner bank is therefore mainly caused by the smaller vessels (Class C1 and C2), while the erosion at the outer bank is mainly caused by the bigger ships (Class A1, A2 and B). At the outer bank 50% of the erosion is caused by the bigger ships (Class A1, A2, and B). At the inner bank only 25% of the erosion is caused by the bigger ships. This can be explained by the fact that the wave height is reduced for the bigger ships, because the travel distances for the waves are longer towards the inner bank.

Class C2 vessels (vessels smaller than 100 m with a draft smaller than 2,5 m) have a big contribution to the erosion problems. This is mainly caused by the large amount of Class C2 vessels. At the outer bend the contribution of this class is 41% while at the inner bend it is even 63%.

Class	Outer bend		Inner bend		Straight section	
	dy [m/year]	Percentage of erosion [%]	dy [m/year]	Percentage of erosion [%]	dy [m/year]	Percentage of erosion [%]
A1	0,09	10	0,05	5	0,06	7
A2	0,27	27	0,13	14	0,16	19
B	0,12	12	0,06	6	0,07	8
C1	0,05	5	0,07	7	0,05	6
C2	0,40	41	0,59	63	0,45	54
D	0,05	5	0,05	5	0,05	6
overall	0,97	100	0,93	100	0,84	100

Table 3-6: Erosion rate due to ship waves

To evaluate the model, the results of this computation are compared with the analysis of the satellite images, as described in paragraph 3.1.1.
After comparison the following remarks can be made

- The mean regression of the river banks at the outer bank was about 1,25 m/year during the last years. The model gives a regression of 0,97 m/year. The difference

between the values can be explained by the presence of normal river flow (containing both meandering effect and discharge variations). The difference can also be caused by errors due to wrong estimation of the critical shear stress, number of waves per ship or other parameters.

- The mean regression of the river banks at the inner bank was about 0,05 m/year during the last years (also some spots with transgression of the river bank were observed). The model gives a regression of 0,93 m/year. The big difference is thought to be caused by the assumption of no presence of wave damping by the bottom. In the inner bend the bathymetry is less steep and less deep, this can cause a significant wave damping by friction. Another explanation would be the presence of a meander movement. Also errors in the input could have disturbed the outcome.

Erosion rate with damping

A shallow part in the river is able to reduce the wave height by frictions means. The formula for this wave height reduction is as follows:

$$H = H_0 e^{-\mu y}$$
$$\mu = \frac{\tan(\alpha)}{H_0} \qquad (3\text{-}22)$$

The parameter y is the length of the shallow part and α is the angle of the bottom slope of the shallow part. According to a bottom survey (not at the Paraná de las Palmas) done for several shores in front of a river bank the slope varies between 1:20 and 1:100. In the case of a H_0 of 0,239 m, which is the case at the inner bank, the value of μ varies between 0,04 and 0,21. In Figure 3-17 the reduced wave height is plotted against the length of the shallow part for various values of tan(α). In Figure 3-18 the resulting erosion rate is plotted. It can be seen that the erosion rate can be reduced to a large extent in the case of shallow parts, which are likely to be present in the inner bend of a river. A foreshore only reduces the waves if the water depth is smaller than two times the wave height. Because the Paraná de las Palmas is subjected to a large variation of water levels the effect of a foreshore will not always be present. So the plots of the reduced wave height and erosion rate need to be observed with the knowledge that the real reduction is less. Only if the foreshore is large enough to cover all the water levels the reduction of the plots is the actual reduction. Due to a lack of information about the exact bathymetry near the river bank it is hard to conclude something from these plots.

If the bathymetry data, see paragraph 2.3.1, is extrapolated towards the inner bend values for tan(α) vary between 1/7 and 1/4 (cross section 14-17). If such a foreshore has an effective length of 1 m the erosion is already reduced to 0,15 m/year.

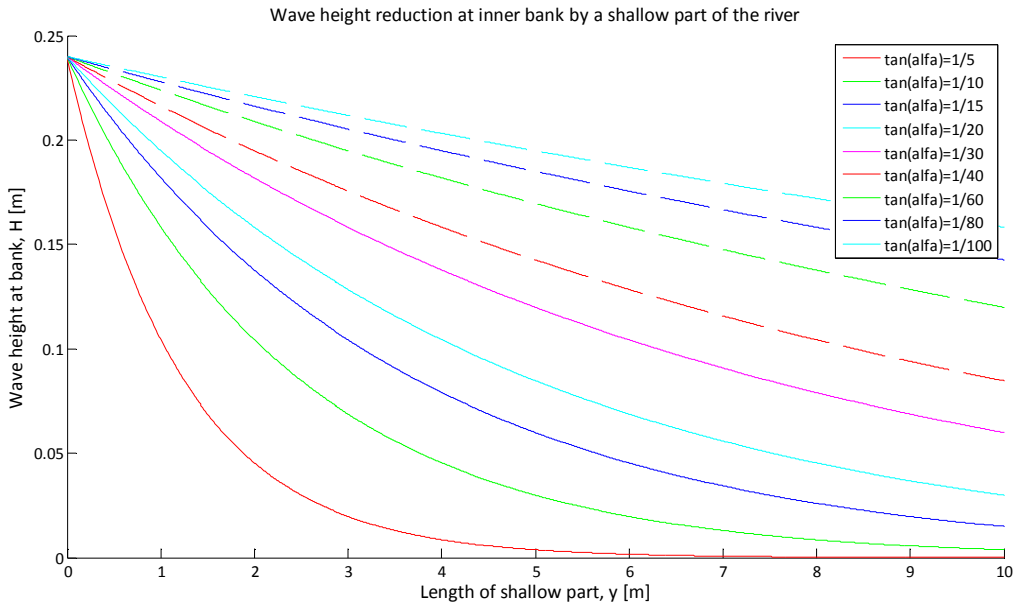


Figure 3-17: Reduced wave height at the inner bank in case of a foreshore

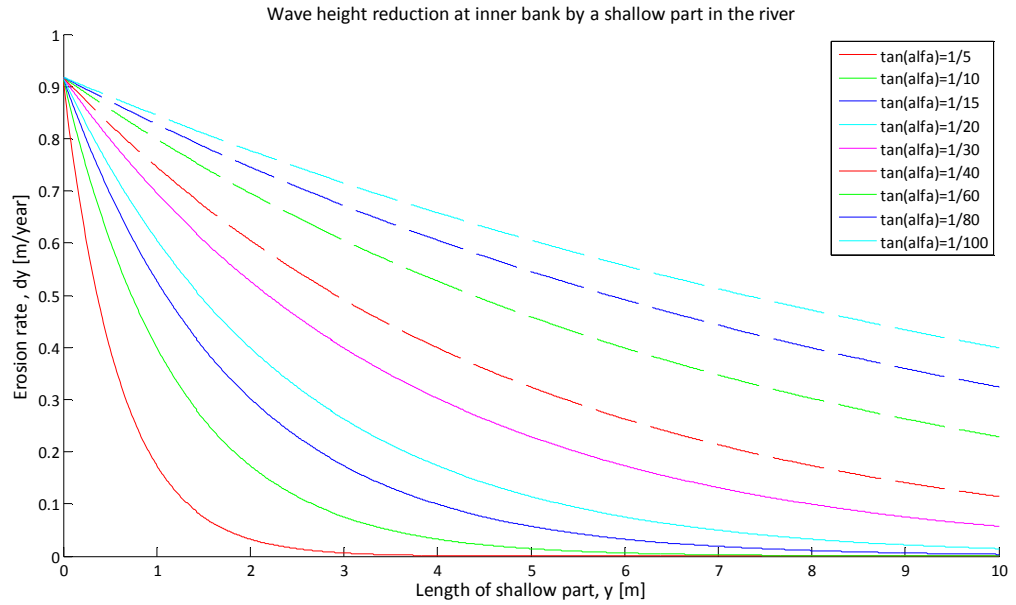


Figure 3-18: Reduced erosion rate at the inner bank in case of a foreshore

Sensitivity of the BEM

For the erosion rate at the outer bend, inner bend and along straight sections a cumulative distribution function can be plotted (result of Monte Carlo simulation). In Figure 3-19 the cumulative distribution function for the erosion rate along a straight river section is given. It shows that the range of the erosion rate is between 0,2 m/year and 2,25 m/year. To obtain a more accurate result, validation of the BEM is needed. But the model shows that significant erosion due to ship waves is reasonable.

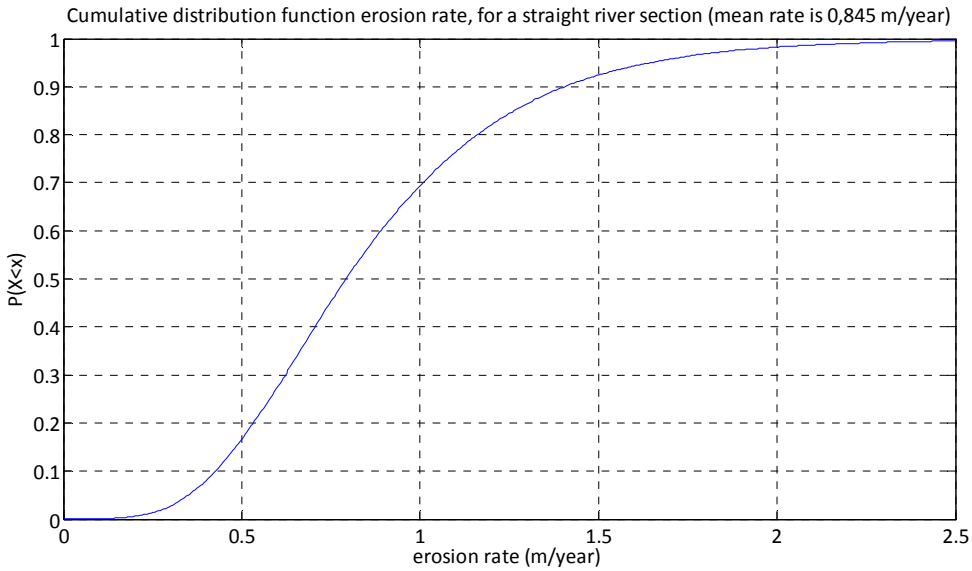


Figure 3-19: Cumulative distribution erosion rate, straight river section

The cumulative distribution functions of the other locations can be found in the appendix D.

3.4 Conclusion of problem analysis

The analysis of the satellite pictures of paragraph 3.1.1 shows that the erosion of the river banks of the Paraná de las Palmas River is significant: the average erosion rate is 0,68 m per year (averaged over inner bends, outer bends and straight parts). In the outer bend the satellite images show an erosion rate of 1,25 m/year.

After investigating both erosion due to rapid drawdown, discharge variations, meander movement (increased flow) and ship waves, it can be concluded that rapid drawdown doesn't have a significant contribution. Only when the local soil consists of less cohesive layers than the assumed soil structure flooding can cause erosion.

The erosion rate due to ship waves which is calculated with a Bank Erosion Model is 0,9 m erosion per year due to ship waves. The sensitivity of this calculation is investigated with a Monte Carlo probabilistic approach and shows that the erosion rate is in a range of 0,2-2,5 m/year. However 60% of the possible outcomes lie in between 0,6 m and 1,2 m erosion per year. Apart from the large uncertainty of the values for C_0 (coefficient to calculate c_E) and n (number of waves per ship) a significant contribution of the total sensitivity of the erosion rate is caused by the inaccuracy of H (wave height). This sensitivity of the erosion rate with respect to the wave height is caused by the fact that the erosion rate is proportional to H^2 and to a much less extent by the inaccuracy of H itself. The height of the measured ship waves correlates reasonable well with the theory of Schiereck.

The effects of river flow (meander movement and discharge variations) are also calculated with the BEM. Unfortunately the BEM is very sensitive for the used input, especially for the used shear strength of the soil. Because the shear stress is hard to determine a calculation of the erosion rate due to river flow with the BEM doesn't product reliable results. Therefore the effect of the river flow is calculated with satellite imagines and the BEM for erosion due to ship waves. This leads to an erosion rate due to river flow of about 0,25 m per year.

From these findings it can be concluded that it is highly probable that the majority of the erosion problems are caused by ship waves. The solutions will thus be designed to reduce

the erosion by ship waves. Because the river flow also has a significant contribution to the total erosion rate, the erosion due to river flow will also be taken into account, if possible, in the design of solutions.

In order to improve the results of the BEM calculations one should improve the quality of the different input parameters, especially the soil parameters since the BEM for river flow is very sensitive to these parameters.
Furthermore it would be interesting to validate the BEM on a straight (non meandering) river section in order to check whether the calculated erosion due to ship waves is comparable to the observed erosion at the straight river section which is free from erosion due to meander movement.

4 Computational modelling

4.1 General modelling considerations

4.1.1 Modelling goal

The goal of the computational modelling of the Paraná de Las Palmas is to get an idea of the overall behaviour of the river without the ship waves (velocity field, water levels, meandering and morphological development), to help determine the relative importance of all the erosion agents.

4.1.2 Important physical processes

When modelling the erosion problem, some choices have to be made, because simplification of reality is inherent to modelling. The physical processes that are important for the erosion problem will have to be defined and have to be accounted for in the modelling. Processes that are of little or no importance to the problem will not be included in the model.

First and foremost, to look at morphological development, erosion, sedimentation and sediment transport processes need to be taken into account.

One of the stretches of river to be modelled is a river bend. River bends are prone to a 3D flow pattern called spiral flow. The bend in the river causes a flow in the surface layer pointed to the outer bend, and a flow close to the bed pointed to the inner bend. This flow pattern has a large impact on the sedimentation/erosion pattern and should be included in the modelling. To do that, Delft3D-FLOW will have to be run in 3D mode (having more than 1 grid cell in vertical direction).

4.2 Delft3D model

4.2.1 Model characteristics

The modelling will be carried out using the Delft3D suite [version 3.28.04, July 2009, Deltares]. The FLOW module is used for the actual simulation. The RGFGRID is used to construct the grid and the QUICKIN module is used to process the bathymetrical data.

Delft3D-FLOW can simulate 2D or 3D hydrodynamics and transport. It can calculate non-steady flow and transport induced by meteorological and tidal forcing. The program uses recti- or curvilinear grids. When the 3D mode is used, the vertical grid is constructed with the sigma coordinate method. [Deltares, 2009a]

4.2.2 Computational grid

The computational grid used in all the Delft3D simulations was created using a polygon defined in the Google Earth program [version 5.2.1.1588, 01-09-2010, Google Inc.]. This polygon followed the river banks depicted on the most recent satellite images (23-01-2010).

This polygon was originally in the latitude/longitude (WGS'84) format, so it had to be converted to the Argentinean POSGAR94 format (the same format as the bathymetrical data).
The converted polygon was entered into Delft3D-RGFGRID as a land boundary. Subsequently, splines were defined following the curvature of the river, to eventually obtain a curvi-linear grid (Figure 4-1).

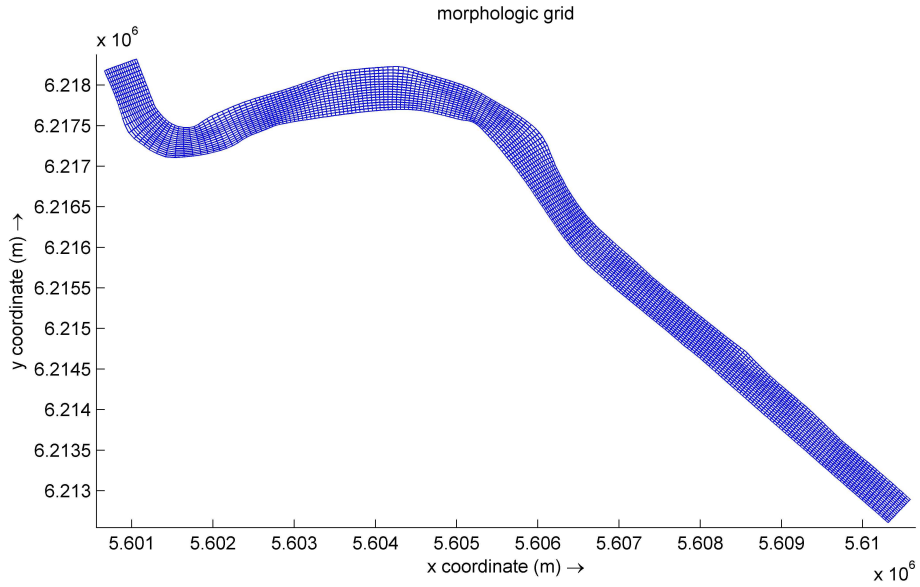


Figure 4-1: The computational grid used for the simulation

4.2.2.1 Grid parameters

To guarantee the computational stability of the simulation, the grid has to meet a few demands. Firstly the orthogonality has to be checked; this is the measure in which the sides of each cell meet each other at an angle of 90° (the lower the number, the more the angle approaches 90°). In the inner part of a computational grid the orthogonality has to be in between 0,02 and 0,04. In this particular grid, the maximum value is 0,02.

Furthermore, the aspect ratio is relevant; this is the length/width ratio of each cell. Normally the aspect ratio should be in between 1 and 2, but when the flow is predominately along only one of the grid lines, the aspect ratio may be larger than 2 (this is indeed the case since the grid is used to model a river). The grid has a maximum ratio of 5,6 which is acceptable regarding the previous [Deltares, 2009b].

4.2.2.2 Bathymetry

Eventually every grid point in the grid has to have a depth assigned to it, so the (irregular) bathymetrical data has to be interpolated. The bathymetrical data is mostly concentrated in the fairway, with some cross-sections in the river bends. This has consequences for the methods that can be used for interpolation. Due to the scarcity of data points, triangular interpolation is a good option. This requires all grid points to be inside a triangle of data points, but this isn't true for all grid points (especially those at the edges of the grid). This

causes the need for a second interpolation method for the remaining grid points, so the internal diffusion method is used (a repetitive smoothing method to fill in the gaps in the bathymetry) [Deltares, 2009c]. In Figure 4-2 the final bathymetry used in the simulation is shown.

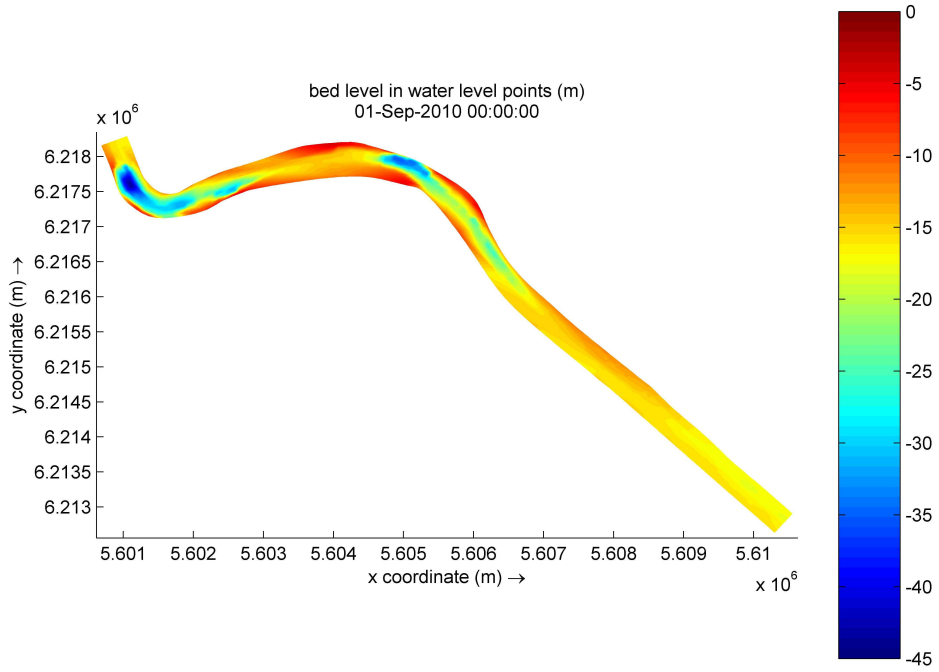


Figure 4-2: The river bathymetry used in the simulation

4.2.3 Delft3D-FLOW input

The complete input parameters for the Delft3D-FLOW model can be found in appendix F.

4.2.3.1 Simulation time span

The size of the time step is limited by the Courant number, which is defined [Deltares, 2009a]:

$$Courant = \frac{\Delta t \sqrt{gH}}{\{\Delta x, \Delta y\}} \qquad (4\text{-}1)$$

In which Δt is the computational time step, g is the gravitational acceleration, H is the water depth and Δx/Δy is the width of the grid cells.

In Delft3D the Courant number should not be larger than 10, except for problems like this with small variations in space and time (then it can be taken substantially larger). The time step used is one minute and the smallest side of a grid cell is 25 m. The H ofcourse varies over the river cross-section, and the maximum depth is 43 m. The characteristic length of a grid cell (in the direction of the river axis) is about 50 m. With these numbers, the Courant number turns out to be 24,6 and is acceptable for this simulation

The time span of the simulation is 35 days. The morphological factor used in the model is set to 10. The inclusion of a morphological factor greater than 1 is that the erosion and sedimentation take place n times as fast (where n is the morphological factor). This means

that the run represents a period of 35·10 = 350 days (so almost one year) of morphological development.

4.2.3.2 Physical parameters

The water is fresh, so a density of 1.000 kg/m^3 is assumed. The gravitational acceleration is set to 9,81 m/s^2. The slip condition for the calculation of the wall roughness is set to 'free' because of the relatively large scale of the simulation.

The turbulence model used is the widely applicable k-ε model and the horizontal eddy viscosity and diffusivity are kept at the default values of 1 m^2/s and 10 m^2/s respectively.

For the roughness, a Manning coefficient of n = 0,035 s/m$^{1/3}$ is used, which is a representative value for rivers.

4.2.3.3 Sediment characteristics

The river sediment is cohesive and has a dry bed density of 1380 kg/m^3 and a specific density of 2650 kg/m^3. The sediment consists of mostly silt with a reasonably large clay fraction and a smaller sand fraction. At the time of the simulation, the exact grain diameter distribution was not known, so an estimation for the D_{50} was made. Because the bottom was assumed to be silty, a D_{50} was estimated at 31 µm (between coarse and medium silt). Later obtained information caused this estimation to be off (see Figure 2-15). Due to time constraints, it was not possible to take this new data into account in a new simulation.

The unhindered settling velocity is calculated with the following formula [De Vriend, 2010]:

$$w_s = \frac{\Delta g D^2}{18\nu} \quad (4\text{-}2)$$

$$\Delta = (\rho_s - \rho)/\rho \quad (4\text{-}3)$$

$$\nu = \frac{\eta}{\rho} \quad (4\text{-}4)$$

In which w_s is the unhindered settling velocity, g is the gravitational acceleration, D is the sediment diameter, ρ_s is the specific sediment density, ρ is the density of the water (assumed fresh, 1000 kg/m^3), ν is the kinematic viscosity of water and η is the dynamic viscosity of water (assumed 10^{-3} kg/ms).

With these values the unhindered settling velocity of the sediment becomes $8{,}64 \cdot 10^{-4}$ m/s.
The critical shear stress for erosion is assumed at 1,5 N/m^2. Due to the difficulties determining the critical shear stress for sedimentation in the case of cohesive sediment, the default value in Delft3D-FLOW will be used, which is 1.000 N/m^2. Therefore, the sedimentation in the model result is expected to deviate from reality.

4.2.3.4 Initial and boundary conditions

There are two boundaries in the model, the upstream and downstream boundaries. To create a stable river model, there has to be a discharge specified upstream and a water level

downstream. The discharge varies during the year, with a mean summer discharge of 4.400 m^3/s and a mean winter discharge of 3.700 m^3/s. In the simulation, the discharge will vary with time to represent the seasonal discharge variability (Table 4-1).

Hours of simulation [hr]	Discharge [m^3/s]
0	3.700
7.200	3.700
18.000	4.400
32.400	4.400
43.200	3.700
50.400	3.700

Table 4-1: Discharge at the upstream boundary (the increase between different discharges is linear)

The sediment concentration in the river is known to be between 0,1 and 0,25 kg/m^3 (see paragraph 2.4.1). In the simulation the inflowing water and the water present in the model at the beginning of the simulation both have a sediment concentration of 0,2 kg/m^3.

At the downstream boundary, a water level is required. In this case, the mean water level is used, which is 0,671 m above RD.

4.3 Modelling results

The results from the Delft3D model consist of a water level, a flow velocity field and an erosion pattern.

4.3.1 Water level

In Figure 4-3 and Figure 4-4 the water level for the whole river is shown.

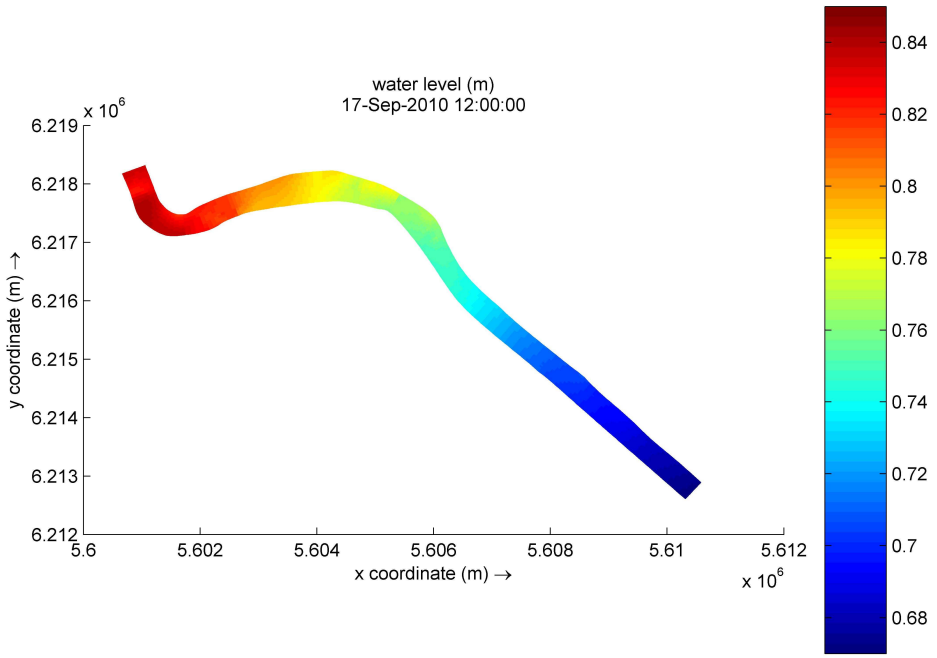


Figure 4-3: Water level with summer discharge

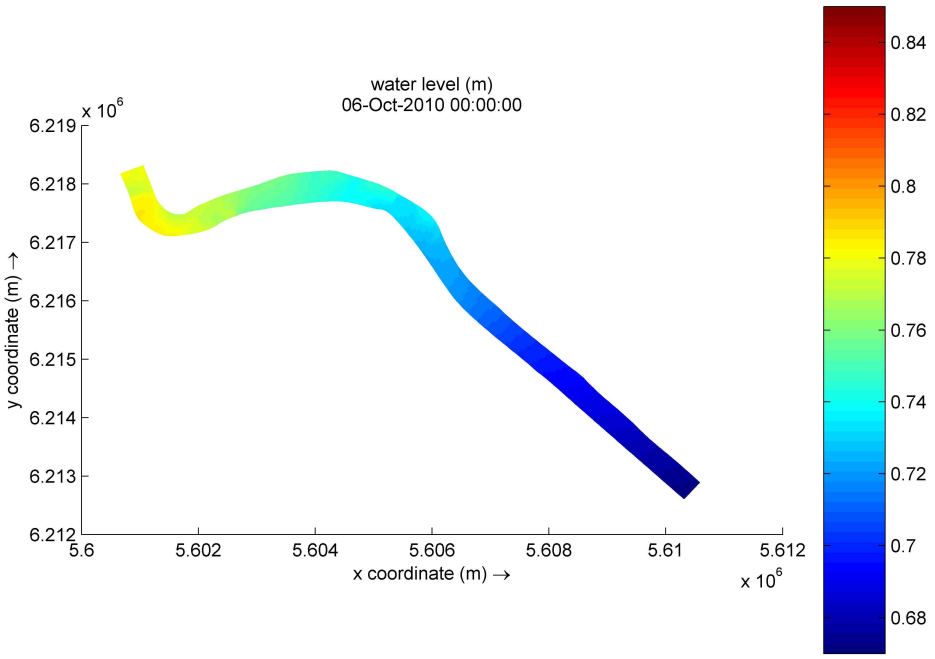


Figure 4-4: Water level with winter discharge

It can be seen that the water levels are higher with a summer discharge, particularly for the two bends. Also the water level in the outer bend is somewhat higher than in the inner bend, as expected.

4.3.2 Flow field

In Figure 4-5 and Figure 4-6 the fully developed depth averaged velocity field for summer and winter discharge is shown. Figure 4-7 to Figure 4-10 show details of the upstream and downstream bends.

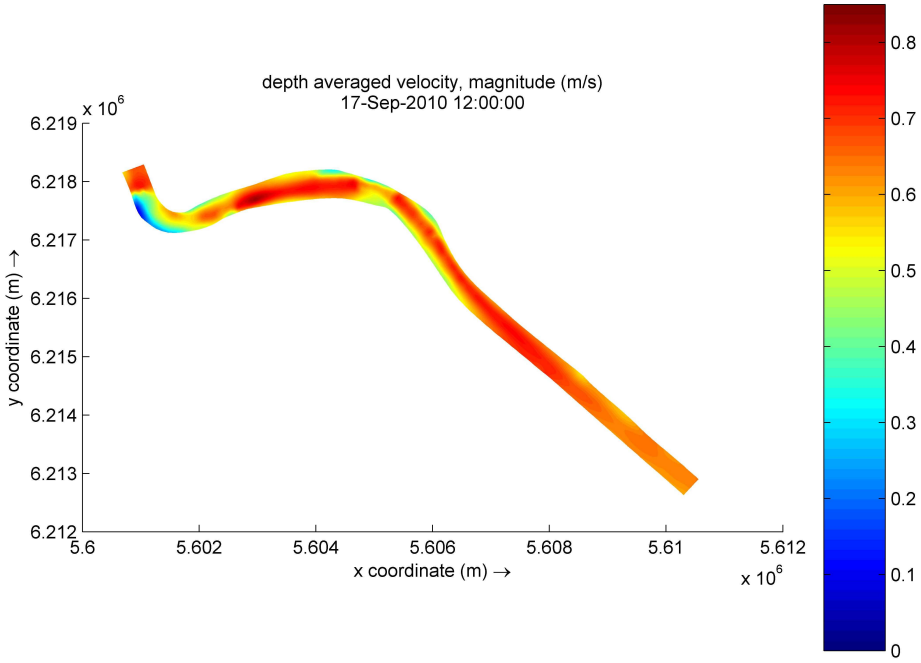


Figure 4-5: Depth averaged velocity with summer discharge

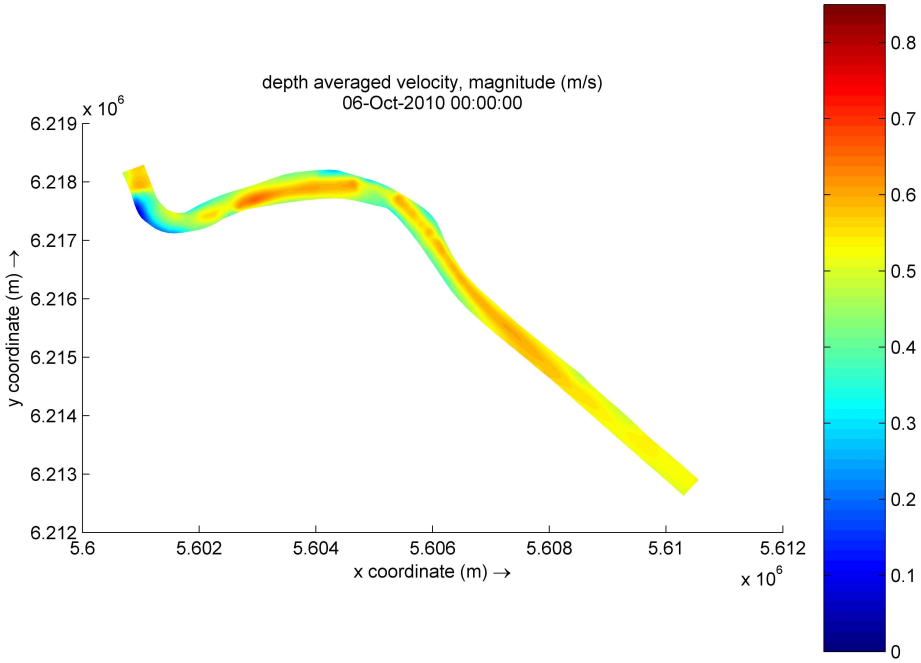


Figure 4-6: Depth averaged velocity with winter discharge

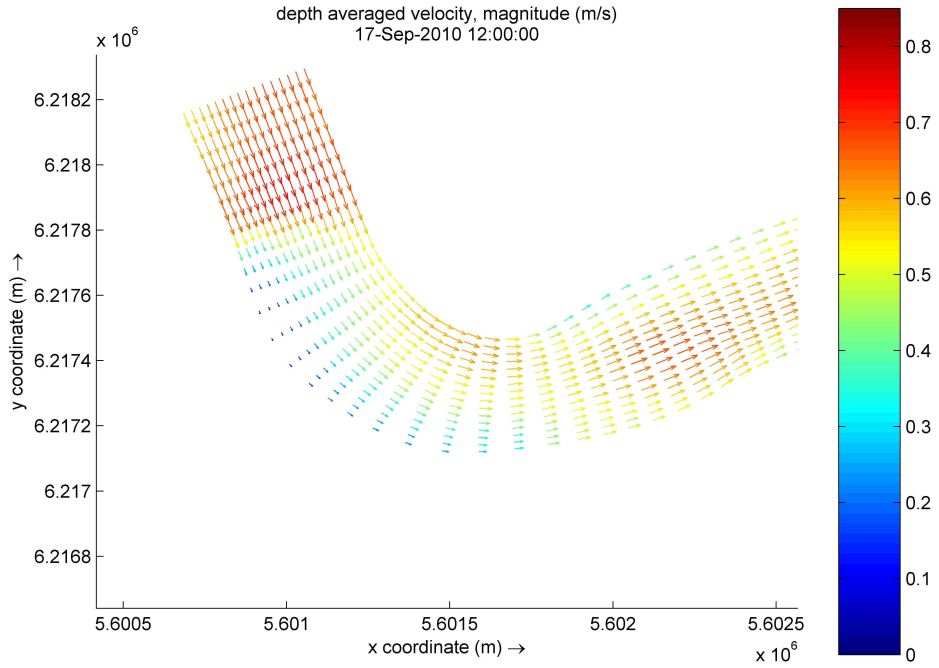


Figure 4-7: First bend, summer (both length and colour of the arrows are proportional to the velocity)

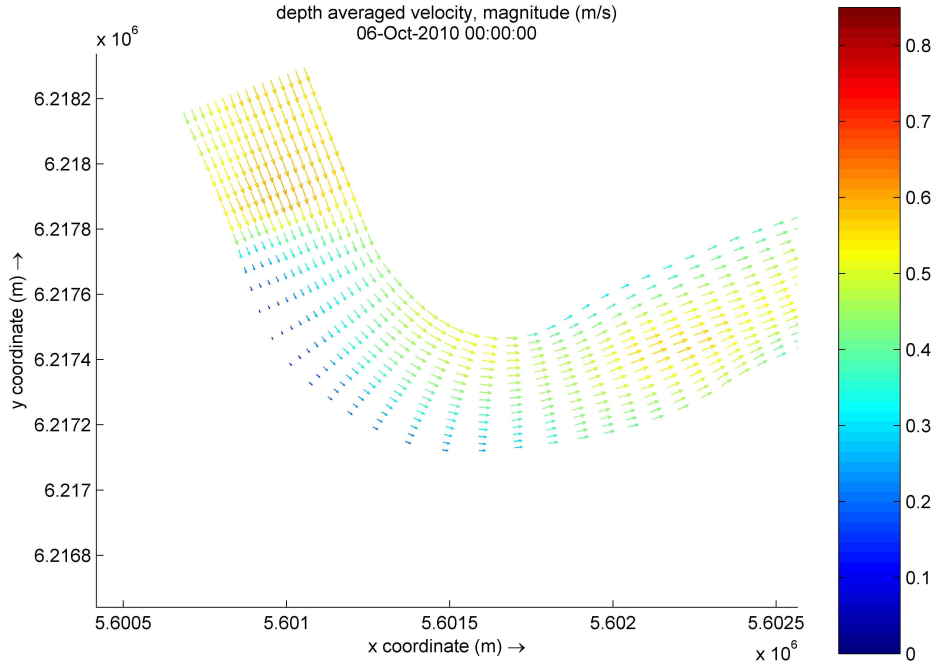


Figure 4-8: First bend, winter (both length and colour of the arrows are proportional to the velocity)

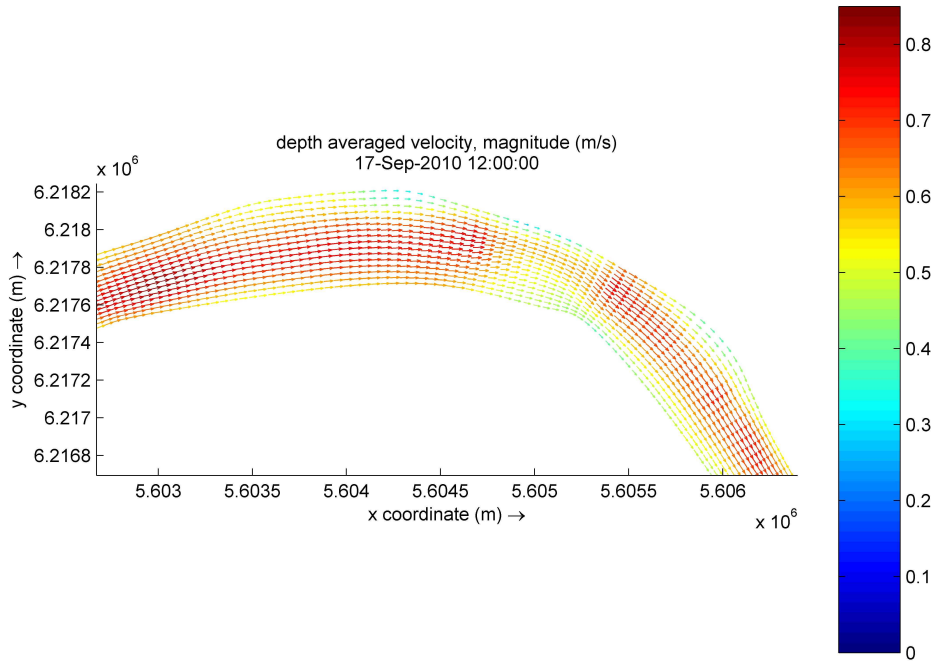


Figure 4-9: Second bend, summer (both length and colour of the arrows are proportional to the velocity)

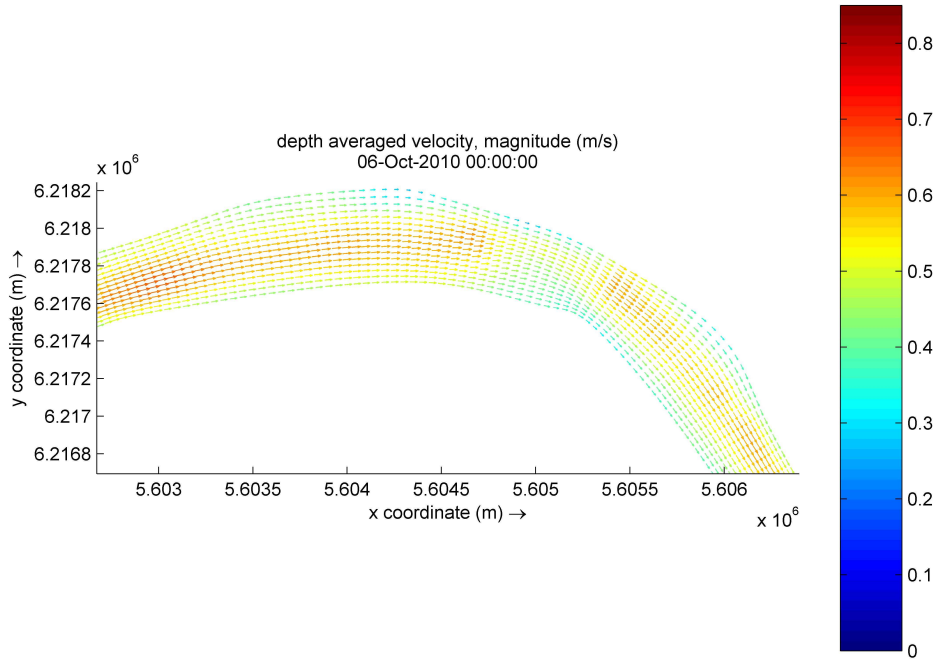


Figure 4-10: Second bend, winter (both length and colour of the arrows are proportional to the velocity)

The first general observation regarding the flow pattern in the river is that it's heavily influenced by the sudden deep pits that are present in the bends. Due to the increase in the cross-sectional area, the velocity drops radically. Especially in the first bend this results in a larger velocity in the inner bend, which is counterintuitive.

Furthermore, higher velocities can be seen at the parts of the river where the depth decreases; both in between the bends and after the second bend.

4.3.3 Erosion

The erosion/sedimentation of the bed at the end of the simulation is shown in Figure 4-11. For reference the initial and eventual bed levels are shown in Figure 4-12 and Figure 4-13 respectively.

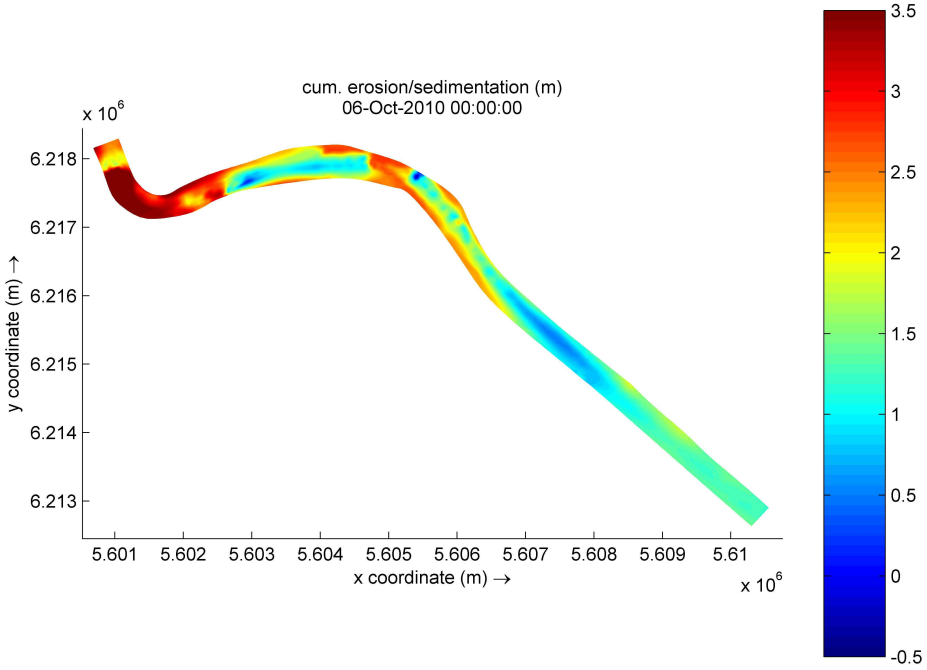


Figure 4-11: Cumulative erosion (negative) sedimentation (positive) at the end of the simulation

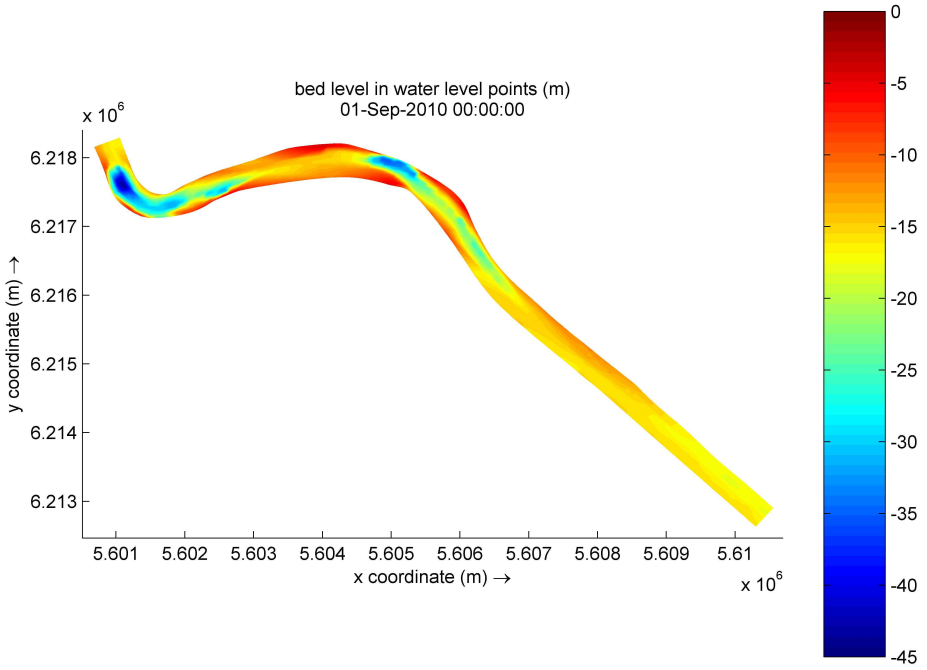


Figure 4-12: Initial bed level (before simulation)

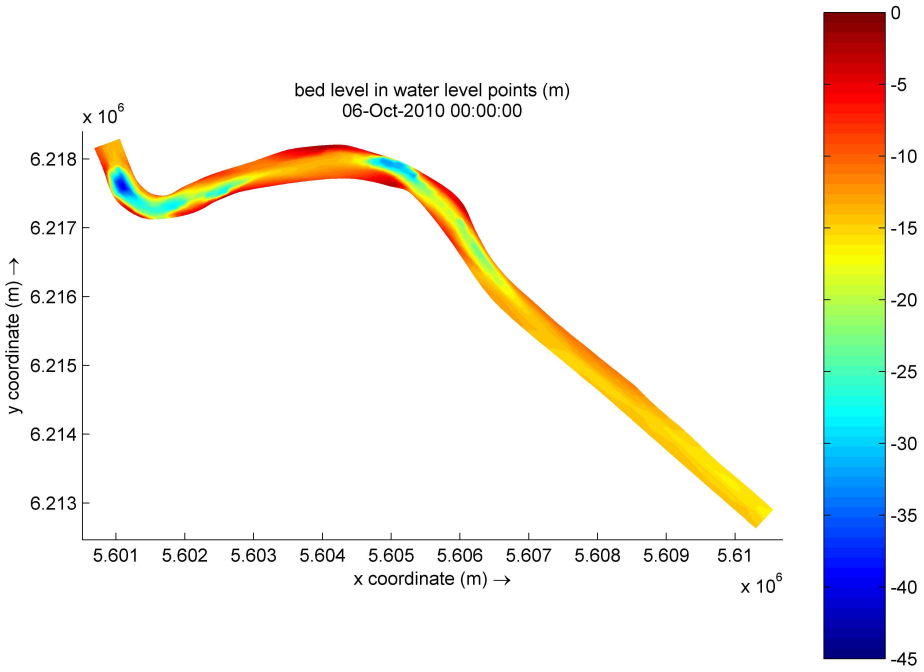


Figure 4-13: Eventual bed level (after simulation)

After a first look at the cumulative erosion/sedimentation plot, a couple sedimentation 'hotspots' can be defined (Figure 4-14); 1. the whole of the first bend and 2. the deep pit in the second bend.
Hotspot 1 lies in the deep inner bend. Two effects probably attribute to this; boundary effects and a deep pit. Due to the proximity to the upstream boundary, it's possible that the sedimentation is caused by boundary effects. If the sediment concentration of the inflowing water is higher than the sediment transport capacity of the river, much of the suspended sediment will deposit close to the upstream boundary.
Due to the sudden increased depth in the first bend, the flow velocity decreases (see paragraph 4.3.2) and the suspended sediment gets the time to settle.

Hotspot 2 is similar to hotspot 1, in the sense that it's also caused by the deep pits in the bend.

Besides the hotspots, a general trend towards sedimentation is observed, except for the shallowest parts in between the bends and after the second bend.

The amount of sedimentation that occurs in the simulation is strongly dependent on the critical shear stresses for sedimentation and erosion, which are not exactly known in this case. This means that the whole erosion/sedimentation pattern that results from the simulation isn't very dependable and should not be used to draw any conclusions about the morphological behaviour of the river.

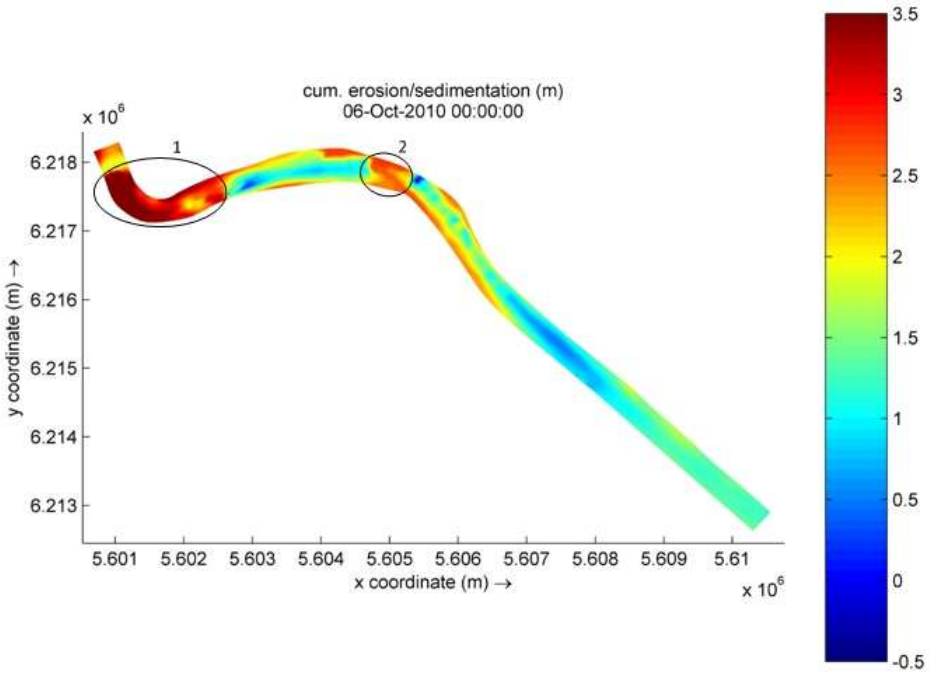


Figure 4-14: Sedimentation 'hotspots' (sedimentation is positive, erosion is negative)

4.4 Conclusion

The results of the simulation give a good picture of the course of the water level and the flow velocity. However, some side notes should be placed.

Firstly, the bathymetric data points used were concentrated in the fairway (in the middle of the river). Only in the bends cross-sectional data was available. That means the bathymetry near the river banks isn't very accurate, which could influence the model results significantly.

Secondly, the influence of the water level setup from the Sudestadas (paragraph 2.3.3) isn't accounted for in the simulation. To correctly represent that setup effect, the water level variations it generates would have to be included in the downstream boundary condition.

Finally, the sedimentation in the model should be regarded in a qualitative way, as said earlier. Besides, if sedimentation would be thoroughly investigated, it's likely that the water level setup from the Sudestadas (paragraph 2.3.3) also needs to be included, because these will probably lead to a temporary decrease in flow velocities and thus contribute to the settling of the sediment.

5 Preventive measures

5.1 Introduction

As is concluded in chapter 3 the mean erosion rate of the outer bend is 1,25 m/year (about 1 m/year caused by shipwaves and 0,25 m/year caused by river flow), at the inner bend the erosion rate is only 0,05 m/year and the averaged erosion rate over the whole stretch is 0,68 m/year. When the current policy is continued it is expected that these erosion rates will be unchanged in the nearby future.
In order to protect the river bank, three types of solutions are possible. First of all, it is possible to take measures in order to damp the incoming waves. A second type of solution is armouring of the river banks in order to cope with the hydraulic loads. Furthermore the generation of waves can be limited or the land use along the river can be relocated.

5.1.1 Damping of incoming waves

River bank vegetation
It is possible to plant certain types of vegetation in the water in front of the river bank. This vegetation includes for example reed and water plants. The wave energy of the incoming wave is partially absorbed by this vegetation which leads to a wave height reduction and a lower load on the bank.

Foreshore
A foreshore is a relatively shallow water section just in front of a river bank. The incoming waves are damped in the shallow water which leads to a lower hydraulic load on the bank.

Longitudinal dams
A longitudinal dam is a detached dam some meters in front of the river bank. Depending on the height of this dam, waves can overtop this dam and the transmission of the waves depends on the properties of the dam (height and permeability). The reduction of the wave height depends on the transmission of the waves through and over the dam. Normally longitudinal dams are constructed of rubble. In some cases a row of piles are used which is less effective but cheaper. Since the implementation of costly solutions is not feasible for this project, the focus in this report is on longitudinal dams composed of piles.

Groyne (transverse dams)
A groyne is a transverse dam which is connected to the river bank at one side and extends into the river. A groyne partially blocks the incoming wave, depending on the distance between the groynes. Furthermore the eroded sediment is trapped between the groynes, which leads to the creation of somewhat of a foreshore that also damps waves. A last (and in a lot of cases the most important) feature of groynes is that it relocates the main flow to the centre of the river which reduces the meander movement of the river and deepens the fairway. Normally groynes are constructed of rubble. In some cases a row of piles are used what is less effective but cheaper. Since the implementation of costly solutions is not feasible for this project the focus in this report is on groynes composed of piles.

Floating wave absorbing constructions
A floating construction with a width greater than the wave length damps part of the wave height. So if these floating constructions are implemented along the river banks, the wave load on the banks will decrease.

5.1.2 Armouring of the river banks

Vegetation on the bank (soft bank armouring)
A number of vegetation species are able to strengthen the soil by their root system, for example trees and vetiver grass.

Revetment (hard bank armouring)
A revetment is a structure that is able to withstand (and absorb or reflect) the incoming waves completely. A revetment can be impermeable for soil particles, but it is generally permeable for water (except asphalt and poured concrete revetments). Another way a revetment prevents soil particles from being washed out is that it reduces the hydraulic load on the soil particles.
A revetment can be constructed with natural stones, rubble, pre-constructed concrete blocks or asphalt. Also, instead of granular filter layers, a geotextile can be used.

Foreshore nourishment
A foreshore is already mentioned as a method to decrease the height of the incoming waves. It can also be a method to compensate the eroded material that is washed away, though it obviously has to be done on a regular basis. The solution is not further investigated due to the expected high costs.

5.1.3 Reduction of wave generation

Limitations to vessel velocities
The height of the generated wave is strongly dependent on the velocities of the passing vessels. A reduction of the velocities of the passing vessels leads to a height reduction of the generated waves.

Limitations to the number of vessels (detour)
When less vessels travel along the river, less waves will be generated and the erosion will be less. These seagoing vessels that are travelling from or to harbours upstream of the bifurcation (where the river splits into Paraná de las Palmas and Paraná Guazú) could take the Martin Garcia Channel on the River Plate and take the Paraná Guazú, as many empty vessels travelling upstream already do. The problem is that the determining depth of the Martin Garcia is smaller (9,75 m) than that of the Emilio Mitre Channel (10,60 m). Besides, the depth in the Paraná Guazú isn't maintained by dredging [Asociación Civil Prácticos del Río Paraná, -]. To implement this solution, huge amounts of dredging are required, and that is not considered realistic due to the high cost.

5.1.4 Relocating of land use

In certain locations it may be possible to relocate the present land use. Protective measures against erosion are generally quite expensive and in certain cases it may be cheaper to relocate the present land use to a not or less attacked area.

5.2 Vegetation

The use of vegetation as bank protection works in two different ways; load reduction and increasing of strength. Firstly, some kinds of vegetation have a dampening effect on the wave height of the waves approaching the river banks. To be effective in dampening the wave height, the vegetation has to occupy a reasonable part of the water column and has to be rigid enough (it has to be able to stand vertical on its own). Secondly, the root system of the vegetation has an armouring effect on the underlying soil.

5.2.1 Load reduction by vegetation

When regarding load reduction, vegetation with long stalks is assumed (like reed and several kinds of grasses). Also, the vegetation is assumed to be emergent from the water (the stalks are longer then the water depth). The load reduction is twofold; both the flow velocity and the wave height are reduced.
The presence of the vegetation results in a larger roughness, and thus in smaller flow velocities.
The vegetation has two different effects that reduce wave height; both the drag caused by the stalks and the movement of the stalks (perpendicular to the direction of wave propagation) cause a decrease in wave height. There have been several attempts at quantifying the transmission of waves through a vegetation field, mostly by defining a transmission coefficient.
For example the formulae found in [Verheij, 1995]:

$$C_T = 1 - p(1 - \exp(-0{,}001 N^{0{,}80} B_{eff}))$$
$$B_{eff} = \frac{B_{veg}}{\cos(\beta)} \qquad (5\text{-}1)$$

In which C_T is the wave height transmission coefficient, p is a season dependent coefficient, N is the number of living stalks per m^2, B_{veg} is the width of the vegetation zone and β is the angle of wave incidence (where 0° is a perpendicular incidence). The factor p is a measure of the seasonal state of the vegetation (worse in winter than in summer) and p = 0,2 for the months July – September, p = 0,8 for October – December, p = 1,0 for January – March and p = 0,6 for April – June (all values are adapted for the seasons on the Southern Hemisphere, the Northern Hemisphere has the same values shifted for six months).
The varying parameter p means that the transmitted wave height also varies throughout the year. The rate of erosion is proportional to the square of the wave height, so the erosion in the winter months is much larger than the erosion in the summer months (Table 5-1).

	p [-]	C_T [-]	Erosion reduction
July - September	0,2	0,9414	11,38%
October – December	0,8	0,7654	41,41%
January – March	1,0	0,7068	50,05%
April – June	0,6	0,8241	32,09%
Yearly average	-	-	33,73%

Table 5-1: Erosion reduction for a reed bed with B_{veg} = 5, N = 100 and θ = 55°

5.2.2 Soil conservation by root systems

Besides the reduction of the load on the river bank, the root systems of vegetation also have an effect on the erosion mechanisms. In appendix B particle entrainment and mass failure of river banks is discussed.

The root systems help in fixing the soil particles and increase the critical shear stress through apparent cohesion. Also, the root systems of vegetation work like a filter and help fixing the soil particles, thus reducing the amount of particles that gets entrained. It is very difficult to quantify this 'armouring' of the soil by root systems [Jaspers Focks, 2006].

Mass failure can occur either by planar failure of rotational failure. Both of these mechanisms have a sliding plane or sliding circle which the roots penetrate. Thereby the resistance against mass failure increases (see Figure 5-1). This means that, to be effective, the roots need to be long enough to penetrate the failure planes and failure circles. If they do, the shear stress in the soil is transferred by skin friction into tensile stress in the roots, adding apparent cohesion. The magnitude of the apparent cohesion is strongly dependent on the number and the diameter of the roots and the magnitude of the soil distortion and is thus difficult to quantify beforehand.

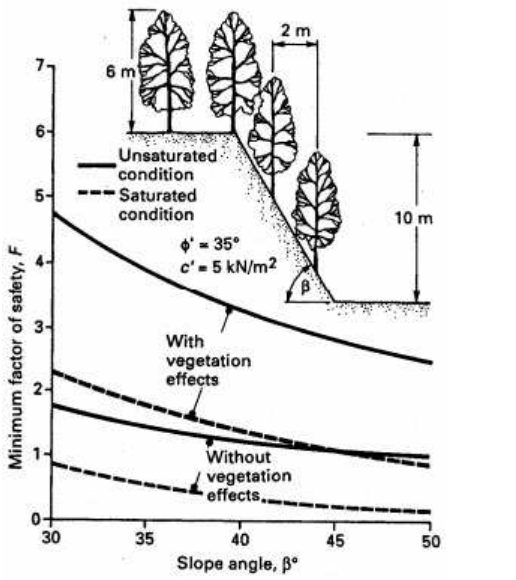


Figure 5-1: Roots as armour against sliding [Schiereck, 2004]

5.2.3 Suitable plants

Below, several plant species known for their use in erosion prevention are discussed in terms of suitability.

5.2.3.1 Phragmites australis – common reed

Common reed (Figure 5-2) is found at soil-water surfaces worldwide. *P. australis* is widespread over the whole world and native to Argentina. It's a perennial plant with a height between 1,5 m and 6 m. The stalks of the reed common to river banks have a diameter of around 10 mm. *P. australis* forms large reed beds with characteristic density of about 100 stalks/m^2 [Kortlever, 1994]. Reed can grow in both fresh and brackish water and both nutrient rich and depleted soil.

P. australis is tolerant of fluctuating water levels and prolonged flooding, though it performs best with water levels between 0,20 m above and 0,20 m below the soil surface. However, it is known to grow in water depths up to 1,80 m. A heightened water level during the growing season impacts the growth of the reed most severe (in the Northern Hemisphere, *P. australis* is known to start growing in February, so growth in the Southern Hemisphere is expected to begin in August). Likely mortality has been observed for water depths of more than 1 m after three years. [Gucker, 2008]

The ability of reed to reduce wave height contributes to the prevention of erosion of the river banks.

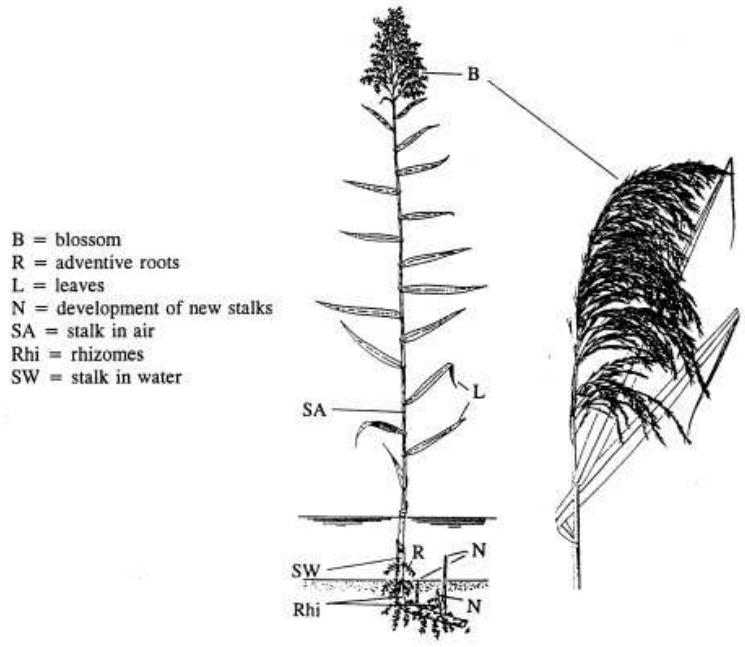


Figure 5-2: Different parts of the P. australis [Kortlever, 1994]

Reed is suited for wave height reduction due to the long stalks and favourable conditions for growth.

5.2.3.2 Spartina alterniflora – smooth cordgrass

Smooth cordgrass (Figure 5-3) is a perennial grass that is often found on intertidal flats and in salt marshes around the world, also in Argentina. It tolerates high salinity values, but high salinity is not a requirement for growth. Cordgrass can reach a height of between 0,30 m and 2,40 m with a stalk diameter of about 10 mm. Densities between 100 and 600 stalks/m^2 have been observed [Augustin et al., 2009].



Figure 5-3: Spartina alterniflora [University of Florida, 1998]

Smooth cordgrass is known for its ability to provide significant erosion protection along coasts due to its ability to reduce the wave height. As said before, salinity isn't a requirement for growth, however several field trials have shown that it's difficult to establish a durable bed of cordgrass in fresh water conditions [USDA/NRCS 2008]. This fact would probably limit its effectiveness when applied to the banks of the Paraná de las Palmas.

5.2.3.3 Chrysopogon zizanioides – vetiver grass

Vetiver grass (Figure 5-4) is a perennial bunch grass originating from India. It reaches heights up to 2 m and has stiff stems. Vetiver grass is characterised by a deep root system that can reach 3 m to 4 m in the first year of growth [Truong et al., 2008a]. The roots don't show a large horizontal spread and generally stay within a 0,60 m radius from the plant. Vetiver is highly resistant to drought, floods and strong variations in temperature (from -15° to 55°). However, the growth rate is highest for a climate with an average temperature between 18°C and 25°C. It's also resistant to various heavy metals and both acidic to alkaline soils [Jaspers Focks, 2006].



Figure 5-4: Vetiver grass [Truong et al., 2008a]

Vetiver grass can be used effectively for slope and bank stabilisation due to its deep root system. When used for river banks, it's often placed in a square grid to both dampen the incoming waves and reduce the flow velocity. However, vetiver grass can only stay submerged for maximum of 3 months without being affected in its growth [Truong et al., 2008b]. This means it's not suited to be planted on the lower river bank that is submerged for most of the year.

Because vegetation can be combined well with other solution an elaboration of this solution can be found in paragraph 5.7.

5.3 Foreshore

A foreshore is a shallow part of a river just in front of a river bank (see Figure 5-5). A foreshore can arise naturally or can be constructed artificially. Whether a foreshore is formed naturally depends on the characteristics of the waterway.
When the wave height of the incoming waves is more than half of the water depth, which is usually the case on a shallow foreshore, the incoming waves will decrease due to breaking [Verheij 2000].

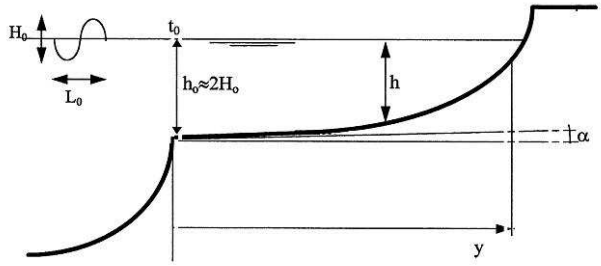


Figure 5-5: Foreshore in a waterway [Verheij,2000]

5.3.1 Wave damping

As stated before the incoming waves will decrease due to breaking. Waves will start to break if:

$$\frac{H_0}{h_0} \approx \gamma_b \qquad (5\text{-}2)$$

The value of γ_b is determined from experimental research. Miche was the first to formulate this parameter and set it at γ_b=0,88. As can be seen in Figure 5-6 the lowest value at which waves start to break is about γ_b=0,5-0,6 and this increases with an increasing Iribarren number [Schiereck, 2004].

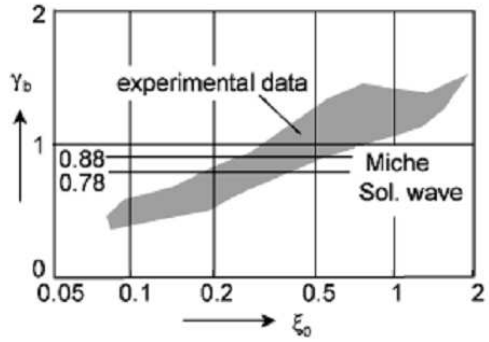


Figure 5-6: Breaker depth as function of ξ [Schiereck, 2004]

Since waves start to break at γ_b=0,5-0,6, waves break on the foreshore which has a depth less than double the wave height. Verheij [2000] gives a relation for the decrease of the incoming wave height due to breaking on a foreshore:

$$H = H_0 e^{-\mu y} \qquad (5\text{-}3)$$

For which H is the wave height at the end of the foreshore, H_0 is the wave height at the beginning of the foreshore, y is the width of the foreshore and μ is a damping term correlated to the foreshore. Verheij [2000] also gives a solution for μ which is:

$$\mu = \frac{tan(\alpha)}{H_0} \qquad (5\text{-}4)$$

With tan(α) the slope of the foreshore and μ between 0,02 and 0,1.

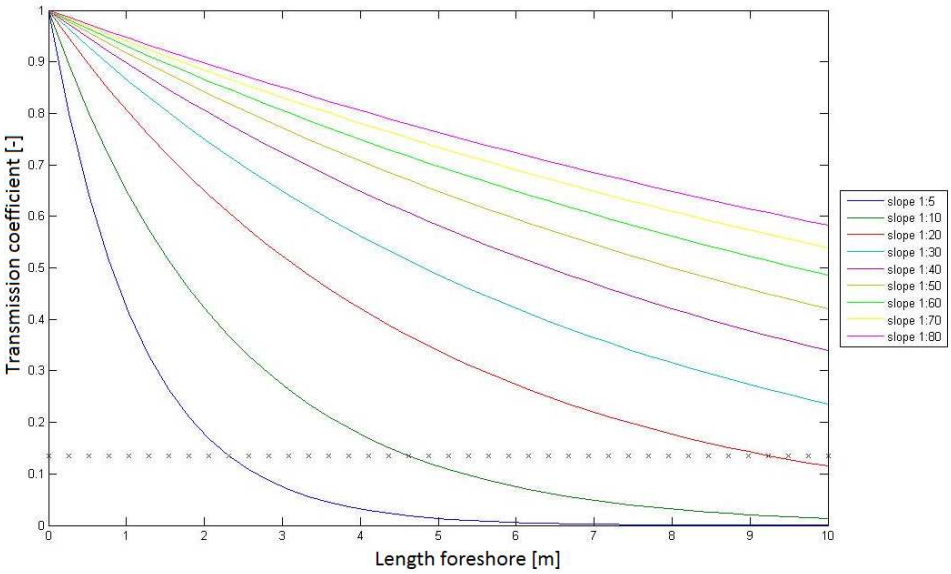


Figure 5-7: Wave transmission as function of the length of the foreshore for different slopes. Expressions are invalid under the horizontal line (Transmission = 0,1353).

Also bottom shear has an effect on the wave height. However as stated in Verheij [2000] the bottom shear of the waves on the foreshore is more than an order smaller than the effect of the wave breaking, it is therefore neglected.

5.3.2 Stability

As stated in the introduction a foreshore can arise naturally or it can be constructed artificially.
Wind waves and ship generated waves will erode only the top part of the bank till a depth of about two times the wave height, the vessel induced return flow will erode the lower part of the bank and the normal river flow will erode the bank at every depth [Verheij 2010]. When wind waves and vessel generated waves are the governing load on the bank a foreshore will arise naturally. When the foreshore is generated naturally and the river characteristics stay the same, the foreshore is stable. However when a foreshore is created artificially it is not certain that the foreshore will remain and some sort of protection may be necessary. This can be for example a hard protection or groynes.
It is advised to check the stability of a foreshore in a modelling program like Delft3D.

5.3.3 Conclusion

As can be seen in Figure 5-7 a long foreshore with a steep slope is very effective. However one has to keep in mind that the waves are breaking at the foreshore, which imposes a big load on the soil particles of the foreshore. This will lead to erosion of the foreshore slope until a gentler slope is formed. Of course one can protect the foreshore with the use of larger sand particles or stones, but this will lead to a revetment-like structure which wasn't the intention.
Also, the stability of the river profile just under the foreshore is not guaranteed for every situation since it's affected by the flow. Once again one can protect this part with heavy stones which again leads to some kind of revetment. Therefore one is advised only to

implement a foreshore when flow velocities are rather low, which is not the case in the Paraná de las Palmas.

5.4 Pile screens, longitudinal dams and groynes

Waves can be reduced by pile screens; the wave is partially reflected and another part is dissipated, so the transmitted wave behind the screen will have less energy and thus a smaller wave height.

$$E = \frac{1}{8}\rho g H^2 = \frac{1}{2}\rho g a^2 \qquad (5\text{-}5)$$

Behind the piles jets will occur, see Figure 5-8. The difference in velocity that occurs behind the piles will induce a turbulent shear stress, which will lead to an energy transfer from the mean motion to turbulent motions. Energy is repeatedly transferred from large turbulent length scales to smaller turbulent length scales (energy cascade) till it reaches the viscous length scale where energy is dissipated.

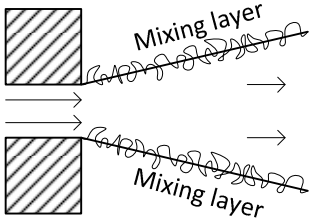


Figure 5-8: Jet behind the piles

The amount of energy that is reflected is expressed in the reflection coefficient (C_R), the amount that is transmitted is expressed in the transmission coefficient (C_T). Both coefficients depend on the space between the piles, the width and shape of the piles, the amount of pile rows, the length, height and period of the wave, the water depth and the angle of incidence.

$$H_T = C_T H_I, \quad H_R = C_R H_I \qquad (5\text{-}6)$$

A lot of information can be found about the subject of wave reduction by pile screens. In this study the focus will be on screens with vertical, squared piles that are higher than the average water depth. When a pile screen is the most promising measure a more thorough study must be performed to compare different pile shapes and different pile screens, such as screens with horizontal slots, screens with vertical slots, screens that are submerged, screens which are not directly attached at the bottom or a combination of the above.
A squared pile shape is expected to give the lowest transmission coefficients [Van der Linden, 1985] so this first approach will give a good approximation of the maximum possible reduction of erosion by a screen consisting of one row of piles.

Hartmann [Schiereck, 2004] found a relation between the transmission coefficient and the relative closure between the piles (W = pile width (b) divided by the centre to centre distance between the piles (e)) for rectangular piles.

$$W = \frac{b}{e}$$
$$C_T = \sqrt{1 - W^2} \qquad (5\text{-}7)$$

The amount of energy and thus the wave height that is transmitted through the pile screen depends only on the relative closure between the piles and not on wave characteristics, but Van der Linden [1985] concluded that the formula of Hartmann is a good approximation for squared piles.

When a wave approaches the pile screen under an angle the incoming (and with the incoming also the transmitted) wave energy per unit length of the pile screen is less than when the same wave approaches perpendicular to the pile screen. Correction factors should thus be applied to the formulae of C_t to account for the angle of incidence. Grüne and Kohlhase [Van der Linden, 1985] gave the following expression:

$$C_T = \frac{1}{2} C_{T0} \left(1 + cos^a \beta\right) \qquad (5\text{-}8)$$

For rectangular pile they found that a =0,5 and $C_{T0} = C_{T,Hartmann}$ resemble the experimental results the best.

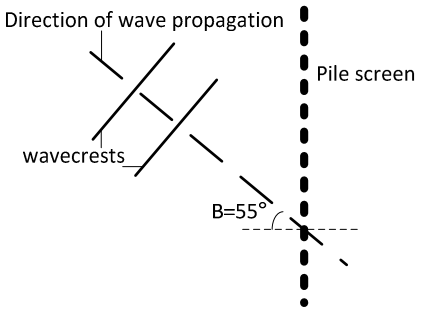


Figure 5-9: A wave approaching the pile screen under an angle β

In Figure 5-10 the formula of Hartmann is plotted for perpendicular incoming waves (red), for waves incoming under an angle of 55°, the situation with a longitudinal dam (blue) and for waves incoming under an angle of 35°, the situation with a groyne (green).

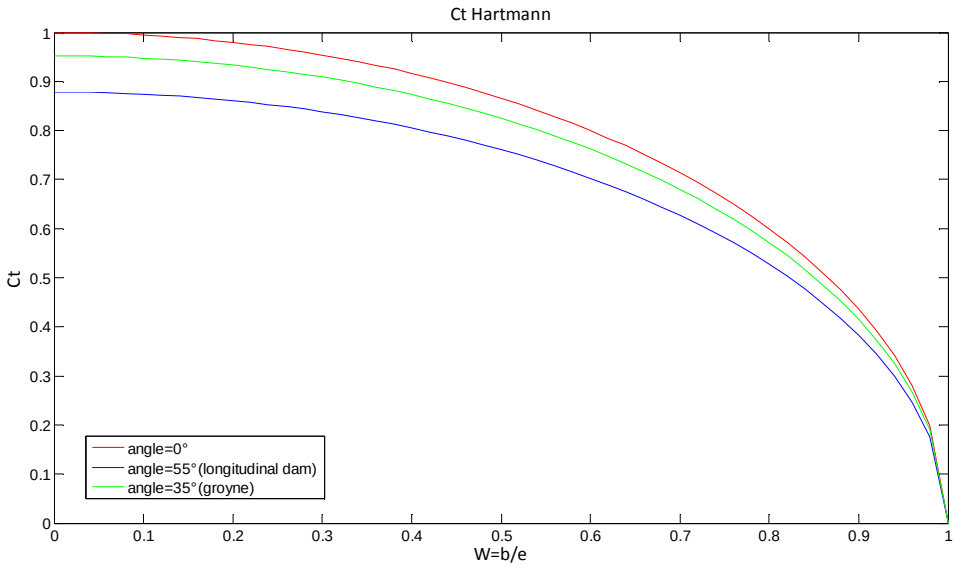


Figure 5-10: C_T from the formulae of Hartmann

As can be concluded from Figure 5-10 a pile screen will only have a significant effect when piles are placed very close together. Placing the piles very close together can have negative effects on environment aspects. Stagnant water behind the pile screen will drastically decrease the water quality. A solution for these environmental negative effects, without increasing the transmission coefficient, will be to place the piles in multiple rows. In this study the effect of multiple rows isn't taken into account.

5.4.1 Pile screen as longitudinal dam

One should bear in mind that a pile screen that functions as longitudinal dam only reduces the secondary waves significantly and not the primary wave [De Roo, 2010]. In the Paraná de las Palmas a pile screen can be effective, because the secondary waves will contribute significantly more to the total bank erosion than the induced shear stress by the return current or the drawdown of the primary wave, see paragraph 3.3.
When using squared piles with of width of 0,25 m that are placed 0,10 m apart the transmission coefficient for a longitudinal dam becomes 0,615. This leads to a reduction of the wave induced erosion rate of 62,2%.

5.4.2 Pile screen as groyne

A groyne will reduce the bank erosion due to ship waves and due to the river flow. Ship waves will always approach the bank under an angle of 35° (see appendix B). When the space between two groynes is less than 10/7 *L (where L is the length of the groyne) the waves will not directly hit the bank. Due to diffraction along the tip of the groyne waves will still approach the bank in the shadow area, but these waves are decreased in amplitude and thus in energy due to the diffraction, see Figure 5-11. Reflection at the groyne will also direct waves to the bank.
When dealing with permeable pile breakwaters the wave pattern and amplitude in the shadow area of the diffraction will be dominated by the transmitted waves through the groyne, because the energy of the diffracted waves will generally be smaller than that of the transmitted (depending of course on the transmission coefficient). The shadow area of the

reflection will contain both the transmitted waves or the unaffected waves and the reflected waves.

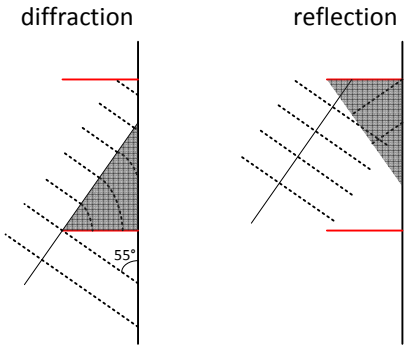


Figure 5-11: Diffraction and reflection in a groyne field (groynes are in red)

At average flow conditions a groyne will decrease the flow velocities near the bank and increase the flow in the main channel. By doing so erosion of the bank is decreased and a large navigation depth can be guaranteed. At extreme high discharges a groyne can have a disadvantageous effect, because it will increase the flow resistance of the channel and thus the water level during high discharges.
The flow field between two emerged impermeable groynes consists of three horizontal gyres [Rupprecht, 2004]. Because the water is shallow the main turbulent processes will be horizontal. In the mixing layer mass and momentum is exchanged from the main motion to the primary eddy, after which it is transferred to the secondary eddy. Near the tip of the groyne the velocity gradient is highest and it decreases in downstream direction with a widening of the mixing layer. The large velocity gradients in the mixing layer will lead to large turbulent intensities which will cause bottom erosion. The scour hole that will exist behind the tip of the groyne can lead to instability of the structure.
The primary eddy has a velocity of approximately 30% of the velocity of the main motion. The secondary eddy is much smaller in size and in velocity than the primary eddy. The dynamic eddy is regularly shed from the tip of the upstream stream groyne and moves downstream till it merges with the primary eddy.

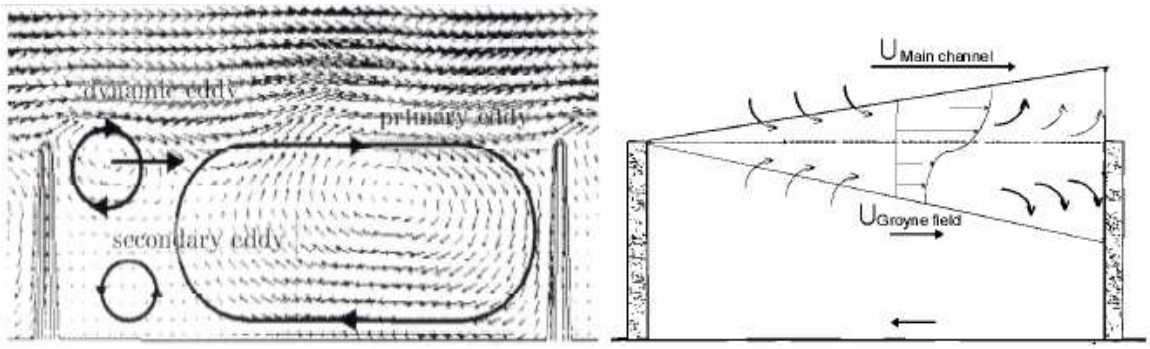


Figure 5-12: Flow patterns and mixing layer in groyne field

Because the flow velocity in the groyne field is much smaller than the flow velocity of the main motion, sedimentation will occur in the groyne field when sediment is transported from the main motion to the primary eddy. This sedimentation will decrease the water

depth in the groyne field which can lead to a reduction of the wave height (see paragraph 5.3).

When dealing with permeable pile groyne the above patterns are less pronounce, depending on the permeability of the groyne. When the permeability is high the flow through the groyne will suppress the circular motions and a unidirectional flow will exist. The velocity gradients between the main flow and the flow in the groyne field and thus the associated mixing layer will still be present, but the dynamic eddy that is shed from the tip of the groyne will not. Due to the permeability of the groyne the dynamic eddy is advected with a velocity that is much bigger than the advection velocity of an impermeable groyne. This larger advection velocity doesn't provide enough time for vorticity to accumulate before detachment [Uijttewaal, 2005].

When a pile groyne is submerged the velocities near the bank will increase significantly [Uijttewaal, 2005]. In an emerged situation a pile groyne will give a rather uniform vertical flow profile, while in a submerged situation the upper part of the water column will have a much bigger flow velocity than the lower part, with a maximum velocity gradient at the level of the groyne crest. This will lead to a momentum exchange over the vertical and thus large turbulent intensities in the upper part of the water column.

Because both the longitudinal dam and the groyne can be combined well with the vegetation, an elaboration of this solution can be found in paragraph 5.7.

5.5 Floating wave absorbing constructions

Floating structures can be used to damp the incoming wave heights. Generally three types of floating structures are known, mainly ordered by the way they reduce the wave energy:

- Dissipating structures (c, d, e and f Figure 5-13):
  Reduction of wave energy is caused by friction or breaking of waves. These structures will transform the wave energy into turbulence. An example of this type of structures is a tyre screen.
- Reflecting structures (a, b and f in Figure 5-13):
  The incoming waves are reflected by the structure, so not the entire wave height can transmit through (under) the structure.
- Absorbing structures (g in Figure 5-13):
  The wave energy will be used to deform an inelastic structure, which causes a loss of wave energy.

It can be said that dissipating and reflecting structures are the better performers in this context, see Figure 5-13.

In Figure 5-13 the value of C_T is visualised for different types of structures [van der Linden, 1985]. The horizontal axis stands for the ratio between the width of the structure and the wave length. The higher this ratio, the lower the transmitted wave height.

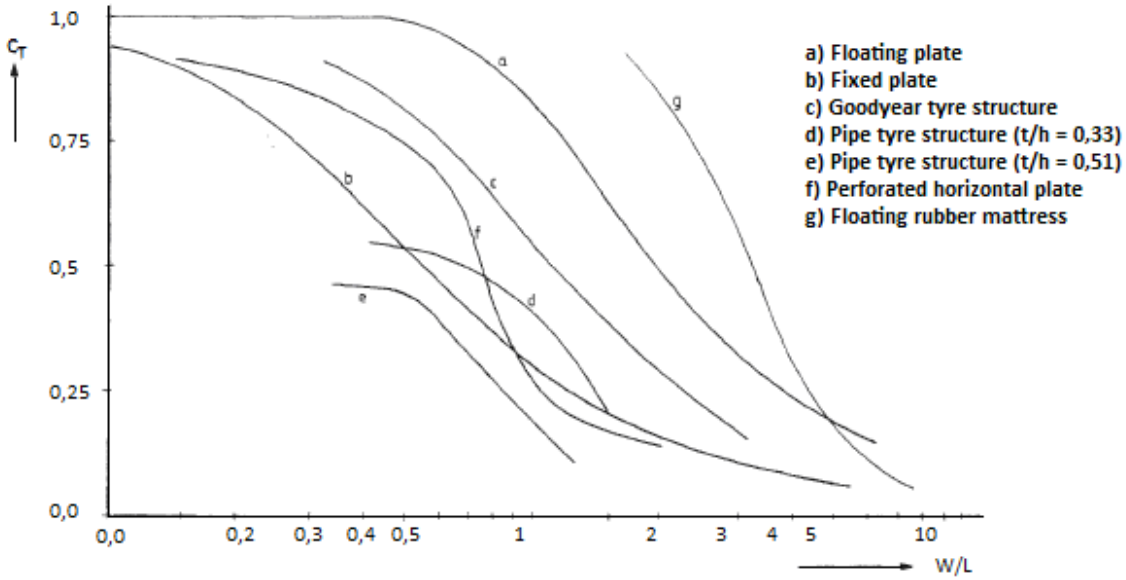


Figure 5-13: C_T for different floating structures

In this report, due to time constraints the focus is only on a floating plate, taking in consideration the water level variations.

It might not be a good idea to use these floating structures along the whole river, because of the major impact on the esthetical value of the river. If the erosion problem is not solved over the whole river stretch this type of structure can be used by private parties, who want to protect their own land. When using a floating plate the structure can be combined with a jetty. The floating plate can therefore be considered as the best solution of this problem. Part of the structure can be designed as a perforated structure.

Dimensioning

The width of the structure depends on the desired amount of wave damping, which is related to the amount of erosion reduction. The erosion rate is proportional to H^2 (see paragraph 3.2.1). Therefore a wave height reduction of for example 50% results in an erosion rate reduction of 75%. Because of the variability of the water levels the best way to anchor the structure is with a pile anchorage, see the next paragraph. The exact curve for the floating plate anchored with piles has to be determined during further investigation, but the curve of the floating plate can be taken as a lower limit.

The damping character of the floating structures, which can be seen in Figure 5-13, is based on wave propagation perpendicular to the length axis of the structure. In the case of ship waves this propagation is not perpendicular but under an angle (35° between bank and wave propagation line). In that case the structure has to absorb less energy per unit length than in case of perpendicular propagation waves.

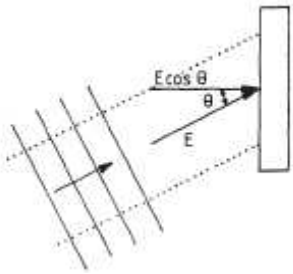


Figure 5-14: Wave attack on an angle

If the situation is schematised as in Figure 5-14, the equivalent energy of the waves can be assumed as follows:

$$E_\theta = \frac{1}{8}\rho g H^2 L_\theta$$
$$L_\theta = L \cdot \cos(\theta) \qquad (5\text{-}9)$$
$$\text{with } \theta = 55^\circ \rightarrow L_\theta = L \cdot \cos(55) = L \cdot 0{,}57$$

The representative wave length for all the ship classes together is 10,2 m, see Table 3-4.
The exerted wave length on the floating structure is than, L_θ = 5,8 m

In Table 5-1 the erosion reduction can be found for several values of W/L (ratio of the width of the structure and the wave length)

W/L	W [m]	C_T	Erosion reduction* [%]
1,3	7,5	0,75	44
2,0	11,6	0,5	75
3,8	22,0	0,25	94

Table 5-2: Erosion reduction for different values of W/L

* This erosion reduction only yields for erosion caused by ship waves. The erosion caused by river flow won't be stopped by this type of structure.

As can be seen in Table 5-2, to reduce the wave height significantly, very wide floating structures will need to be constructed.

Anchorage
Because of the tidal influence at the Paraná de las Palmas and water level variations due to surge at the Rio de la Plata and the discharge variations, the structure must be able to move up and down. The most suited anchorage is a pile anchorage (see Figure 5-15). The floating structure can adjust to the water level by moving up and down along the four piles. The piles are connected to the structure with brackets. The piles will reduce the freedom of movement of the structure. Therefore the given values of Figure 5-13 are very conservative, but the exact curve has to be determined with a model configuration.

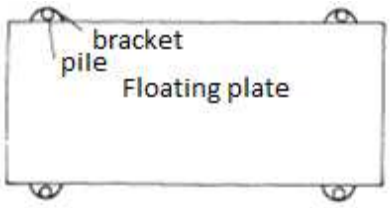


Figure 5-15: Pile anchorage

5.6 Limitations to vessel velocities

By limiting the speed of the vessels the generated waves will be smaller and therefore the exerted loads on the river bank will be less. It is good to keep in mind that the erosion reduction only yields for the erosion caused by ship waves. This type of solution will not influence the erosion caused by the river flow. In this paragraph 'vessel speed' refers to the speed of the vessels relative to the ground. If the speed relative to the water is meant, it will be mentioned explicitly.

5.6.1 Model

The velocity of a ship, relative to the water, has a large influence on the generated wave height, see appendix B.

$$\frac{H}{h} = \zeta \left(\frac{s}{h} \right)^{-\frac{1}{3}} Fr^4 \qquad (5\text{-}10)$$

The formula above shows that H is proportional to v^4 (vessel speed relative to the water), because Fr is proportional to v.

The reduction of the representative wave height is calculated with the measurement track as input. If for example the representative wave height is calculated for a speed limit of 5 m/s only the waves of vessels which were sailing with a higher speed are transformed. Because for a single vessel the parameters h, ζ, s and g are constant, the transformation of the wave height is as follows:

$$H_{new} = \left(\frac{v_{old}}{v_{new}} \right)^4 * H_{old} \qquad (5\text{-}11)$$

With this new wave height the representative wave height is calculated. Also a new ζ-value is calculated in order to estimate the representative wave heights for the inner bank and for a straight river section. To be able to compare this solution with other possible solutions like a pile screen, the effect of the reduction is expressed as:

$$\frac{H_{repr,new}}{H_{repr,old}} \qquad (5\text{-}12)$$

This is in fact the same as a transmission coefficient, although it is physically not correct to call it a transmission coefficient in this case.

5.6.2 Results

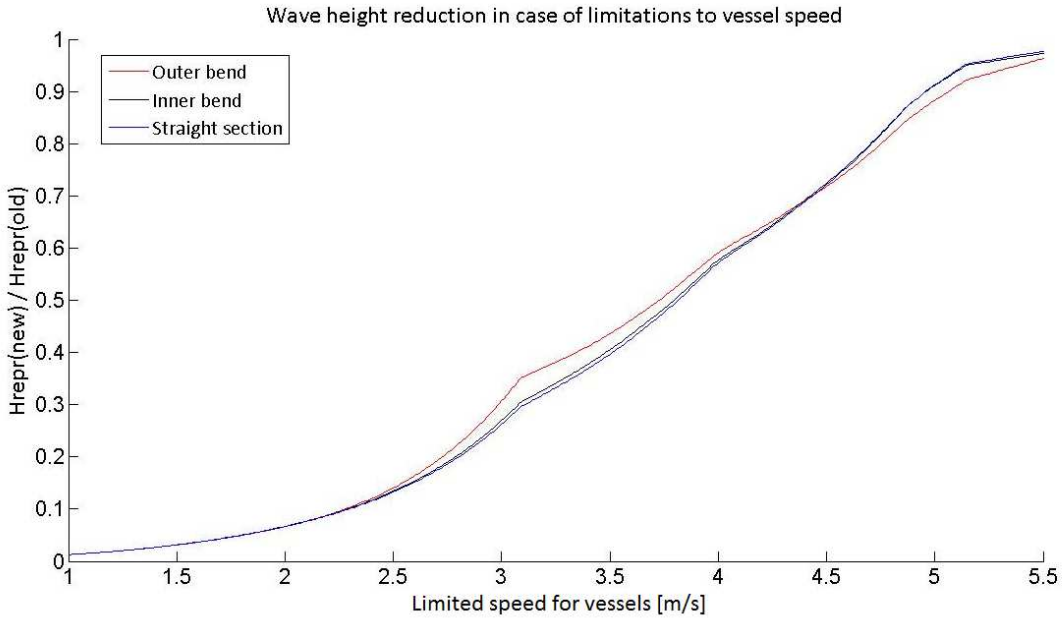


Figure 5-16: Wave height reduction in case of limitations to vessel speed (relative to the ground)

In Figure 5-16 the change of representative wave height is plotted against the speed limit. Distinction is made between the outer bank, the inner bank and a straight river section. The actual speed limit at the Paraná de las Palmas is set to be 10 kts (5,14 m/s). It is assumed that this speed limit is a velocity relative to the ground. During measurement it is observed that a lot of vessels don't obey this limit. Enforcing this speed limit would result in a reduction of the representative wave height in the order of 5% (inner bank and straight section) or 10% (outer bank). A new speed limit of 7,8 kts (4 m/s), for example, would result in a reduction of the representative wave height of 40% and a reduction of the erosion rate of about 64%.

The curves of Figure 5-16 show some discontinuities. These are mainly caused by data points which do not correlate well with the other measured data. The discontinuity at a speed limit of about 3,1 m/s is mainly caused by data of a tanker which sailed quite slow (2,1 m/s relative to the water, 3,1 m/s relative to the ground), but had a relatively large wave height. A better understanding can be created by studying Figure 5-17. The tanker is represented by the dot with a Fr-value of 0,17. This specific large wave height starts to reduce for a speed limitation of 3,1 m/s. For speed limitations above 3,1 m/s the wave height is not reduced and significantly affects the total representative wave height, which result in a discontinuity. Because the tankers sailed 120 m out of the outer bank, the effect on the representative wave height at the outer bank is larger than the effect on the representative wave height at the inner bank. This explains the difference between the curves for the outer bank and the inner bank near a speed limit of 3 m/s.

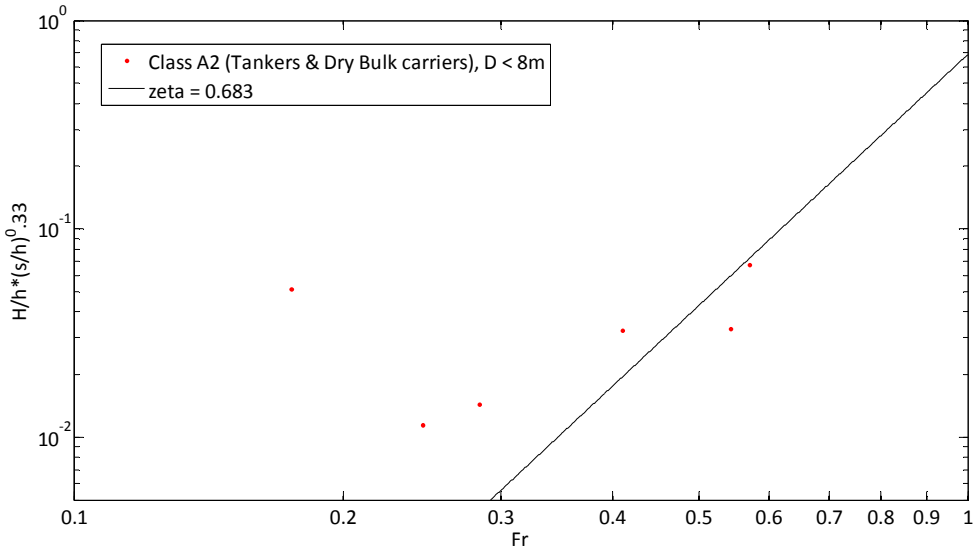


Figure 5-17: Cause of discontinuity in previous plot

It is hard to recommend a specific speed limit, because of the enormous economic consequences of such a measure. Another important thing is that a lot of vessels need to have a certain speed to be able to maneuver in the river. The last problem is stated in paragraph 3.3.3.1. A Ro Ro vessel needs for example 11 knots (5,65 m/s) to maintain ruder control in bad weather conditions (storm perpendicular to the length axis of the vessel). So a low speed limit will frequently be exceeded by a part of the passing vessels. Another problem with this solution is that enforcing the speed limit leads to an intensive monitoring of the vessel speed by, for example, the coast guard.

5.7 Revetment

5.7.1 Observed revetments

During analysis of the erosion problems it is observed that some people have defended their bank with one layer of stone rubble (concrete), which can be seen in Figure 5-18. The mean diameter of this stone rubble is in the order of magnitude of 0,3 m. According to Jansens [2000] it can be said that bigger stones upon a base layer can increase erosion, because of the increased turbulence between the bigger stones.



Figure 5-18: Bank protection with stone rubble

An indication of the type of flow between the stones can be characterised by the Reynolds number:

$$\mathrm{Re} = \frac{U \cdot L}{\nu} \qquad (5\text{-}13)$$

In which U is the velocity inside the pores, L a characteristic length of a pore, in this case assumed to be $0{,}5 \cdot d_{n50}$, and v is the kinematic viscosity (for water $1 \cdot 10^{-6}$ m^2/s). For Re>2000 the flow is assumed to be turbulent. For lower values of Re the flow is laminar. The velocity at the bottom in shallow water can be estimated according to:

$$u = a\sqrt{\frac{g}{h}}\sin(\omega t + kx) \qquad (5\text{-}14)$$

In which a is the amplitude of the wave (H/2) and h is the water depth. To make an assumption of the possible velocities between the stones, a wave height of 0,25 m and a water depth of 0,1 m is taken. The resulting velocity at the bottom is 1,2 m/s. Although this

formula is not totally correct for breaking waves, it gives an indication of the magnitude of the velocity. The velocity will hardly be reduced by the big stones. If a pore velocity (velocity inside the filter) of 0,6 m/s is assumed (50% reduction) the Reynolds number has a value of 90.000, so the flow between the stones is extremely turbulent, which causes extra erosion instead of improving the situation.

In order to create an erosion reducing revetment, one or more filter layers have to be placed between the original cohesive bed and the top stones. In this section the size of the top stones as function of the waves, the slope of the bank, the number of filter layers and the stone sizes of these layers are calculated.

There are two types of filters; a closed granular filter and an open granular filter. The difference between these types of filters is discussed in paragraph 5.7.2.

5.7.2 Closed and open granular filters

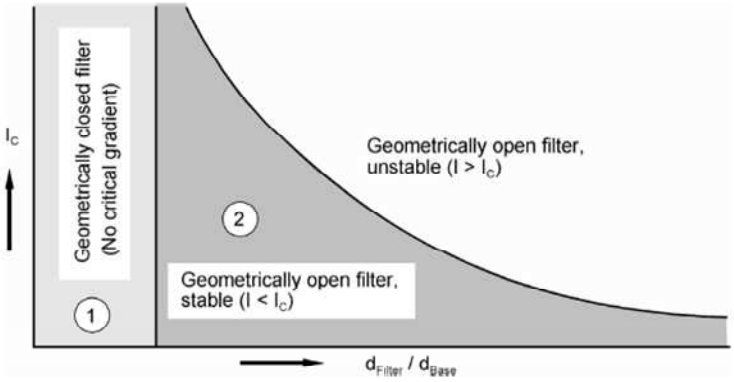


Figure 5-19: Design criteria for granular filters

Figure 5-19 presents the relation between the critical gradient, which is a measure for the loading of the filter layer (ΔH/L), and the relation between the grain sizes in the filter and the base layer. The gradient can be split in a parallel component and a perpendicular component.

Closed filters

In Figure 5-19 it can be seen that in case of a small ratio between d_{filter} and d_{base} no critical gradient exists. For these filters the pores in the filter layer are small enough to prevent grains of the base layer to travel through the filter (Terzaghi filter rules [Schiereck, 2004]). This leads to a conservative design of the filter, because it can stand any hydraulic load. For these filters it is important to check the permeability of the filter, because high pressures can be build-up if the filter is less permeable than the base layer.

Open filters

The grains in an open filter are larger than those in closed filters. The pores in the filter are big enough for the base layer to move in and out. But there will only be erosion if the load is higher than the critical gradient. Because in this design the hydraulic loads are taken into account, it leads to a more economic design. Permeability is generally not a problem because of the open structure of these filters

For the design of a granular filter in this specific situation a closed filter is not convenient, because of the small particle sizes in the base layer (in the order of 20 µm). A closed filter should lead to a structure with a lot of layers, from the small particle size in the base layer to a top layer with a grain size which is stable during wave attack. Furthermore a closed filter approach doesn't take the cohesive properties of the soil into account. Because of these considerations the bottom filter layer (see Figure 5-20) of the filter will be designed with an open filter layer approach (based on the hydraulic load on the soil) and the other layers will be designed as a conventional filter using the filter rules of Terzaghi.

5.7.3 Design of a granular filter

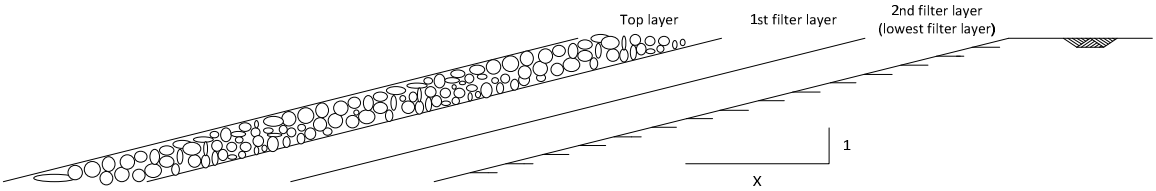


Figure 5-20: Composition of granular revetment

The aim of the granular filter is to reduce the velocities above the base layer. The base layer consists of sandy silt with a critical shear stress of 1,5 Pa. The critical velocity can be calculated with:

$$u_c = \sqrt{\frac{\tau_c}{\rho}\frac{C^2}{g}} \qquad (5\text{-}15)$$

$$u_c = 0{,}56 \text{ m/s}$$

The velocities above the base layer need to be reduced to a value of 0,56 m/s. First it will be calculated what kind of pore velocities can be reached with a filter in which the flow is laminar. If the new pore velocities are small enough, a granular filter can be used as a solution. Then the maximum size of d_{n50} of the lowest filter layer will be computed, for which still laminar flow occurs. After that the top layers of the granular filter will be discussed. In this computation it's assumed that only the bottom filter layer directly upon the base layer will reduce the velocities. Because the top layers always consist of bigger stones, it's assumed that these layers hardly reduce velocities and even introduce some extra turbulence (see paragraph 5.7.1). These assumptions result in a conservative design. For the granular filter two variants are designed:

- A granular filter on a slope of 1:4
- A granular filter on a slope of 1:7,5

This is done because the variant with the slope of 1:4 needs in total three layers, while the variant with a slope of 1:7,5 needs only two layers. The disadvantage of the second variant is that the filter needs more space, because of the milder slope.

5.7.3.1 Maximal grains size of the lowest filter layer

Little is known about the velocity reduction in filter layers. According to Jansens [2000] the mean pore velocities can be estimated with:

$$\frac{1}{\rho_w \cdot g}\frac{\partial p}{\partial x} \cdot T \propto \overline{u}_p \rightarrow i \cdot T \cdot C_i = \overline{u}_p \quad (5\text{-}16)$$

In this formula i is the pressure gradient and T is the wave period. Jansens used a value of C_i of 0,4. The theoretical background of this coefficient is not given. Jansens used the formula to predict the pore velocities in a filter on a horizontal bed. It is therefore questionable whether this formula can be used for pore velocities in a filter on a slope. But it is expected that this formula gives an indication of the pore velocities.

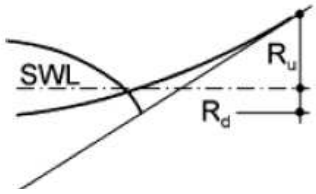


Figure 5-21: Run-up and run-down

The maximum gradient occurs during run down [Zoon, 2010]. An estimate of this gradient can be made with:

$$i = \frac{R_u + R_d}{L_{//}} \quad (5\text{-}17)$$

In which R_u is the wave run up (see Figure 5-21), R_d is the wave run down and $L_{//}$ is the length parallel to the slope. The value of the run up and run down depends on the type of wave breaking. Because the bank should be stable for extreme loading conditions, the significant wave height in this calculation will be 0,34 m. The wave length is 10,8 m and the wave period 2,3s. The type of breaker can be indicated with the Iribarren number:

$$\xi = \frac{\tan(\alpha)}{\sqrt{\frac{H}{L}}} \quad (5\text{-}18)$$

In which ξ represents the ratio of slope steepness and wave steepness. For ξ between 0,5 and 2,5 the behaviour of the waves can be called plunging (breaking waves). The wave impact doesn't cause a big load on the base layer in case of some filter layers, because the impact pressure will be completely reduced by the filter [Zoon, 2010].

The values of R_u, R_d, i and $\bar{u}_p$ can now be calculated:

$$R_u = H \cdot \xi$$
$$R_d = R_u (1 - 0{,}4\xi)$$
$$i = \frac{R_u + R_d}{(R_u + R_d)/\sin(\alpha)} \qquad (5\text{-}19)$$
$$\bar{u}_p = i \cdot T \cdot C_i$$

Although the flow in the filter should be laminar, there are still some velocity fluctuations. The velocity fluctuations can have the same order of magnitude as the average velocity [Zoon, 2010]. So the actual velocity can be taken as two times the mean velocity. The actual velocity above the base layer is lower than the critical velocity of the base layer, so the objective of the design is achieved.

The grain sizes in this filter layer should cause a laminar flow. The maximum value of d_{n50} for laminar flow (Re<2000) is:

$$d_{n50} = 2\frac{\mathrm{Re} \cdot \upsilon}{u_p} \qquad (5\text{-}20)$$

Zoon [2000] has analysed that the reduction of the velocity and velocity fluctuations mainly occurs in the upper part of the filter (<5d_{n50}). Below that part the reduction of the velocity and velocity fluctuations is negligible.

5.7.3.2 Grain size of top layer

The top layer is designed with the Van der Meer formula [Schiereck, 2004]. This formula determines the minimum stone size of stones on a slope under wave attack as function of the significant wave height (H_s), number of waves (N), acceptable damage (S), Iribarren number (ξ) and permeability (P).

$$\frac{H_s}{\Delta d_{n50}} = 6{,}2P^{0.18}\left(\frac{S}{\sqrt{N}}\right)^{0{,}2}\xi^{-0{,}5} \quad \textit{(plunging breakers)}$$
$$\frac{H_s}{\Delta d_{n50}} = 1{,}0P^{-0.13}\left(\frac{S}{\sqrt{N}}\right)^{0{,}2}\xi^{P}\sqrt{\cot\alpha} \quad \textit{(surging breakers)} \qquad (5\text{-}21)$$

The Van der Meer formula consists of a set of two formulae; one for plunging breakers and one for surging breakers. Which formula has to be used is determined by the comparison of the Iribarren number with a transition Iribarren number:

$$\xi_{transition} = \left(6{,}2P^{0{,}31}\sqrt{\tan\alpha}\right)^{\left(\frac{1}{P+0{,}5}\right)} \qquad (5\text{-}22)$$

When the Iribarren number is bigger than the transition Iribarren number the formula for surging breakers has to be used. When the Iribarren number is smaller than the transition Iribarren number the formula for plunging breakers has to be used. In the calculations a value of 0,1 is used for P, which corresponds to a situation “armour + filter on clay or sand” [Schiereck, 2004]. The number of waves is in reality more than 7500 but since according to

Schiereck [2004] an equilibrium is reached for N=7500 this value is used. The value for the threshold of damage is between 2 and 3 and therefore S=2 is used.

5.7.3.3 Grain size of filter layers

The filter layers between the top layer and the layer directly on the bank are determined with the Terzaghi filter rules for closed filters. As stated before, the stability of these filter layers depends on the difference in grain size between the fraction with the smallest grains of the top layer and the grain size of fraction of the biggest grains of the underlying layer. Furthermore, internal stability and permeability have to be assured. The Terzaghi filter rules are adopted from Schiereck [2004] and read:

$$\textit{Stability: } \frac{d_{15F}}{d_{85B}} < 5 \quad \textit{Internal Stability: } \frac{d_{60}}{d_{10}} < 10 \quad \textit{Permeability: } \frac{d_{15F}}{d_{15B}} > 5 \qquad (5\text{-}23)$$

5.7.3.4 Dimensions of top layer and filter layers

The calculation of the dimensions of the top layer and filter layers is done in MATLAB. The results are presented in Table 5-3. As input a stone density of 2400 kg/m^3 is used since people are currently applying concrete rubble. A H_s of 0,34 m is used which is calculated from the measured wave record (appendix C). The wave length of 10,3 m and period of 2,6 s correspond to this wave height. The grading (W_{85}/W_{15}) of all calculated layers is set at 2,7 (smallest value in wide gradation category [Schiereck, 2004]). The sieve curve is linearized between D_{10} and D_{85} in order to calculate D_{10}, D_{15} and D_{85} from D_{50}. Therefore, the measure for internal stability (D_{60}/D_{10}) only depends on the grading and is 1,3355 (stable) for all layers.

	Double layer	Single layer
Slope [-]	1:4	1:7,5
Dn50 Toplayer (Van der Meer formula) [mm]	120,0	88,0
W50 Toplayer {kg}	4,2	1,6
Maximum grain size lowest filter layer [mm]	7,8	12,9
Dn50 1st filter layer [mm]	21,0	13,0
W50 1st filter layer [g]	21,0	4,9
Stability 1st filter layer (D15 toplayer/D85 1st filter layer) [-]	4,2	4,9
Permeability 1st filter layer (D15 toplayer/D15 1st filter layer) [-]	5,8	7,0
Dn50 2nd filter layer [mm]	3,6	-
W50 2nd filter layer [g]	0,11	-
Stability 1st filter layer (D15 toplayer/D85 2nd filter layer) [-]	4,2	-
Permeability 1st filter layer (D15 toplayer/D15 2nd filter layer) [-]	5,8	-

Table 5-3: Results of Revetment calculations with MATLAB

As one can see in Table 5-3, it's possible to construct a revetment with just one filter layer between the original soil and the top layer. However this leads to a very mild slope of at least 1:7,5 (7,6 degrees), which may be impractical. The mild slope also leads to an increase of the amount of stones to be used. Therefore a revetment with two layers on a slope of 1:4 (14 degrees) seems to be the economically preferable option. The minimum thickness of each layer is $2*d_{n50}$, with a minimum of 20 cm [Schiereck, 2004]. This gives for the top layer a thickness of 24cm, and for the second and first filter layer a thickness of 20 cm.

5.7.4 Conclusion revetment

The present hard protections with large stones are insufficient and mostly counterproductive. A filter layer prevents the soil particles from washing out. A stone revetment does have a drawback: it's a good solution for straight sections without meander movement, but in bends where meander movement is present it's less successful. The reason for this is the undermining of the toe of the structure by the meander movement, which leads to instability of the whole structure. In order to prevent this toe erosion, a stone (hard) revetment should be constructed up to sufficient depth, which is more difficult and leads to higher costs.

5.8 Geotextile

To prevent the washing out of particles at the river bank, a geotextile can be used instead of a granular filter. Geotextiles are permeable textiles made from artificial fibres. A geotextile can have (some of) the following functions [Schiereck, 2004]:

- Separation: The geotextile forms a barrier between two layers, to prevent mixing.
- Filtration: The textile prevents loss of soil particles and allows water movement.
- Reinforcement: The geotextile can be used to strengthen the soil, to prevent sliding, for example.
- Fluid transmission: If the permeability of the textile is larger than the surrounding layers, the geotextile can act as a drain.

In order to use the geotextile for the prevention of erosion, the filtration function is the most important.

The permeability of the geotextile should be about 10 times larger than the permeability of the subsoil to prevent pressure build up under the geotextile [GEOfabrics, 2010]. The permeability of silt is in the order of 10^{-7} m/s. The permeability of the geotextile should therefore be 10^{-6} or larger.

To prevent loss of soil material the O_{90} of the geotextile should be smaller than 10 times the d_{n50} of the base layer. This is only valid for cohesive soils, for non-cohesive soils the O_{90} should be smaller than d_{n50}. The d_{n50} of the base layer is in the order of 20 µm. The resulting O_{90} should therefore be smaller than 0,2 mm.

The geotextile should be armoured with stones that can withstand the hydraulic forces of the waves. The size of the d_{n50} of these stones is 0,12 m, as calculated in paragraph 5.7.3. In the design manual of GEOfabrics [2010] the required strength of the geotextile can be calculated according to the weight of the armour units. For armour units with a weight below 100 kg, the weakest geotextile can be used. For armour units with higher weight the

required strength of the geotextile needs to be calculated. The weight of the biggest stones in this design is in the order of 4 kg, which is far below 100 kg. Therefore the strength of the geotextile is not a significant factor in this design.

It is also possible to apply a geotextile with the stone protection directly attached to it. This solution seems very promising but is not further considered due to time constraints.

5.9 Combined solutions

Some of the above mentioned solutions have a degree of synergy, so it's probably a good idea to combine them. These combinations are discussed below.

5.9.1 Longitudinal pile dam with vegetation

Behind a longitudinal pile dam, there is some distance to the river bank. It's possible to add a bed of reed to combine the two wave damping effects. An example of such a setup can in Figure 5-22.

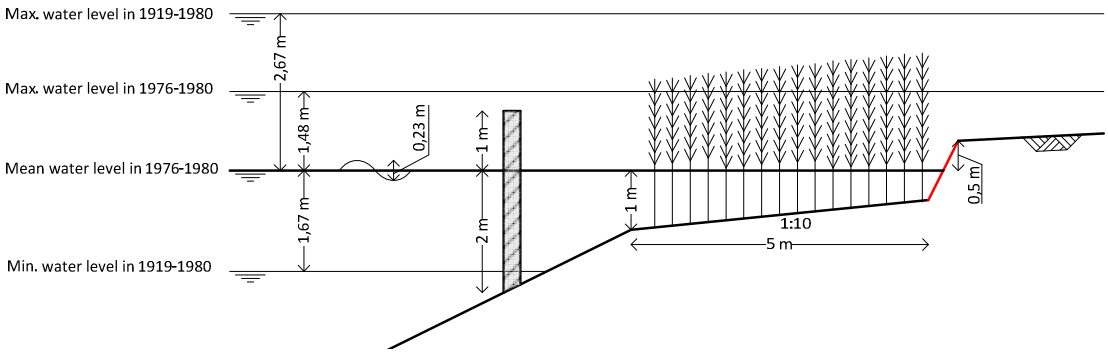


Figure 5-22: Schematic design of a protection consisting of a longitudinal pile dam and a reed bed

In this design, square piles are used with sides of 0,25 m and they are placed 0,10 m apart. This means that the transmission coefficient becomes 0,615 (with β = 55° and W = 0,71; see paragraph 5.4). The strip of reed is 5 m wide. Both measures result in a transmission coefficient and these can be multiplied to calculate the combined result.

Period	$C_{T,reed}$	$C_{T,piles}$	$C_{T,total}$	Erosion reduction
July - September	0,9414	0,615	0,579	66,5%
October – December	0,7654	0,615	0,471	77,8%
January – March	0,7068	0,615	0,435	81,1%
April – June	0,8241	0,615	0,507	74,3%
Yearly average				74,9%

Table 5-4: Combined effect of a longitudinal pile dam and reed in wave induced erosion reduction

Thus yearly the erosion due to wave attack reduces with 74,9%, which is a significantly larger reduction than is obtained with only the strip of reed. At the straight river section the erosion due to ship waves will decrease from 0,84 m/year to 0,21 m/year, when the water level is such that both the reed strip and the piles will reduce the waves.

However, it needs to be said that in the case of very low water, the water level is below the level of the reed bed and then only the longitudinal dam will decrease the wave height (the total transmission coefficient becomes 0,615). In that case the erosion is reduced with only 62,2%. These very low water levels are expected to occur less than once per year, so the extra erosion they cause should be minimal.

Furthermore, for some water levels, the water depth at the reed strip is sufficiently low that it will function like a foreshore, and reduce the wave height even more. This effect is not accounted for in the calculated erosion reduction.

The height of the piles and the level on which the strip of reed is placed, are chosen such that there will be a maximum reduction of bank erosion when the waves attack the most frequently attacked bank level (given in red). When the water level is higher than the piles and the reed the reduction will be drastically less, because the wave energy is concentrated in the upper part of the water column. But these situations don't occur frequently so the bank that is attacked at that level will not have a high erosion rate.

Obviously, this erosion reduction doesn't apply to the erosion caused by the river flow. This is also expected to decrease, because the presence of the reed will reduce the flow velocity close to the river banks. At the outer bank the erosion due to ship waves will reduce from 0,97 m/year to 0,24 m/year and the total erosion rate will decrease from 1,25 m/year to 0,5 m/year, when taking into account a very small decrease of the erosion due to meander movement.

A last comment with respect to the longitudinal dam is that it will be a barrier for the people living along the Paraná de las Palmas River. The river will be less accessible and less visible from the river bank.

5.9.1.1 Probabilistic approach

Because of the uncertainties in calculating the reduction in wave induced erosion, it can be valuable to employ a probabilistic approach. To do this a Monte Carlo simulation is used to generate a large number of realisations of each variable involved in the calculation (much like the probabilistic approach to calculating erosion in paragraph 3.3.3.5). The number of realisations per variable used in this Monte Carlo simulation is 100.000.

The outcome of the simulation (Figure 5-23) is similar to the outcome of the deterministic calculations. The mean of the Monte Carlo simulation is slightly higher at 75,4% (against 74,9% in the deterministic approach).

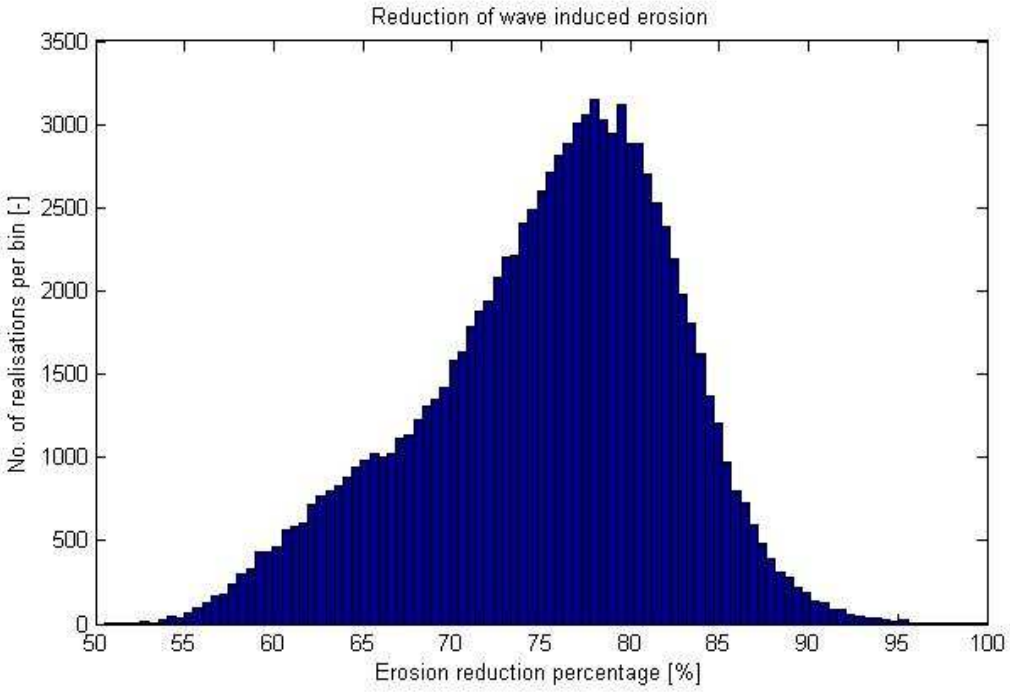


Figure 5-23: Monte Carlo simulation (N = 100.000) of the percentage of reduction of wave induced erosion for a longitudinal dam in combination with a reed bed

One should keep in mind that this probabilistic approach is performed for the erosion due to ship waves only. The percentages give the reduction of the erosion due to ship waves, not the reduction of the total erosion. As is stated above the total reduction of the erosion will be far less than the reduction of the erosion due to ship waves, because longitudinal dams combined with a reed bed will not decrease the erosion due to flow much.

5.9.2 Groynes with vegetation

Another combination is constructing pile groynes with reed beds in between the groynes. The groynes in this example consist of the same piles with the same distance in between as the example with the longitudinal dam. The distance in between the groynes is less than 10/7 times the length of the groyne (see paragraph 5.4.2) at the mean water level, so that all the incoming ship waves are damped by the groynes. When the water is lower than mean water level, especially when it reaches the 1:10 slope of the reed bed, the favourable ratio of 10/7 between the distance between the groynes and the length of the groyne isn't present anymore. In this case the water depth over the reed bed is so low that it will perform as a foreshore. An even lower water level in which the effect of the groyne is negligible occurs with such a low frequency that the design of the groyne is not be adapted to that level.
The groynes in the bends are shorter than the groynes on the straight stretches of river. The reason for this is the (outer) bends are deeper close to the shore, and longer piles are needed in deeper water. Consequently the groynes in the bends are closer together. Additionally, a reed bed is planted on the river banks in between the groynes.

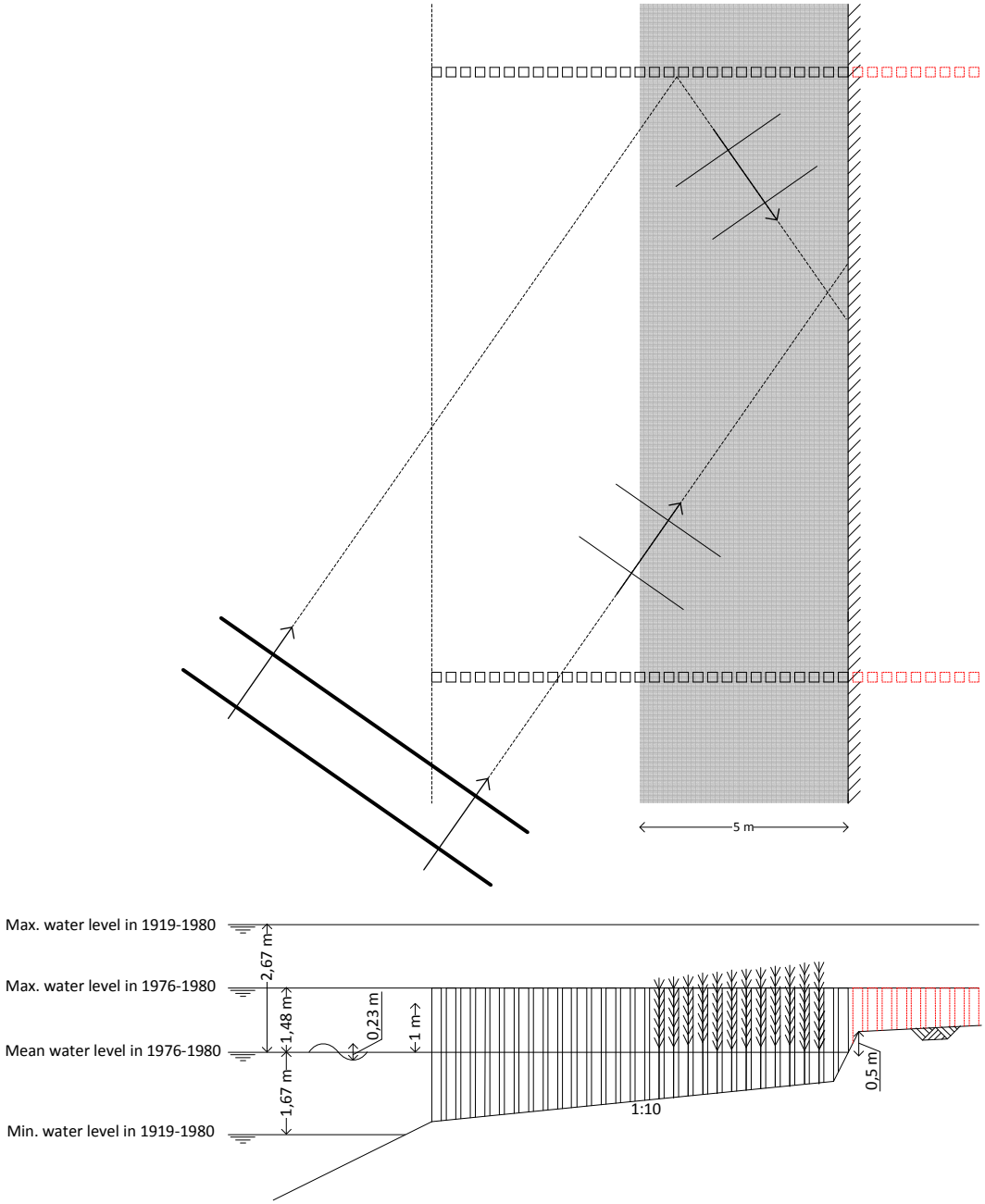


Figure 5-24: Schematic design of a protection consisting of a pile groyne and a reed bed

The space in between the groynes is expected to fill up to some extent with sediment, because of the reduced flow velocity in between the groynes. When that happens, the reed bed is expected to spread even further towards the river.

When using groynes, the ship waves are approaching at an angle of 35° instead of 55°, so the damping effect of the piles is slightly reduced. In this example, the reed bed is still assumed to be 5 m wide.

Period	$C_{T,reed}$	$C_{T,piles}$	$C_{T,total}$	Erosion reduction
July - September	0,9414	0,667	0,628	60,6%
October – December	0,7654	0,667	0,511	73,9%
January – March	0,7068	0,667	0,471	77,8%
April – June	0,8241	0,667	0,550	69,8%
Yearly average				70,5%

Table 5-5: Combined effect of a pile groyne and reed in wave induced erosion reduction

When the ship wave reaches the pile groyne, there is some wave transmission (as calculated above) but also some wave reflection. In this situation therefore, the wave erosion reduction will be somewhat less than 70,5%.
The amount of wave reflection from a pile row can be calculated but the combined load of the reflected and the transmitted waves is hard to calculate within the given time span. With a W of 0,70 the reflection coefficient en thus the reflected waves are much smaller than the transition coefficient and the transmitted waves. A first estimate of the reduced load can thus be made with only the transmitted waves. But one should keep in mind that the combined reflected and transmitted waves will lead to a somewhat higher load on the river bank, especially when the piles are placed very close together and W approaches 1.

The groyne field in combination with the reed bed will also have a significant effect on the flow field in the whole river. When the height of the pile groyne is chosen 1,5 m above mean water level, the chance that the groyne will be submerged is once in 2,5 year. When the groyne is emerged the flow in the groyne field is changed in such a way that it can be expected that the erosion due to river flow will decrease significantly. This is especially important in the bends, because the meander movement of the river will be hindered.
When the groynes are submerged the flow patterns in the groyne field will changes and flow velocities near the bank will increase, this can lead to erosion of the bank. Because the flood plain isn't protected in this schematic design during a flood flow velocities on the flood plain will be higher than in the situation when no groynes are placed. Because of the high resistance, due to a lot of vegetation in the flood plain, the protection on the flood plain (red piles) is considered unnecessary. In further research a balance must be found between the amount of piles and the protection of the flood plain.
When the red piles are placed and a water level above the flood plain is reached the waves are even more reduced, because some part of the waves will encounter two groynes before they reach the bank.

The solution with groynes and a reed bed will reduce the erosion rate due to ship waves somewhat worse than the solution with longitudinal dams, but it will reduce the erosion rate due to river flow significantly better. When the groynes are constructed in such a way that they can prevent all bank erosion due to the meander movement the total erosion is already reduced by 20%. This should be taken into consideration when comparing the reduction of erosion due to ship waves by both alternatives.

5.9.2.1 Probabilistic approach

Just as in paragraph 5.9.1.1, a Monte Carlo simulation is used to model the uncertainties in the input variables. Again, 100.000 realisations are being generated of each variable.

In Figure 5-25 it can be seen that the mean of the probabilistic approach agrees quite well with the deterministic approach; for the Monte Carlo simulation a mean of 71,0% is found compared to the deterministic value of 70,5%. However, again the reflected waves are not taken into account here, so the wave induced erosion reduction is also an overestimated.

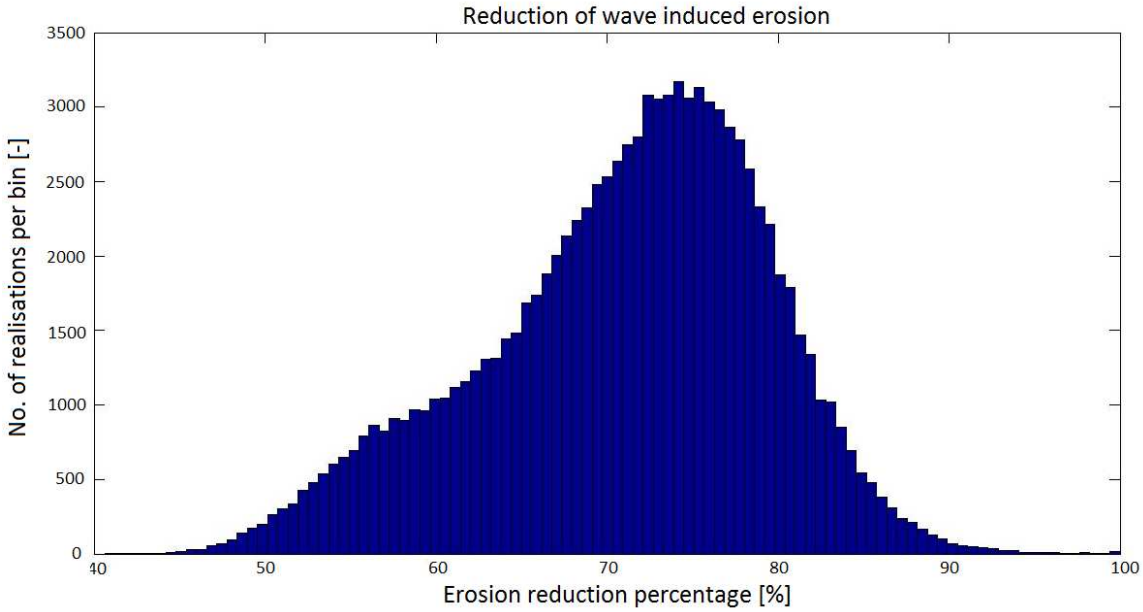


Figure 5-25: Monte Carlo simulation (N = 100.000) of the percentage of reduction of wave induced erosion for a groyne field in combination with a reed bed

One should keep in mind that this probabilistic approach is performed for the erosion due to ship waves only and only the transmitted waves are accounted for, not the reflected waves. The percentages give the reduction of the erosion due to the transmitted ship waves, not the reduction of the total erosion.

5.10 Evaluation

In Table 5-6 the main advantages and disadvantages of all the protective measures are given.

	Advantage	Disadvantage
Foreshore	- Esthetical and recreational value - Creation of a shallow area where waves are small which will increase the ecological value	- The foreshore needs to be wide, especially due to varying water level - The foreshore probably needs to be protected
Floating structure	- Individual solution - Same effectiveness for varying water level - Can be combined with jetty	- Esthetical value - Least effective for higher and longer waves that cause the most erosion
Limitations to vessel speed	- No constructions are needed - Flexible solution	- Hard to maintain/control - Large economic impact
Granular revetment	- Individual solution - Durable solution, especially for straight sections	- Constructability - Designed with open filter rules, which induces uncertainties
Geotextile	- Individual solution - Quality can be guaranteed because product can be tested	- Constructability
Longitudinal dam combined with vegetation	- Vegetation will not only decrease (wave)forces, but also increase the soil strength - Creation of an area where waves are small which will increase the ecological value	- The river will be less accessible and visible - Effectiveness of the vegetation depends on season - When piles are placed too close together stagnant water can decrease the ecological value
Groyne combined with vegetation	- Also a reduction of erosion due to meandering - The flow is concentrated, so future dredging costs will be reduced - Vegetation will not only decrease (wave)forces, but also increase the soil strength - Creation of an area where waves are small which will increase the ecological value	- Extremely changed river landscape - Effectiveness of the vegetation depends on season

Table 5-6: Evaluation of protective measures

5.11 Conclusion of preventive measures

In this chapter, various possible solutions are discussed in paragraph 5.2 and onward, some more promising than others. Firstly, several solutions are not suitable to either effectively mitigate the problem or to be implemented at the Paraná de las Palmas. Regarding the vegetation solutions; the smooth cordgrass probably won't grow very well in the fresh water conditions in the river. Furthermore the vetiver grass doesn't tolerate long periods of being submerged, so it could only be planted on the upper bank, and doesn't provide much protection to the lower part of the bank.

The construction of a foreshore at the river bank is possible, but inconvenient because the width of the foreshore has to be very large to be effective, due to the variation in water levels in the river.

Constructing a hard revetment is also inconvenient, because a gentle slope is needed and causes the requirement for a large amount of stones. The alternative is a steeper slope with two layers, but the extra layer makes it a lot harder to be constructed properly by individuals and still requires a large amount of stones.

The remaining solutions are at least somewhat promising, but some are more suitable being implemented as an integral solution along the whole problem area on Paraná de las Palmas, while others are more suitable being implemented by individuals protecting their own land and property.

The first of the promising integral solutions is the longitudinal pile dam combined with a reed bed. It reduces the wave induced erosion quite effectively, but especially the pile dam forms an obstruction in reaching the river from the river bank. This can be a significant disadvantage for the residents of the houses along the river.

A similar solution is the combination of a field of pile groynes and a reed bed. This in itself is somewhat less effective in reducing the wave induced erosion than the pile dam and reed bed combination. The main reason for this is the fact that a groyne partially reflects the incoming waves, and in turn the reflected wave also attacks the river banks. However, the added advantage of the groyne field is that it drastically reduces the bank erosion due to river flow, and concentrates the river flow in the middle of the river. Besides that, it forms far less of an obstruction for the residents along the river and it forms almost no obstruction to shipping.

A whole other solution is applying a stricter limitation to the maximum vessel velocities. This reduces the problem at its source, so doesn't need implementation of measures along the river banks. Also, it has no negative impact on the residents along the river. However, it is an obstruction to shipping that will have an economic impact due to the increased travelling time along the Paraná de las Palmas. Besides that, the stricter limitations will, of course, have to be enforced (just like the current speed restrictions).
The individual solutions are solutions that are impractical to implement along the whole length of the river. The floating structure, for example, is a solution that is possible for

individuals to construct themselves in front of their land to protect it, while it would be impractical to apply this solution to the whole river.
Another individual solution could be the application of a geotextile, weighed down with stone rubble, although the placement of the geotextile can be quite challenging for individuals.

6 Conclusions and recommendations

6.1 Conclusions

In this section the answers to the research questions, described in chapter 1, will be discussed.

- *What are the contributions of the different erosion agents to the total bank erosion rate?*

The analysis of the satellite pictures of paragraph 3.1.1 shows that the erosion of the river banks of the Paraná de las Palmas River is significant: the average erosion rate is 0,68 m per year (averaged over inner bends, outer bends and straight parts). In the outer bend the satellite images show an erosion rate of 1,25 m/year.
After investigating both erosion due to flooding, meandering movement (increased flow velocity) and ship waves, it can be concluded that flooding doesn't contribute significantly to the observed erosion. Only if the local soil consists of less cohesive layers than the assumed soil structure indicates, flooding could cause erosion.
The erosion rate due to ship waves, which is calculated with a Bank Erosion Model, is 0,9 m per year. The sensitivity of this calculation is investigated with a probabilistic approach (Monte Carlo simulation) and shows that the erosion rate is in the range of 0,2 to 2,5 m/year. However 60% of the possible outcomes are between 0,6 m and 1,2 m erosion per year. Apart from the large uncertainty in the values for C_0 (coefficient to determine c_E, a soil strength parameter of the BEM) and n (number of waves per ship), a significant contribution of the total sensitivity of the erosion rate is caused by the inaccuracy of H (wave height). This sensitivity of the erosion rate with respect to the wave height is caused by the fact that the erosion rate is proportional to H^2 and to a much less extent by the inaccuracy of H itself. The height of the measured ship waves correlates reasonable well with the theory of Schijf.
The meandering movement is also calculated with the BEM. Unfortunately the BEM is very sensitive for some of its input parameters, especially for the critical shear stress of the soil. Because the critical shear stress for cohesive soils is hard to determine, a calculation of the erosion rate due to meandering with the BEM doesn't product reliable results. Therefore the meandering movement is calculated with analysis of satellite imagines and erosion due to ship waves is calculated with the BEM. This leads to a meandering movement of about 0,25 m per year.
From these findings it can be concluded that it's highly probable that the majority of the erosion problems are caused by ship waves.

- *What kind of measures can be taken to decrease the erosion rate?*

The possible measures can be divided into three types: damping of incoming waves, armouring of the river banks or reduction of wave generation. Furthermore a relocation of land use should be considered when the other solutions are not feasible due to economical reasons.

The most promising wave damping solution is a pile screen combined with vegetation. In areas where meandering movement doesn't play a role this pile screen could be executed as a longitudinal dam. In other areas a pile groyne is more suited.
Armouring of a river bank can be done by vegetation or by a revetment. The present armouring measures (rip rap) will increase the turbulence, because the armouring stones are too big, and thus increase the hydraulic load on the bank.
A stricter speed limit for vessels can also reduce the erosion rate. But because of the many political and economic interests it is hard to draw conclusions on the feasibility of this measure.

6.2 Recommendations

- In this report the computation of the slope stability after a flood is based upon an assumed bathymetry near the river bank. The angle of the slope of the bathymetry in front of the river banks influences the strength of the slope. Therefore it is important to obtain the bathymetry of the river near the river bank (the first 10 a 20 m from the river bank). This should be done on several places at the outer bank, inner bank and at straight river sections. If the bathymetry near the inner bend is known accurately, the damping of waves can be calculated according to Figure 3-17. For the Delft3D simulation it is also important to know the bathymetry near the river bank, so the flow velocities near the river bank can be calculated more accurately. These velocities can then be used to quantify the erosion rate due to flow.
- The assumed soil stratigraphy in this report is based upon a Standard Penetration Test, which was done several kilometres from the river. Some more Standard Penetration Tests or Cone Penetration tests should be done near the river banks to get a more accurate idea of the soil stratigraphy and soil properties.
- In order to quantify the erosion, caused by ship waves and river flow, it is important to get a better estimate for the critical shear stress of the soil. This soil parameter can best be obtained with laboratory research.
- The representative wave height is solely based on a measurement record of about two days. One should extend this period to reduce the influence of rare events. During this measurement the wave length and period should be measured with measurement devices instead of visual observations, which seemed to be unreliable. However, the wave height can be estimated quite well with visual observations along a gauge rod, but shouldn't be done near a reflection concrete wall. It is better to place the gauge rod in front of a less reflecting boundary.
- The uncertainty of the BEM results is mainly caused by the uncertainty of the number of waves per ship. During measurements not only the maximum wave should be measured, but also the other, smaller waves. From this secondary wave train record the representative wave height and n (number of representative waves per ship) can be calculated for each ship class.
- To get more reliable results from the Bank Erosion Model it's necessary to validate the model. The erosion rate of a river section, without meandering influences, should ideally be used for the validation process.

- In this report only an initial design of the preventive measures is given. During further research a more detailed design and evaluation of the different possible

measures is necessary. Giving a full set of recommendations for this first stage of design seems a bit out of place; it seems better to give an idea of the further design phases:

- A second design, based on the more detailed bathymetry. Especially for the constructability, the bathymetry is of great influence.
- Evaluation of the feasibility of the different measures, not only based on effectiveness, but also on economic, ethical, environmental and constructability aspects.
- A detailed design, including technical drawings, quantities of needed materials/vegetation/etc. and construction method of the most promising measure.

Literature list

Asociación Civil Prácticos del Río Paraná, (-). *Guidelines towards passage planning: Acces to/from Río de la Plata – Río Paraná.* "Passage Plan" IMO-Resolutions A.485(XII) and A.893(21)

Augustin, L.N., et al. (2009). Laboratory and numerical studies of wave damping by emergent and near-emergent wetland vegetation. *Coastal Engineering, 56, 332-340*

Deltares (2009a). *Delft3D-FLOW: Simulation of multi-dimensional hydrodynamic flows and transport phenomena, including sediments, User Manual.* Version 3.14, revision 7864

Deltares (2009b). *Delft3D-RGFGRID: Generation and manipulation of curvilinear grids for Delft3D-FLOW and Delft3D-WAVE, User Manual.* Version 4.00, revision 7821

Deltares (2009c). *Delft3D-QUICKIN: Generation and manipulation of grid-related parameters such as bathymetry, initial conditions and roughness, User Manual.* Version 4.00, revision 7567

Depetris. P.J. (2007). The Parana river under extreme flooding: a hydrological and hydro-geochemical insight. *Interciencia*. 32 N^0 10. 656-662

D'Onofrio. E.E. et al. (1997). Return periods of extreme water levels estimated for some vulnerable areas of Buenos Aires. *Continental Shelf Research*. 19. 1681-1693

Duclos, G. et al. (2004).Wave propagation through arrays of unevenly spaced vertical piles. *Ocean Engineering*, 31, 1655-1668

FUNDAR (2010), *Technical report. Report of final information delivered by FUNDAR to the project group (15 November 2010).*

GEOfabrics (2010). *Designing rock and rip-rap structures with geotextiles.* Leeds

Groenveld, R. (2008). "Inland Waterways". Lecture notes CT4330, Delft University of Technology

Gucker, C.L. (2008). *Phragmites australis. In: Fire Effects Information System*. http://www.fs.fed.us/database/feis/
Consulted on 18 October 2010

Halcrow (2008). Termoeléctrica Manuel Belgrano S.A. Estudio de Obra de toma de planta TMB

Hydrovía (consession company of Jan de Nul), 2010a. Bathymetry data of years 2008, 2009 and 2010

Hydrovía (consession company of Jan de Nul), 2010b. personal conversation with Tom Ceupens, Project Manager Argentina. 12-10-2010

INTA (2006). *Estudio de suelos en la reserva de biosfera delta del Paraná.* San Fernando.

Irondo, M. (2004). The littoral complex at Paraná mouth. *Quaternary International,* volume 114, issue 1, 143-154.

Jansen, P.PH., ed (1978). "Principles of River Engineering", Delftse Uitgevers Maatschappij

Jansens, R.J. (2000). *Het doordringen van golven in een filterlaag. MSc thesis,* Delft University of Technology

Jaspers Focks, D.J. (2006). Vetiver grass as bank protection against vessel-induced loads. MSc. Thesis, Delft University of Technology

Kim, Y.C. (2010). *Handbook of Coastal and Ocean Engineering*. 2010 edition. World Scientific Publishing Co., Singapore

Kortlever, W. (1994). *Wave Attenuation by Using Reed for Bank Protection.* Delft University of Technology. Report No. 1-94

Lievens, A. (1997). "The River Plate Experience; Maintenance Dredging by Means of Privatisation". Terra et aqua (sep-1997-68)

Ligteringen, H. "Ports and Terminals". Lecture notes CT 4330, Delft University of Technology

Van der Linden, M. (1985). *Golfdempende constructies*. Delft University Press

Longuet-Higgins, M.S., Steward, R.W. (1964). Radiation stresses in water waves; a physical discussion, with applications. *Deep-Sea,* 11, 529-562

Meccia, V.L. et al. (2009). Sea surface height variability in the Rio de la Plata estuary from synoptic to inter-annual scales: results of numerical simulations. *Estuarine*, *Coastal and Shelf Science*, 85, 327-343

Mosselman. E. (1989). Communications on hydraulic and geotechnical engineering, Theoretical investigation on discharge-induces river-bank erosion. Report No. 89-3

Mosselman. E . (1996). Formula of BEM, internal memo Waterloopkundig Laboratorium / Delft Hydraulics betreft Q2185.11, MER Zandmaas, aanpak oevererosie, versie 2, 31 january 1996

Pacific Marine Environmental Laboratory. http://www.pmel.noaa.gov/tao/elnino/nino-home.html. Consulted on 1 September 2010.

Parchure. T.M., Mc Anally W.H. jr, Teeter. A.M. (2001). Desktop Method For Estimating Vessel-Induced Sediment Suspension. *Journal of Hydraulic Engineering,* July 2001

Peck, P.B., Hanson, W.E., Thornburn, T.H. (1974). *Foundation Engineering,* second edition, John Wiley and Sons, New York.

Piedra-Cueva, I. et al. (2005). Residual currents and corridor of flow in the Rio de la Plata. *Applied Mathematical Modelling*, 31, 564-577

Piedra-Cueva, I. et al. Finite element Modelling of the Rio de la Plata. *International Conference on Estuaries and Coasts*, November 9-11, 2003, Hangzhou, China

Rinaldi, V.A., Abril, E.G., Glariá, J.J.(-) *Fundamental geotechnical aspects of the Paraná Delta river and Rio de la Plata estuary formations.*

De Roo, S. et al. (2004). Response of technical-biological bank protection to ship-generated wave actions- first results. *Fluvial Hydraulics*, 5th International conference

Rupprecht, R. (2004). *Modelling of the morphological interaction between a river and its groyne fields*. MSc. Thesis, Delft University of Technology

RWS/DHL (1988). Aantasting van Dwarsprofielen in Vaarwegen Report M1115 XIX

Sarubbi, A., Pittau, M.G., Menéndez. (2004). *Delta del Paraná: balance de sedimentos. Proyeto simulación y predicción del crecimiento del frente del delta del río Paraná. Instituo Nacional del Agua.*

Simon. A. et al.(1991). Bank and near-bank processes in an incised channel. *Geomorphology*. 35. 193-217

Simionato, C.G. et al. (2009). On the path of plumes of the Rio de la Plata estuary main tributaties and their mixing scales. *Geodata*, 34, 87-116

Sivrikaya, O, Toğrol, E. (2006). Determination of undrained strength of fine-grained soil by means of SPT and its application in Turkey. *Engineering Geology,* volume 86, 52-69.

Schiereck, G.J. (2004). *Introduction to bed, bank and shorelineprotection*. Delft University Press,

Stewart, R.H. (2003). *Introduction to Physical Oceanography*. September 2008 edition. Texas A&M University

Thorne. C.R. (1991). Bank erosion and meander migration of the red and Mississippi rivers, USA. *Hydrology for the Water Management of Large River Basins*. 201.

Truong, P., Tan Van, T. & Pinners, E. (2008a). *Vetiver system applications: technical reference manual.* 2nd ed. The Vetiver Network International

Truong, P., Tan Van, T. & Pinners, E. (2008b). *The Vetiver system for slope stabilization.* 1st ed. The Vetiver Network International

Uijttewaal, W.S.J. (2005). Effects of Groyne Layout on the Flow in Groyne Fields: Laboratory Experiments. *Journal of Hydraulic Engineering*, 131, No 9, 782-791

United States Department of Agriculture/Natural Resources Conservation Service (2008). *Plant fact sheet: Smooth Cordgrass.* USDA NRCS Plant Materials Program

Verheij, H.J. (1995). *Golfdemping door riet.* Report Q2037, WL

Verheij, H.J. (2000). *Samenwerkingsproject Modelering Afslagoevers – voortgangs-rapportage 1999.* Report Q2529, WL / Delft Hydraulics

Verheij, H.J. (2001). *Calibratie van een oeverafslagmodel voor de Zandmaas.* Report Q3060, WL / Delft Hydraulics

Verheij H.J. (2010), personal note via email 07-10-2010

Verruijt, A. (2005). *Grondmechanica*. 7th print. Delft University Press.

De Vriend, H.J. et al. (2010*). Lecture notes CT4345 River Engineering*

Vrijling, J.K. et al. (2006*). Lecture notes CT4130 Probability in Civil Engineering*

Zoon, A. (2010). *Cobble sea defence: Hydraulic interface stability of sand underlying a single filter layer.* MSc thesis, Delft University of Technology

Appendices

A. Pictures of the erosion
B. Erosion theory
C. Measurements of ship waves
D. Analysis of ship waves and movement
E. Sensitivity analysis BEM
F. Delft3D input

A. Pictures of the erosion

To get an impression of the erosion problems at the Paraná de las Palmas, some images of the river banks are added to the report. The images show clearly the straight shape of the river banks and some local protection methods. They also show that trees are not able to prevent the bank erosion.



Figure A-1: Bank erosion 1



Figure A-2: Bank erosion 2



Figure A-3: Bank erosion 3

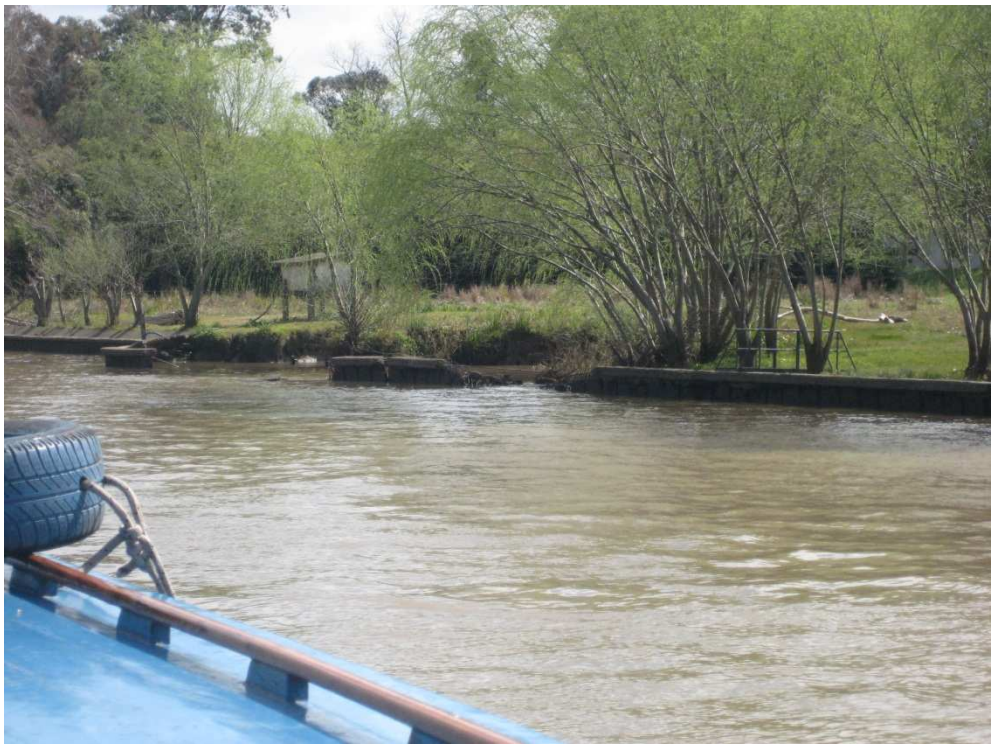


Figure A-4: Failed quay wall



Figure A-5: Bank erosion 4



Figure A-6: Improvised revetment 2

B. Erosion Theory

B.1 Erosion processes

Erosion of non-cohesive soil

Non-cohesive soil is usually detached and entrained grain by grain. The grain starts to move when the forces exerted by the flow or waves exceed the friction forces. A flow will exert destabilizing forces: a drag force, a lift force and a shear force on the grain. These forces can be compensated by friction and by the submerged weight of the particle.

Shields gives a formula on grain stability on a horizontal bed in a uniform flow that uses a relation between the dimensionless shear stress (including lift, drag and shear forces) and the particle Reynolds number, Re_*, (a measure of whether the particle protrudes into the turbulent boundary layer or stays within the viscous sub layer) [Schiereck, 2004].

$$\Psi_c = \frac{\tau_c}{(\rho_s - \rho_w)gd} = \frac{u_{*c}^2}{\Delta g d} = f(Re_*) = f\left(\frac{u_{*c} d}{\upsilon}\right) \qquad \text{(B-1)}$$

In which Ψ_c is a mobility parameter, τ_c is the critical shear stress, ρ_s is the soil density, ρ_w is the water density, u_{*c} is the crtical shear stress velocity, Δ is the specific density, d is the particle diameter and ν is the kinematic viscosity.

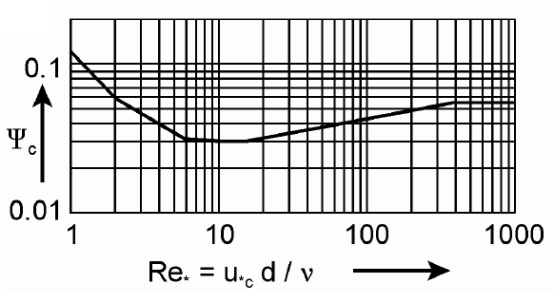


Figure B-1: Shields diagram

In a situation without uniform flow or on a slope several correction factors should be used.

$$d = \frac{K_v^2 \overline{u_c}^2}{K_s \Psi_c \Delta C^2} \qquad \text{(B-2)}$$

K_s, slope factor, indicating a strength reduction, $K_s < 1$.
K_v, velocity/turbulence factor, indicating a load deviating from uniform flow.

In which C is the Chézy coefficient.

When the grain is placed on a slope, the down slope component of the submerged weight will decrease the stability of the grain and the component normal to the slope will increase it stability.

Acceleration causes a decrease of the boundary layer thickness and an increase of shear stress.
The same phenomenon happens in waves. In waves the motion changes sign every half period, which limits the growth of the boundary layer; every half period the boundary layer has to start from scratch. This small boundary layer is responsible for high shear stresses under short waves.

The shear stresses in uniform flow and under waves are given by:

$$For\ turbulent\ flow: \tau = c_f \rho u^2 \quad \text{(B-3)}$$

$$In\ uniform\ flow: \tau_b = c_f \rho \overset{=2}{u} = \rho u_*^2 \quad \text{(B-4)}$$

$$In\ non\text{-}breaking\ waves: \hat{\tau}_w = \frac{1}{2} c_f \rho \hat{u}_b^2, with\ \hat{u}_b = \omega a_b = \frac{\omega a}{sinhkh} \quad \text{(B-5)}$$

In most situations both waves and currents will be present. When waves are dominant the shear stress caused by the current can be neglected. When currents are dominant the velocity vectors of waves and currents should be added, not the shear stresses. From this resulting velocity the total shear stress can be calculated. This resulting shear stress is maximal when the direction of the waves is parallel to that of the current and minimum when the direction of the waves is perpendicular to that of the current. When averaged over a wave cycle however the resulting shear stress becomes independent of the difference of both directions.

Erosion of cohesive soil

The erosion process of cohesive soils can be divided in particle entrainment (surface erosion, fluvial erosion) which is determined by erosion strength, mass erosion under gravity which is determined by the soil's undrained shear strength (yield strength) and sub aerial preparation [Erosion and Sedimentation Manual, 2006].
The destabilizing forces are the same as for the non-cohesive soil, but the stabilizing forces are mainly due to the cohesive properties of the soil. These cohesive properties can be due to real cohesion, when silt and clay fractions are present in the soil, but they can also be due to apparent cohesion. This apparent cohesion exists due to capillary suction (matric suction, negative pore water pressure) in an unsaturated zone or due to the presence of vegetation roots which bind the soil [Thorne, 1991].
The erosion process for cohesive soil is not as well understood as it is for non-cohesive soil, because it is influenced by a lot of different (soil-)properties, such as: bank material weight and texture, shear strength and cohesive strength, physio-chemical properties, bank height and cross-sectional shape, groundwater level and permeability, stratigraphy, tension cracks, vegetation and constructions [Mosselman, 1989] and [Parchure, 2001].

- Particle entrainment

The balance between the shear stress exerted by the flow and the critical shear stress of the cohesive soil, determines whether the particles can be eroded by entrainment, as is also the case with non-cohesive soils. The ability of a cohesive soil to resist particle erosion is known as erosion strength. Cohesive soil is usually more resistant for entrainment than non-

cohesive soil, because of the cohesive forces that exist due to electro-chemical interactions between particles in cohesive soil.

- Mass failure

Mass failure occurs when the driving forces exceed the stabilizing forces and is determined by the undrained shear strength.
Mass failure can be triggered in several ways: by the removal of particles near the toe which leads to over steepening of the bank, the development of tension cracks and their filling with water and the occurrence of high pore water pressures or decrease of matric suction.
A mass failure can also be triggered by a rapid drawdown after a flood, because the change from submerged to saturated conditions approximately doubles the bulk unit weight of the bank material, which increases the destabilizing forces. Even without the absence of high pore water pressure (in permeable riverbanks) this phenomenon occurs, but in undrained banks the probability of a mass failure due to a rapid drawdown is much greater.
The structure of the soil is an important property for the occurrence of high pore water pressures. This will be discussed in greater detail in the paragraph about erosion of stratified soil.

Mass failure can be divided in a planar-type failure and rotational slip [Simon, 1999]. A planar-type failure occurs generally on unstable banks that are steeper than 60 degrees. A crack occurs as the result of a tensile stress, which separates a potential failure block from the intact bank. During failure a slab or block of soil topples forward into the river.
The formulas to calculate if a planar failure occurs are given below.

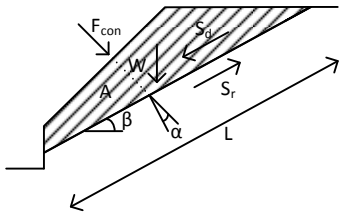


Figure B-2: Schematisation planar failure

$$F_s = \frac{S_r}{S_d}, \qquad \begin{cases} F_s > 1 \rightarrow \textit{stable plane} \\ F_s < 1 \rightarrow \textit{unstable plane} \end{cases}$$
$$S_r = c' + (\sigma - \mu_a)\tan\varphi' + (\mu_a - \mu_w)\tan\varphi^b = c_a + (\sigma - \mu_a)\tan\varphi' \qquad \text{(B-6)}$$
$$S_d = W\sin\beta - F_{con}\sin\alpha$$
$$\sigma = W\cos\beta + F_{con}\cos\alpha$$
$$W = A\gamma / L$$

In which F_s is a safety factor. S_r is the shear strength, determined by the effective cohesion (c'), the effective stress on failure plane at failure (σ-μ_a), the effective friction angle (ϕ'), the matric suction (μ_a-μ_w,): the difference in air pressure and water pressure in the pores and the angle (ϕ_b), that indicates an increase of shear strength due to an increase in matric suction. S_d is the driving force, determined by the gravitation force and the confining pressure of the water.

A rotational slip occurs generally on high banks with slopes less than 60 degrees and slides along a curved surface, passing close to the toe. The soil above the slip surface is divided into vertical slices and a momentum balance along the midpoint of the circle determines whether the bank fails along that slip surface. According to the method of Bishop [Verruijt, 2005] the following equation holds for the failure factor.

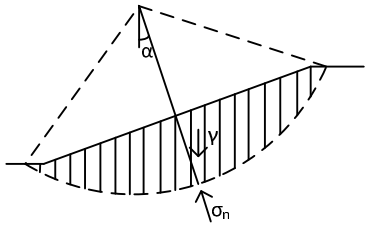


Figure B-3: Schematisation rotational failure

$$F_s = \frac{\sum \frac{c + (\gamma h - u)\tan\varphi}{\cos\alpha\left(1 + \tan\alpha\tan\varphi / F_s\right)}}{\sum \gamma h \sin\alpha} \qquad \text{(B-7)}$$

In which F_s is the safety factor, c is the cohesion, γ is the specific weight, h is the height of the slice, u is the water pressure and ϕ is the angle of repose.

- Subaerial preparation

Subaerial processes like wind, raindrop impact and frost heave are not considered in this study, because of their relatively small contribution to the total erosion.

Erosion of stratified soil

The soil in riverbanks usually isn't totally cohesive or non-cohesive. The riverbank is divided into several horizontal layers that all have different cohesive properties and a different permeability. This structure can lead to other failure mechanisms than discussed in the above paragraphs.
A layer with a low permeability will lead to a poor vertical drainage. Due to this poor vertical drainage other layers that are more permeable will act as horizontal drainage tubes when water can reach this layer, which will result in piping. Sand and silt particles will be washed out of this permeable layer which will not only lead to a decrease of stability of the layer itself, but it will also threaten the stability of the above lying layers.
Furthermore some layers will be less resistant to hydraulic forcing (flow and waves) than other layers. Especially when dealing with water level variations a deeper less resistant layer can fail which can also threaten the more resistant upper layer.

B.2 Main erosion agents, theory

Floods

Floods can lead to erosion of the bank, especially when there is a rapid drawdown after the highest water level is reached, as is described appendix B.1. The most important erosion

process in case of a rapid drawdown is mass failure. The local layering of the soil will induce several other failure mechanisms. Because local information about the soil structure is lacking these failure mechanisms will not be discussed here, even though they may contributed significantly to the erosion due to flooding. Erosion at the upper layer of the bank due to the increased water level and the corresponding flow over the bank can lead to surface erosion and thus a weakening of the bank. The contribution of this surface erosion to the total erosion of flooding is considered to be significantly less than the contribution of mass failure due to a rapid drawdown and it will thus be neglected.

Because of the low permeability the soil will still be saturated when the water level decreases rapidly. The specific weight will not increase from submerged to dry as is the case for permeable soil, but from submerged to saturated. Besides this increase in driving forces due to an increase in specific weight, the resisting forces will be decreased in case of a rapid drawdown. Infiltration of rainwater or stream flow can reduce the matric suction when its duration is long enough to overcome the time lag. Furthermore the confining pressure of the water will not be present anymore in the situation after a drawdown.

Not only a rapid drawdown can lead to erosion but also the increased velocities during floods will increase the hydraulic load on the bank and toe erosion can occur. Furthermore the low water level that can be reached during a low discharge can increase the hydraulic load (wave attack) on deeper layers, which can also threaten the stability of the upper layer, as was mentioned in appendix B.1.

Meander movement

Lowland rivers often exhibit a meandering behaviour. Therefore those rivers are not straight channels, but consist of a lot of bends. The hydrodynamics and morphodynamics of a river bend are totally different from those in straight river sections. The necessary basics of the hydrodynamics and morphodynamics of a river bend are explained in the following paragraph.

To make the water in the river follow the curvature of a river bend a centripetal force is exerted on the flow. The general formula of the centripetal force is:

$$F_{centr} = \frac{mv^2}{r} \qquad \text{(B-8)}$$

This necessary centripetal force will be supplied by an inclination of the water level and by a secondary bed shear stress. This phenomenon can be explained by the following equation [De Vriend, 2010]:

$$-\frac{\overline{u^2}}{r} = -g\frac{\partial \zeta}{\partial r} - \frac{\tau_{be}}{\rho h} \qquad \text{(B-9)}$$

The secondary bed shear stress acts only on a small layer, just above the bottom. The inclination of the water level causes a uniform distributed pressure over the entire depth. This is not valid for the centrifugal force of the water particles, because the velocity is not

uniform over depth. As we can see in paragraph 2.3.5 the velocity near the bottom is smaller than the velocity at the surface. Generally the velocity profile has a logarithmic shape.

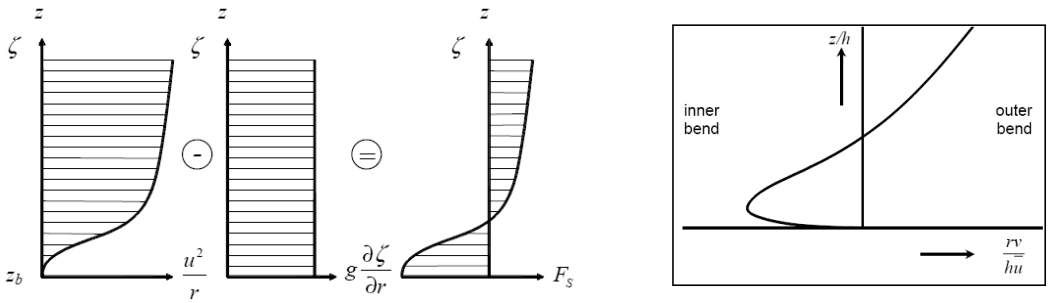


Figure B-3: Left: Pressure distribution over depth; right: velocity distribution over depth

In Figure B-3 the resulting pressure distribution over depth is plotted (left). Because the velocities at the surface are relative large this top layer has also a relative large centrifugal force. The pressure at the surface caused by the water level inclination is not large enough to fully compensate the centrifugal force. Therefore a net pressure is acting in direction of the outer bend at the surface. At the bottom the net pressure is acting in direction of the inner bend. The resulting velocity distribution can be seen in the right plot of Figure B-3. At the surface the water will be transported towards the outer bend, while at the bottom the transport is in direction of the inner bend. This cross-stream circulation is called the secondary flow. This secondary flow also influences the morphologic of the bend. Sediment will be transported from the outer bend towards the inner bend. This will produce a cross-section like Figure B-4.

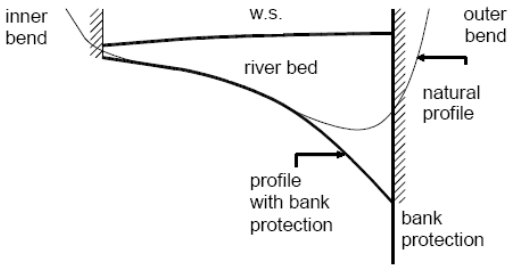


Figure B-4: General cross section in a river bend

The bathymetry of the considered river bend of the Paraná de las Palmas also indicates cross sections which show the presence of a secondary flow (paragraph 2.3.1). Whether or not further bank migration will occur depend on a lot of variables, for example: the actual bed shear stress, critical bed shear stress, actual suspended sediment concentration, equilibrium suspended sediment concentration, etc. A formula used to describe the bank migration rate is [Jansen, 1978]:

$$\frac{\partial n}{\partial t} = E\left(\frac{\tau - \tau_c}{\tau}\right) \qquad \text{(B-10)}$$

More information about the background of this formula can be found in paragraph 3.2.1. The bank erosion rate (at the outer bend) is not always equal to the bank accretion rate (at

the inner bend). A schematization of the bank erosion/accretion rate can be found in Figure B-5.

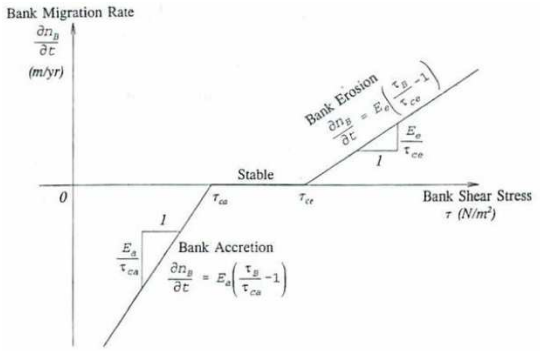


Figure B-5: Schematization of bank migration rate

Ship waves

- Primary and secondary waves

Ships generate waves while travelling through the water by their own propulsion. This creates primary and secondary waves and a propeller wash [Schiereck, 2004]. The primary wave consists of a bow wave at the front of the ship, water level depressions aside the ship, a stern wave and the return current around the ship which reverses behind the ship (Figure B-6). The bow and stern wave induce a secondary wave, which travels towards the river banks.

The propeller wash is not taken into account, because this load is only locally present. The influence on bank erosion is negligible, because the ships normally sail on a considerable distance out of the river bank.

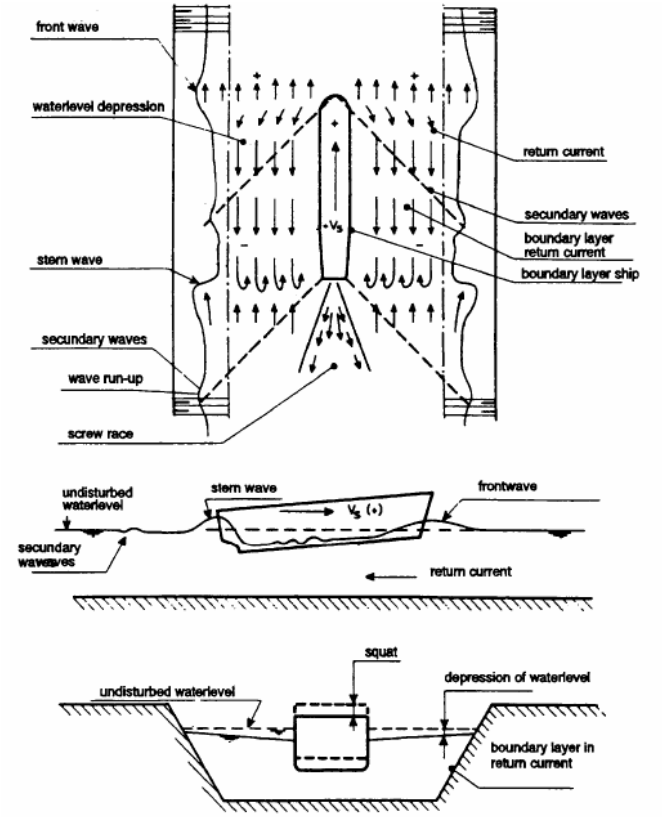


Figure B-6: Water movement around a ship

The primary water movement around the ship is examined by [Groenveld, 2002] who referred to Schijf (1949). Schijf described the primary water movement around the ship by combining the Bernoulli equation with the continuity equation. This approach is called the method of preservation of energy and gives an expression for the water level depression (z) and the velocity of the return current (U_{return}):

$$\frac{V_{ship}^{\ 2}}{gh} = \frac{2 \cdot \frac{z}{h}}{\alpha_{schijf}\left(1 - \frac{A_s}{A_c} - \frac{z}{h}\right)^{-2} - 1} \quad with\ \alpha_{schijf} = 1{,}4 - 0{,}4\frac{V_{ship}}{V_{lim}}$$

$$\frac{U_{return}}{\sqrt{gh}} = \frac{V_{ship}}{\sqrt{gh}}\left(\frac{1}{1 - \frac{A_s}{A_c} - \frac{z}{h}} - 1\right) \qquad \text{(B-11)}$$

For the derivation of V_{lim} see the next paragraph.

The secondary waves are composed of diverging waves and transverse waves, see Figure B-7. These waves originate from the hull where they are generated by discontinuities of the hull. At the point where diverging waves and transverse waves meet cusps are formed.

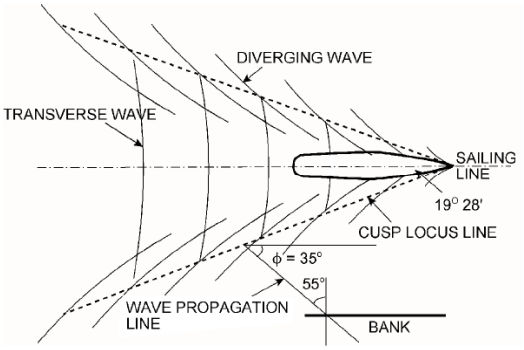


Figure B-7: Secondary waves

Research done about these ship waves by Rijkswaterstaat and Delft Hydraulic Laboratory (now Deltares) shows that the height of the wave cusps can be expressed by the following expression [RWS/DHL, 1998]:

$$\frac{H}{h} = \zeta \left(\frac{s}{h} \right)^{-\frac{1}{3}} Fr^4 \qquad \text{(B-12)}$$

In which H is the height of the cusps, h is the transversal cross section of the river divided by the width, s is the distance between the calculation point and the ship, Fr is the Froude number and ζ is a parameter describing the ship's geometry. The draught of the ship and the shape of the bow appear to be dominant for this parameter. In Figure B-8 measurements are plotted and a value of 1.2 for ζ is found [RWS/DHL, 1998].

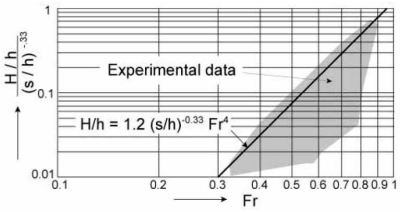


Figure B-8: Determination of ζ

The publication of Rijkswaterstaat and Delft Hydraulic Laboratory is focused on the protection of banks and shore lines. Therefore 1,2 is chosen as value for ζ since this gives high values for the crusp height and leads to a conservative load as input for the design of bank protections. In order to simulate the actual erosion this value may be too conservative and has to be reduced in order to calculate an average crusp height as input for the calculation of the average effect of the waves.

For Fr<0,75 the secondary waves are deep water waves [Schiereck, 2004] which behave in according to the deep water formulae (ϕ=35 degrees as can be seen in Figure B-8):

$$c = \frac{gT}{2\pi} \rightarrow T = c \times \frac{2\pi}{g} = \cos(j) V_s \frac{2\pi}{g} \qquad \text{(B-13)}$$

- Limit speed of ships

The speed of the ships is limited by their maximal hull speed and the limit speed in relation to the return current. Besides these maxima there is a maximum speed set by law in the Paraná de las Palmas river.

The maximal hull speed is determined by the length of the ship. When the speed of a vessel increases also the wave length of the primary wave increases and the Froude number starts to rise. When the wave length of the primary wave approaches the length of the ship the resistance of the hull in the water increases strongly. For an ordinary displacement type of ship this creates a barrier which is called the hull speed. It is possible to sail faster than the hull speed but with a displacement type of ship this is economically unattractive and normally does not happen. The maximal economically speed is about 80% of the hull speed [Schiereck, 2004]. The maximal hull speed is given by the following expression which is the wave celerity of a wave with the wavelength equal to the length of the ship:

$$\left.\begin{array}{l} c = \frac{gT}{2\pi}\tanh\left(\frac{2\pi h}{L}\right) \\ L = cT \end{array}\right\} \longrightarrow V_t = c = \sqrt{\frac{gL}{2\pi}\tanh\left(\frac{2\pi h}{L}\right)} \qquad \text{(B-14)}$$

The limit speed in relation to the return current is dependent of the frontal surface of the ship (As) in relation to the surface of the cross-section of the river (Ac) [Schiereck, 2004]. When the frontal surface is negligible to the river cross-section the limit speed is the same as the hull speed. When the frontal surface is the same as the river cross-section the limit speed is zero since no return current is able to pass. The graph of Figure B-9 visualizes the Froude number (using the limit speed) as function of the frontal surface divided by the river cross-section.

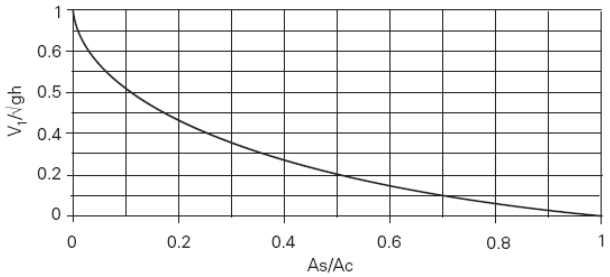


Figure B-9: Froude number (using the limit speed) related to the return current

The limit speed is the minimum of the hull speed and the limit speed related to the return current.

The ships speed is regulated in the Paraná de las Palmas river and has a maximum of 10 kts (5 m/s) [FUNDAR]. However ships are allowed to deviate from this maximum if a higher speed is necessary to keep good control of the ship. This minimum speed for control of the ship depends on the speed necessary to keep rudder control, the minimum speed to compensate the drift of the ship and the speed needed to overcome the current velocity.

The minimum speed to keep rudder control is 4 kts [Ligteringen, 2007]. The minimum speed to compensate the drift is dependent of the wind and currents. The maximal drift angle is 14 degrees [Ligteringen,2007] what means that for every knot a ship drifts perpendicular to its original heading, a ship has to sail under a heading of 14 degrees in the direction of the current or wind with a minimal speed of 4 times the velocity of the current or wind drift.
The ship type that drifts the most due to wind perpendicular to the original heading is an unloaded Ro Ro carrier. At a wind velocity of 30 kts the ship speed perpendicular to the original heading should be about 11 kts. This can be found from equalling the force of the wind on the ship surface with the counterforce of the water on the hull;

$$F_{wind} = \frac{1}{2} \cdot \rho_{air} \cdot v_{wind}^{2} \cdot S_{SchipAboveWaterline} = F_{water} = \frac{1}{2} \cdot \rho_{water} \cdot v_{drift}^{2} \cdot S_{SchipUnderWaterline} \qquad \text{(B-15)}$$

From this expression a drift velocity is found which is 25% of the speed needed to compensate the drift.

C. Measurements of ship waves

During the period of 14 September 2010 till 16 September 2010 the waves generated by the ships travelling the Paraná de las Palmas River at km 86 (lat. 34^0 10.613'S, Long. 58^0 51.811'W) where measured in cooperation with Fundar and the Universidad Nacional de San Martin. The average water level at time of passage was read from a gauge rod. The draught of the ships was read from the markers on the hull. The height of the waves generated by the ship at the point where they hit the bank was measured visually with the help of a gauge rod. The velocity was measured by measuring the passing time between two fixed points. The velocity was also read from the online AIS (Automatic Identification System) of Prefectura Naval Argentina and also the length of the ship and the width of the ship were taken from this system. The distance between the bank and the ship is measured visually.

C.1 Induced Errors

The concrete revetment induced some unspecified reflection what increased the measured cusp height. Furthermore the visual observation of the cusp height may have introduced some small errors.

Also the weather conditions during the measurements are of importance. At the first day the wind speed was about 12 kts which induced wind waves and a set up against the river bank what causes the water level to rise above the top of the revetment. The second day the conditions were perfect. There was almost no wind and the water level was completely flat. The third and last day there was little wind with an estimated speed of about 5 kts which resulted in low waves.

The set up influenced the measurements by the distortion of the visibility of the gauge rod. The rod has been read (the first day) with use of binoculars which is a bit less exact compared to direct reading of the rod (the second and third day). The presence of wind waves influenced the wave pattern and made it harder to measure the correct ship generated waves.

During the measurement the highest cusp height which was visible on the measuring rod was noted. It is not clear whether during the experiments [RWS/DHL, 1988], on which the theoretical approach is based, also the highest cusp height is measured or the average cusp height. This could also introduce some differences between the theoretical and measured wave heights.

Especially due to the reflection of the waves from the concrete revetment and because only the highest cusp height from each wave train is measured it is expected that the wave heights that are used in the calculations are a slight overestimation.
Furthermore the wavelength and wave period that are measured aren't used in the calculations. This is done because it is even hard to get reliable measurements from experienced observers and in this case the observers were inexperienced. The wavelength and wave period are thus calculated from the measured wave height.

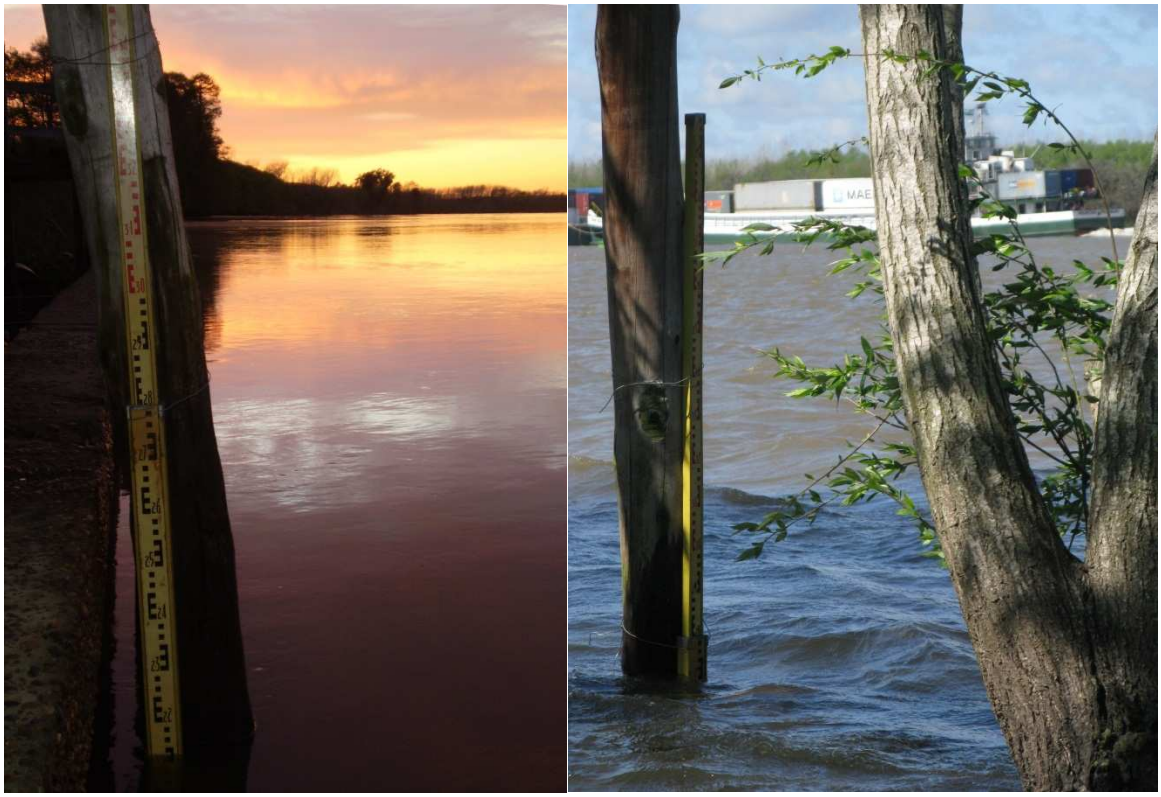


Figure C-1 Measurements during different conditions

C.2 Measurement data

During analysis of the measurement not all the measured data is used. In Table C-1 the used data for all the classes can be found.

Nr.	Day	Time	Water level	Ship type	Draft	Up Down	H	Speed measured	Speed AIS	Distance to bank	LOA	Width
[-]	[-]	[hh:mm]	[m]	[-]	[m]	[-]	[m]	[m/s]	[m/s]	[m]	[m]	[m]
1	14-sep	11:30	2,75	-	-	down	0,25	0,00	0,00	120	-	-
2	14-sep	11:44	2,8	Dry Bulk	11,5	down	0,2	0,00	5,76	120	190	28
3	14-sep	13:00	2,9	Tanker	9,5	down	0,25	0,00	0,00	120	183	32
4	14-sep	13:30	2,9	Dry Bulk	-	up	0,11	0,00	0,00	120	-	-
5	14-sep	13:40	2,9	Tanker	4,6	up	0,25	5,61	0,00	120	99	15
6	14-sep	13:51	2,9	Navy Vessel	2,5	up	0,45	5,94	0,00	40	-	-
7	14-sep	14:04	2,95	-	1,2	up	0,2	4,33	0,00	120	-	-
8	14-sep	15:25	2,95	Navy small supply	3	up	0,2	4,96	0,00	120	-	-
9	14-sep	15:30	2,95	-	3,1	down	0,25	5,06	4,53	120	68	10
10	14-sep	15:41	2,95	Navy Vessel	2,8	up	0,3	5,21	0,00	40	-	-
11	14-sep	15:50	2,95	leisure boat	-	down	0,2	9,68	0,00	215	-	-
12	14-sep	16:10	2,9	Container	5,8	up	0,34	4,78	4,78	80	120	23
13	14-sep	16:30	2,85	leisure boat	-	down	0,25	5,67	0,00	120	-	-
14	14-sep	17:45	2,73	Tanker	10,4	down	0,13	0,00	3,63	120	183	32
15	14-sep	18:00	2,68	Recreational	-	down	0,2	10,27	0,00	300	-	-
16	14-sep	19:30	2,56	Container	-	up	0,27	0,00	0,00	120	-	-
17	14-sep	19:58	2,51	Push boat + 2 barges	-	up	0,08	0,00	2,31	120	-	-
18	14-sep	22:57	2,33	Tanker	7	down	0,37	0,00	3,09	-	159	23
19	14-sep	23:13	2,32	Small log transport	-	up	0,2	4,46	0,00	300	-	-
20	14-sep	23:32	2,31	small cargo	-	up	0,08	3,20	0,00	250	-	-
21	15-sep	0:01	2,31	Container	3	up	0,2	3,27	3,29	180	73	12
22	15-sep	0:21	2,33	small cargo	4,8	up	0,21	5,03	0,00	300	67	10
23	15-sep	0:50	2,35	small cargo	2,4	up	0,12	4,40	0,00	300	68	10
24	15-sep	1:17	2,36	Tanker	5,4	up	0,08	0,00	0,00	300	82	12
25	15-sep	2:03	2,36	small cargo	3,6	up	0,18	4,61	3,86	300	80	14
26	15-sep	2:13	2,36	small cargo	-	down	0,44	0,00	5,14	120	-	-
27	15-sep	2:13	2,36	small cargo	3,7	up	0,12	0,00	3,45	300	90	12
28	15-sep	4:01	2,31	-	-		0,4	0,00	0,00	-	-	-
29	15-sep	4:25	2,29	-	-	down	0,12	0,00	0,00	-	-	-
30	15-sep	5:13	2,25	Push boat + barge	-	down	0,25	0,00	0,00	120	-	-
31	15-sep	6:25	2,21	Small cargo	-	down	0,16	3,97	0,00	120	71	-
32	15-sep	7:45	2,2	IW	-	down	0,4	4,87	0,00	-	80	10
33	15-sep	8:20	2,05	Recreational	-	up	0,18	0,00	0,00	350	20	4
34	15-sep	8:35	2,03	IW	-	up	0,09	3,64	0,00	350	90	13
35	15-sep	8:45	2,03	Recreational	-	down	0,06	3,52	0,00	50	20	4
36	15-sep	9:00	2,02	RoRo+Container	8,3	down	0,2	4,20	5,71	120	213	32
37	15-sep	9:38	1,98	IW	-	up	0,04	3,40	0,00	350	90	12
38	15-sep	10:05	1,97	Container	5,4	down	0,27	6,31	7,20	120	120	23
39	15-sep	10:15	1,95	IW	-	up	0,04	4,04	0,00	350	60	10
40	15-sep	12:10	1,88	Pushboat, no barge	2,3	down	0,07	5,34	0,00	350	35	10
41	15-sep	13:02	1,91	-	2,1	down	0,16	5,15	5,14	120	97	15
42	15-sep	13:20	1,91	log boat	-	down	0,28	0,00	4,63	300	-	-
43	15-sep	13:45	2	log boat	-	up	0,27	3,40	0,00	350	-	-
44	15-sep	14:20	2,06	speedboat	-	up	0,18	10,00	0,00	350	-	-
45	15-sep	14:29	2,1	Dry Bulk	10,6	down	0,26	5,75	5,35	120	225	32
46	15-sep	14:52	2,12	IW	4,8	up	0,3	0,00	0,00	120	-	-
47	15-sep	15:05	2,14	log boat	-	down	0,18	0,00	0,00	300	-	-
48	15-sep	15:06	2,14	El Jilguero boat	-	up + down	0,2	0,00	0,00	350	-	-
49	15-sep	15:07	2,14	push barge	1,8	up	0,17	0,00	0,00	300	-	-
50	15-sep	15:23		Container	6,5m	up	0,5	4,02	3,76	120	164	28
51	15-sep	16:20	2,18	Penin boat	-	up	0,35	5,56	0,00	50	-	-
52	15-sep	16:23	2,18	Dry Bulk	11,8	down	0,4	5,95	0,00	120	225	32
53	15-sep	16:54	2,14	Tanker	4,3	up	0,23	3,86	0,00	120	110	-
54	15-sep	17:22	2,11	IW	4	down	0,2	4,35	0,00	200	52	-
55	15-sep	18:45	2,02	Push boat	-	up	0,36	4,67	0,00	120	-	-
56	15-sep	19:00	2,02	log boat	-	up	0,12	2,75	0,00	300	-	-
57	15-sep	20:10	1,95	Tanker	8,7	down	0,1	0,00	3,70	120	159	25
58	15-sep	20:15	1,95	IW	4,4	down	0,2	0,00	5,09	120	67	10

59	15-sep	20:30	1,95	IW	-	up	0,06	0,00	0,00	300	-	-
60	15-sep	20:45	1,95	Dry Bulk	10	down	0,15	4,94	4,58	120	225	32
61	15-sep	21:00	1,94	IW	-	up	0,16	4,34	4,01	250	67	-
62	15-sep	21:01	1,94	IW	-	up	0,14	0,00	0,00	250	-	-
63	15-sep	22:00	1,88	IW	-	down	0,26	0,00	5,14	-	-	-
64	15-sep	22:40	1,83	IW	3	down	0,25	0,00	4,73	120	80	14
65	15-sep	23:50	1,83	IW	-	down	0,24	0,00	0,00	120	-	-
66	16-sep	0:10	1,87	IW	-	up	0,37	4,98	0,00	250	-	-
67	16-sep	0:35	1,96	IW	4	down	0,12	0,00	4,48	300	76	12
68	16-sep	0:45	1,98	IW	-	up	0,2	3,98	0,00	300	-	-
69	16-sep	1:00	2	IW	-	up	0,08	4,09	0,00	300	-	-
70	16-sep	1:40	2,13	Tug	-	up	0,18	0,00	0,00	300	-	-
71	16-sep	2:00	2,19	IW	3,3	down	0,12	4,10	0,00	200	90	12
72	16-sep	3:30	2,35	Dry Bulk	9,5	down	0,36	0,00	0,00	120	167	-
73	16-sep	4:05	2,36	Tanker	9,4	down	0,44	5,33	0,00	120	148	24
74	16-sep	4:30	2,36	Tanker	9,8	up	0,38	0,00	0,00	80	182	28
75	16-sep	5:00	2,3	Large IW	-	up	0,2	0,00	0,00	120	120	20
76	16-sep	5:35	2,25	IW	3	up	0,12	3,79	3,96	300	61	11
77	16-sep	7:50	2,07	Recreational	-	up	0,06	8,95	0,00	350	-	-
78	16-sep	7:55	2,07	IW	3	up	0,1	3,71	3,60	120	58	11
79	16-sep	8:15	2,05	Dry Bulk	10,5	down	0,3	6,03	5,56	80	225	32
80	16-sep	8:45	2,02	Tanker	5	up	0,5	5,72	5,50	100	117	20
81	16-sep	9:03	2	Tanker	7,9	down	0,1	4,35	4,48	120	124	18
82	16-sep	9:30	1,98	Bulk	4,5	down	0,08	3,89	0,00	120	167	26
83	16-sep	9:45	1,95	Tanker	9,8	up	0,15	3,90	4,78	120	225	32
84	16-sep	10:00	1,94	IW	6,8	down	0,12	5,52	0,00	120	99	15
85	16-sep	10:40	1,9	Dry Bulk	9,2	down	0,18	5,42	0,00	120	194	27
86	16-sep	11:30	1,86	Dry Bulk	10,6	up	0	5,18	0,00	120	230	36
87	16-sep	13:15	1,82	RoRo	-	down	0,3	4,09	0,00	120	200	33
88	16-sep	13:45	1,86	IW	3	down	0,24	0,00	0,00	120	70	-
89	16-sep	14:00	1,86	General Cargo	10,5	up	0,3	4,48	0,00	120	202	27

Class	A1	A2	B	C1	C2	D
Vessel number (in measurement data)	2	5	12	9	20	11
	14	18	21	22	23	13
	45	53	36	25	26	15
	52	80	38	27	31	35
	57	81	50	54	32	44
	60	82	87	58	34	51
	73			64	37	77
	79			67	39	
	83			71	41	
	85			76	61	
	86			78	63	
	89			84	66	
					68	
					69	

Table C-1: Used data for the different classes

D. Analysis of ship waves and movement

In this appendix the background of the analysis of the measurements are given. Section D.1 describes the computation of the ζ values for the different vessel classes. Section D.2 describes the computation of the representative wave height. Section D.3 explains the computation of the wavelengths and wave heights. Section D.4 discusses the yearly ship movement on the Paraná de las Palmas (at km 87).

D.1 Determination of ζ-values

The ζ-value, of formula (D-1), is a highly empirical value and represents the ship's geometry.

$$\frac{H}{h} = \zeta \left(\frac{s}{h} \right)^{\frac{-1}{3}} Fr^4 \qquad \text{(D-1)}$$

Especially the draught and the shape of the bow of the ship are important. For this research it is necessary to determine ζ for different types of ships. The data of the field measurements are the input for this calibration.

Type	LOA [m]	DWAT [m^3]	Displ. [m^3]	Beam [m]	Draft [m]	C_b [-]
Tankers & Product Carriers	220	60.000	74.000	32,20	12,80	0,82
Dry Bulk Carriers	210	50.000	66.000	32,20	12,60	0,82
Container Vessels	185	25.000	33.500	28,50	10,10	0,63
Ro Ro & Car Carriers	198	20.000	35.500	32,20	10,00	0,61
Home Trade Inland Waterway Ships	60	1.150	1.500	10,00	3,25	0,80
Recreational Boats / Cruisers	12	-	-	3,00	0,80	0,60

Table D-1: Vessel characteristics

Based on the vessel characteristics in Table D-, a classification is made, which can be seen in paragraph 2.2. The ships are divided in these classes to compare the influence of the C_b (block coefficient) and the draft on the value of ζ. The mean value of ζ is estimated to be able to calculate a representative wave height used in erosion calculations. For Class B no distinction is made for different drafts, because during measurement the amount of Class B ships was not large. Inland Waterway vessels are the vessels which are smaller than 100 m and cannot be classified as container ships or as tankers. Class C consists of vessels with a length smaller than 100 m, which are transporting sand, wood, general cargo, etc.
If the draft for a ship of the Class A or Class C is not known the vessel is added to Class A2 respective C2.

For calibrating the ζ value for the different classes only the observations are taken during which at least the following data is measured (type of ship, speed, distance from river bank, water level and the wave height). The speed of the ship is firstly corrected, which means that

the speed of upriver travelling ships is increased by 1 m/s (assumed stream velocity), and the speed of downriver travelling ships is decreased by 1 m/s.

The measurements of the wave heights is only done for two days, but the measurement of ship velocities can be done for a much longer period (via the Automatic Identification System). Therefore the ζ values are calibrated in such a way that if the measured velocities are put into equation (D-1) the output wave heights can be used in expression (D-2) to calculate the representative wave height.

Erosion ~ H^2

$H(1,2,..,n)$ (set of wave heights)

$$Hrepr = \sqrt{\frac{\sum_{j=1}^{n} H_j^2}{n}} \qquad \text{(D-2)}$$

The contribution of the higher waves to the erosion is higher and therefore also to the determination of the ζ value. The calibration of the ζ values for the different classes can be seen on the following pages.

Class A: Tankers & Dry Bulk carriers

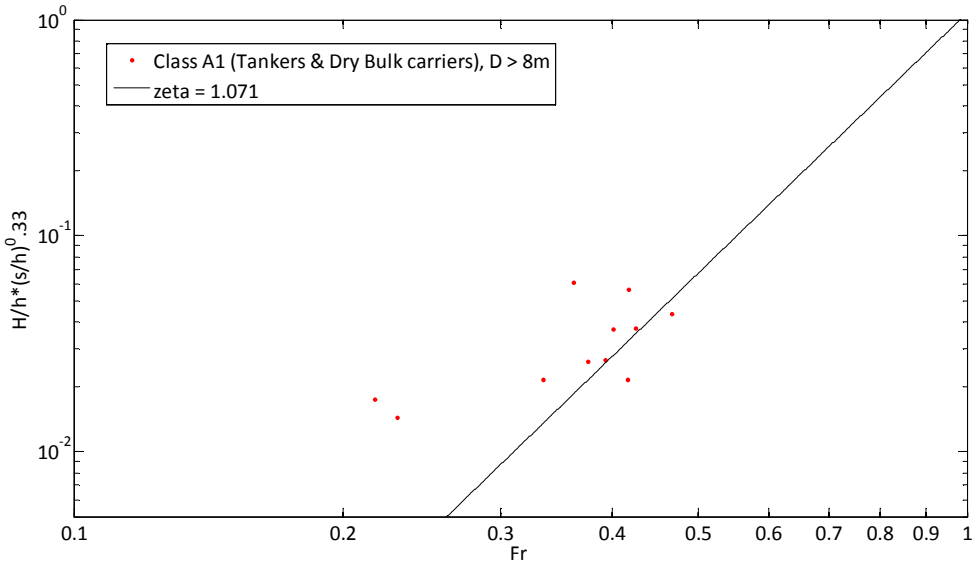


Figure D-1: Calibration of ζ for Class A1, draft > 8 m

In Figure Figure D-1 it can be seen that the graph with ζ=1,071 fits the major part of the measurements. Only two data points are badly correlated with this ζ. As is stated before, the higher wave heights contribute more to the erosion, which causes the line to be directed more to the right of the figure (lower ζ).

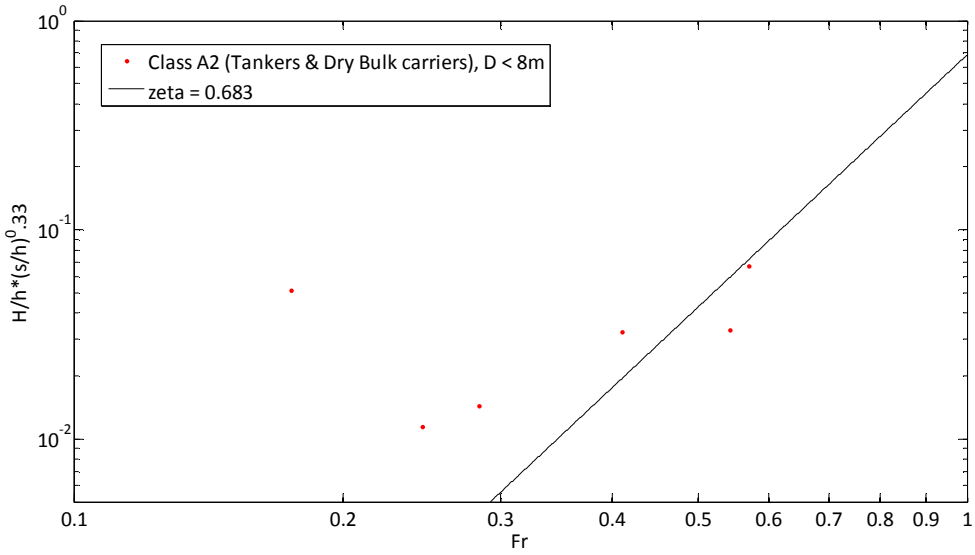


Figure D-2: Calibration of ζ for Class A2, draft < 8 m

Only six data point are gathered for the ships of Class A2, with a draft smaller than 8 m. It is hard to base a reliable fit on this small amount of data. In Figure D-2 it is shown that with ζ=0,683 the best fit is reached, which is smaller than for Class A1 with a draft > 8 m.

Class B: Container ships and Ro Ro

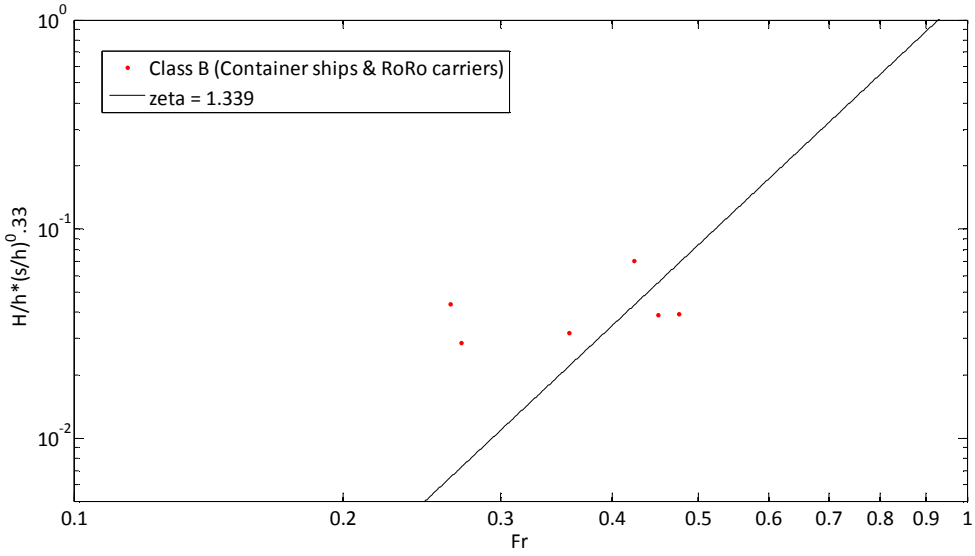


Figure D-3: Calibration of ζ for Class B

During the two day measurements only 6 ships of Class B passed the Paraná de las Palmas. Therefore it is hard to make a reliable fit for this class. In Figure D-3 it can be seen that the Class B ships can be represented by a ζ of 1,339.

Class C: Inland waterway ships and small vessels

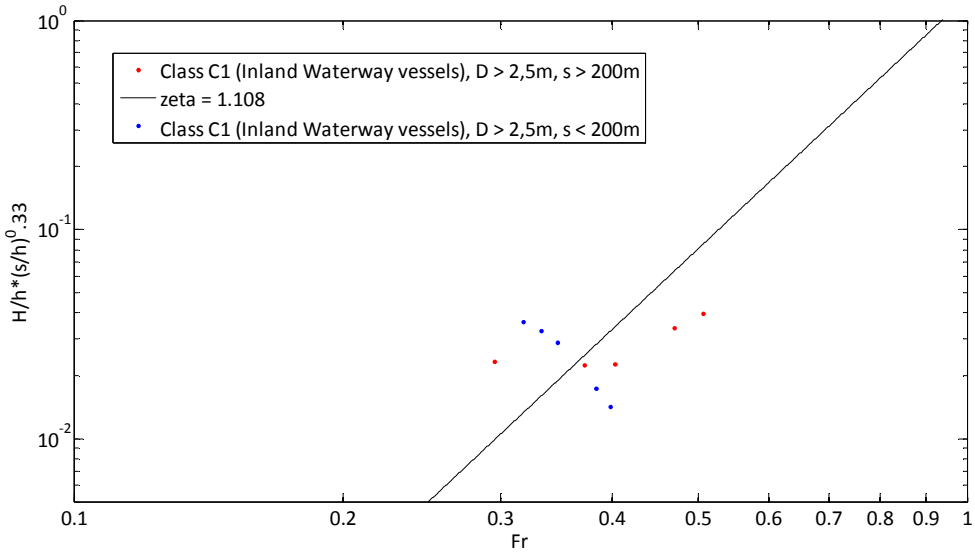


Figure D-4: Calibration of ζ for Class C1, draft > 2,5 m

On first sight the data points for Class C1 (draft > 2,5 m) seem to have a wide spreading. This spreading can be related to the distance between the ship and the river bank. The ships closer than 200 m are marked by blue dots and the ships located further than 200 m are marked with red dots. The general trend is that nearby ships have a larger ζ than ships on a larger distance. The fitted ζ for Class C1 is 1,108

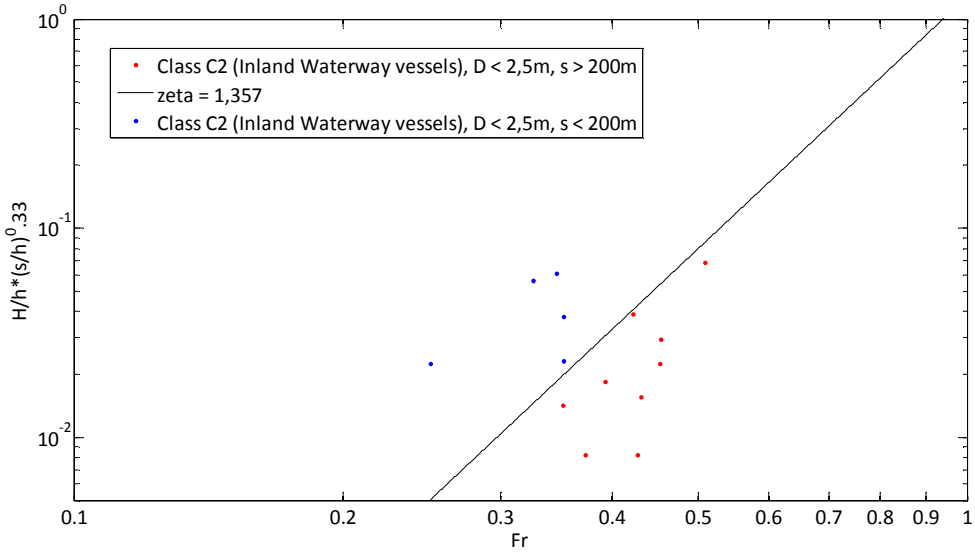


Figure D-5: Calibration of ζ for Class C2, draft < 2,5 m

In Figure D-5 the data points are plotted for Class C2 ships with a draft smaller than 2,5 m. Also in this plot a large difference can be seen between nearby ships and ships which sail further away from the river bank. For this selection the ζ is 1,357. It might be better to sort the data of Class C by distance, see Figure D-6.

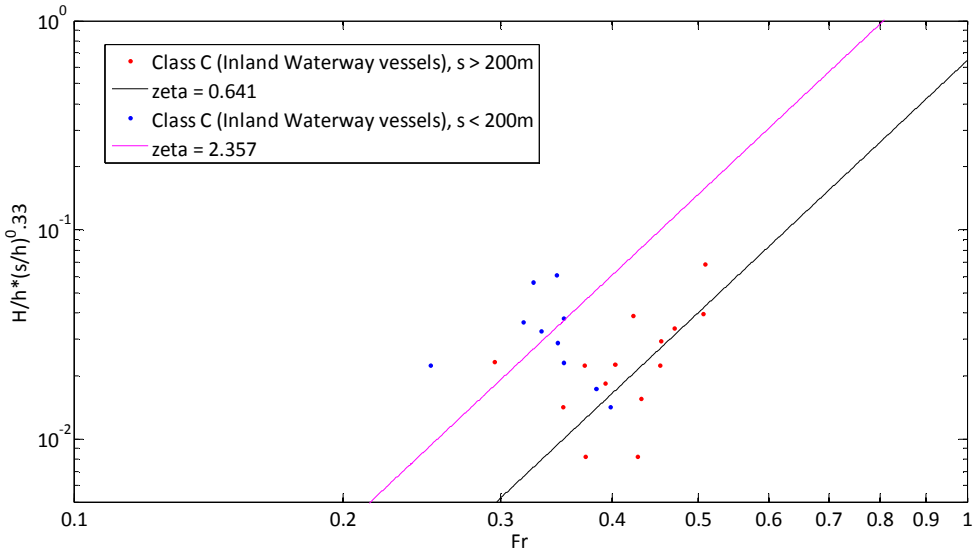


Figure D-6: Calibration of ζ for Class C. Red: s>200 m, Blue: s<200 m

For ships at a maximum distance of 200 m the fitted ζ is 2,357. For ships at a minimum distance of 200 m the mean ζ is 0,641. Although the use of these values will result in a more reliable wave height estimation, it is not very convenient to use these values for further research, because the distance to the coast is normally not given in ship tracks.

Class D: recreational ships

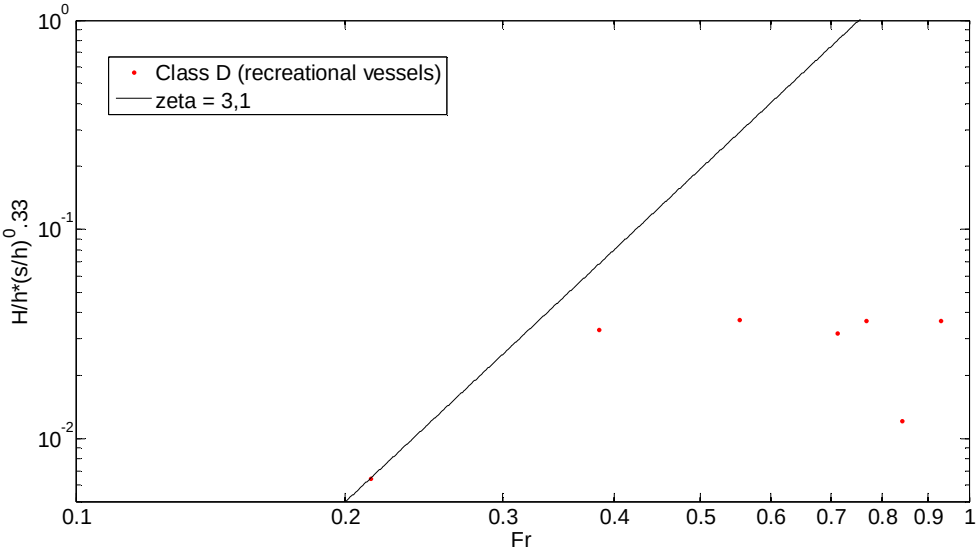


Figure D-7: Calibration of ζ for Class D

The fit of ζ for Class D ships is solely based on one data point, so the accuracy of this estimate is very low. A remarkable observation in Figure D-7 is that the generated wave height is constant for Fr > 0,3. This can be explained with the following expression for the limit speed of ships:

$$\left.\begin{array}{l} c = \frac{gT}{2\pi}\tanh\left(\frac{2\pi h}{L}\right) \\ L = cT \end{array}\right\} \longrightarrow V_t = c = \sqrt{\frac{gL}{2\pi}\tanh\left(\frac{2\pi h}{L}\right)} \qquad \text{(D-3)}$$

Displacement ships can't exceed the celerity of their own generated primary wave. Self-propelled ships can pass this limit if they are able to plane on the water, like speed boats. The wave height of a ship which has passed this border doesn't grow anymore. If a speed boat with a length of 6 m is assumed, and h =14,5 m, the maximum celerity of the primary wave is: 3,06 m/s. The Froude number is than 3,06/sqrt(9,81·14,5)=0,26. Therefore it can be seen in Figure D-7 that for higher Froude numbers the wave generation doesn't vary. For further research the y-value can be assumed constant: 0,035.

Summary

For further research the following ζ values will be used:

Class	ζ	$H/h*(s/h)^{0.33}$
A1	1,071	Var
A2	0,683	Var
B	1,339	Var
C1	1,108	Var
C2	1,357	Var
D	-	0,035

Table D-2: ζ-values for different classes

*D.2 **Representative wave height***

In paragraph 3.2.1.2. it is stated that the erosion rate is proportional to H^2 if no damping is assumed by a foreshore or structure. If there is damping (μ), the erosion rate is proportional to $\ln(c_E \cdot \mu \cdot H^2 + 1)$. For small μ (which is often the case) this proportionality is almost the same as to H^2. Therefore the representative wave height is based on the following proportionality: Erosion rate ~ H^2.

The representative wave height is calculated on the following way:

Erosion ~ H^2

$H(1,2,..,n)$ (set of wave heights)

$$Hrepr = \sqrt{\frac{\sum_{j=1}^{n} H_j^2}{n}} \qquad \text{(D-4)}$$

The measurements have been done at the outer bend of the river. The bigger ships travelled at about 120 m from the coast, while some smaller ships were able to take the inner bend. The wave heights at the inner bend were therefore much smaller than the measured wave heights. In straight river sections the ships will not be restricted to a small channel. Some vessels will travel through the middle, while other ships will travel to the right or left, depending on the other traffic at the river. For further research it is assumed that the ships are travelling in the middle of the river (at 220 m out of the river bank).

For Classes A1, A2, B, C1 and C2 the representative wave height can be determined if H(j) is calculated with the use of (D-1). The corrected measured ship velocities, measured water level and distance to the coast are the input for the expression. For Class D this method cannot be used because no zeta value is determined. For this class the value of $H/h*(s/h)^{0,33}$ is assumed to be constant (0,035).

The representative wave heights are determined for the following locations:

- Outer bend
- Inner bend
- Along straight river sections

Also the significant wave height is determined. The significant wave height is the mean wave height of the highest third of waves. The significant wave height is only calculated for all the classes together because not enough vessels are measured to do this for all the classes separate.

Class	Outer bank		Inner bank		Straight section	
	H_{repr} [m]	$H_{1/3}$ [m]	H_{repr} [m]	$H_{1/3}$ [m]	H_{repr} [m]	$H_{1/3}$ [m]
A1	0,249	-	0,178	-	0,202	-
A2	0,294	-	0,201	-	0,230	-
B	0,319	-	0,213	-	0,244	-
C1	0,174	-	0,205	-	0,182	-
C2	0,226	-	0,272	-	0,240	-
D	0,209	-	0,207	-	0,207	-
Overall	0,244	0,34	0,239	0,27	0,228	0,28

Table D-3: Representative and significant wave heights for all classes

*D.3 **Wave length and period***

The wave length and period of the ships that passed by are also noted during the measurements. Measurement of the wave length and period are less easy than measurement of the wave height. All measured data can be found in appendix C. For estimation of the period and length of secondary ship waves a reliable expression is developed [Schiereck, 2004]:

$$T = \cos(\theta) \cdot v_s \frac{2\pi}{g}$$

$$L = \frac{gT^2}{2\pi} \qquad \text{(D-5)}$$

These expressions are valid in deep water (h/L > 0,5), when Fr < 0,75.

The results of this theoretical approach do not correspond well with the measurements. It seems like the wave length is underestimated during measurements. Because normally this formula gives good results it is decided to use the theoretical wave lengths and periods for

further research. Another reason to use the theoretical approach is that the measured wave lengths are not very reliable.

For all classes the mean wave length and period are calculated. Also the wave length and wave period is calculated which responds with the representative wave height. This is done, for example, for the erosion calculation with the BEM model, which is explained in paragraph 3.2.1. For a calculation without damping the erosion is proportional to H^2 and T. If for example two waves are present (H_1 = 0,5 and H_2 = 0,2) with the following two wave periods (T_1 = 2 and T_2 =1), and n, C_E are assumed to be 1 (for simplicity), the erosion is equal to:

$$dy = H_1^2 \cdot T_1 + H_2^2 \cdot T_2 = 0{,}54m \qquad \text{(D-6)}$$

The fictive erosion can also be calculated with a H_{repr} and a T_{repr}, as:

$$\begin{aligned} dy &= H_{repr}^2 \cdot T_{repr} = 0{,}54m \\ H_{repr} &= \sqrt{\frac{\left(H_1^2 + H_2^2\right)}{2}} = 0{,}38m \\ T_{repr} &= \frac{H_1^2 \cdot T_1 + H_2^2 \cdot T_2}{H_1^2 + H_2^2} = 1{,}86s \\ dy &= 2 \cdot 0{,}38^2 \cdot 1{,}86 = 0{,}54m \end{aligned} \qquad \text{(D-7)}$$

In this way the T_{repr} and L_{repr} are calculated for the different classes. The values for the mean and the representative wave length and wave period can be found in Table D-4.

For all classes together also the significant wave length and period is determined. The significant wave length is the mean wave length of the highest third of waves. The significant wave period is the mean wave period of the highest third of waves: $L_{1/3}$ =10,3 m and $T_{1/3}$=2,5 m. The values are based on the calculated wave lengths and periods of the ships during measurement.

Class	Mean wave length [m]	Mean wave period [s]	L_{repr} [m]	T_{repr} [m]
A1	9,1	2,4	9,6	2,5
A2	9,8	2,3	13,3	2,7
B	8,9	2,3	10,0	2,5
C1	8,4	2,3	8,4	2,3
C2	9,3	2,4	9,1	2,4
D*	10,2	2,4	15,2	3,1
overall	9,1	2,3	10,2	2,5

Table D-4: Mean wave length and period and representative wave length and period for all classes

* For the calculation of the wave length and the wave period only the vessels with a speed lower than 9 m/s (Fr = 0,75 for v_s=9 m/s,) are taken.

*D.4 **Ship movement***

The Coast Guard at Zárate (Km 106) delivered a database of ship tracks between the 1st and 24th (up to 9 am) of September [Prefectura Naval, 2010].

The location of measurements was at km 87. Between km 106 and km 87 there is one side channel, 'Canal Gobernador', and the harbour of Campana. Some of the ships in the record could therefore pass Zárate without passing through km 87 of the Paraná de las Palmas, see Figure D-8.

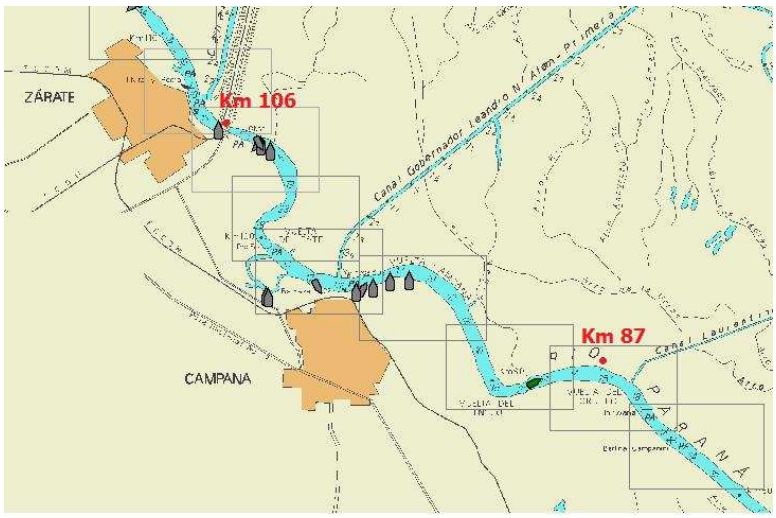


Figure D-8: Paraná de las Palmas between km 87 and km 106

During measurements 89 vessels were measured, while in the record of the coast guard 117 vessel were tracked. A lot of these vessels didn't pass the measurement area. After comparing the record of the coast guard and the record of the measurements it can be concluded that mainly the number of smaller ships (Class C) differs between both records. The bigger vessels (Class A1, A2, and B) are found in both records. During the measurement period 86 Class C vessels passed km 106, of which only 32 were measured at km 87. Nine class C ships did pass km 87 but didn't pass km 106. In total 41 vessels of Class C were measured at km 87, instead of 86 vessels at km 106. According to this analysis it is assumed to reduce the number of Class C ships in the coast guard track with 50%.

All different ships are divided in the four classes, as described in appendix D.1. In the database a lot of types of ships are mentioned. Below it can be seen which type is added to which class.

- Class A
    - Crude oil tankers
    - Product tankers
    - Chemical tankers
    - Bulk carrier
    - Wood transporters (length > 100 m)
- Class B
    - General Cargo (length > 100 m)
    - Ro Ro ships

    - Container ships
- Class C
    - Sand barges
    - General Cargo (length < 100 m)
    - Small vessels
- Class D
    - Passenger ships
    - Cruise ships

The distribution of classes at the Paraná de las Palmas can be found inTable D-5.

Class	Number of ships per year at km 87 (extrapolated)	Percentage [%]
A1	2.367	8,9
A2	4.457	16,7
B	1.813	6,8
C1	2.567	9,6
C2	11.372	42,5
D*	1.374	5,1
Remaining**	2.798	10,5
Total	26.739	100

Table D-5: Distribution of classes

* The number of Class D ships is based upon extrapolation of the measurement track
**The remaining ships are mainly push boats and tugs.
In the record it can be seen that 40 of the 83 push boats and tugs were supporting other ships. It would be too conservative to account all these remaining ships, because the ship wave of for example of a tanker can't be added to the ship wave of the supporting tug. Therefore only 50% of these remaining ships are taken into account in the erosion computations. During the measurement only two push boats/tugs were measured, so a reliable estimate for the representative wave height is very hard to make. For simplification 50% of the remaining vessels are added to the Class C2 (not included in the table).

D.5 ***Calculation example***

In this section an example will be given for the calculations done in paragraphs D.1 up to D.2. In these sections a distinction is made between the different ship classes, as can be seen in Table D-3 In this section only the calculations for class A2 are given. This class is chosen because only six vessels of this class were measured.

The following class A2 ships were measured:

Nr.	H_{rod} [m]	Ship type	D [m]	Up/down	H [m]	V_s [m/s]	s [m]	LOA [m]	W [m]
5	2,9	Tanker	4,6	up	0,25	5,61	120	99	15
18	2,33	Tanker	7	down	0,37	0,00	120	159	23
53	2,14	Tanker	4,3	up	0,23	3,86	120	unknown	unknown
80	2,02	Tanker	5	up	0,50	5,72	100	117	20
81	2	Tanker	6	down	0,10	4,35	120	124	18
82	1,98	Dry Bulk	4,5	down	0,08	3,89	120	167	26

Table D-6: Characteristics class A2

ζ-values

The zeta values are calibrated in such a way that if the measured velocities are put into equation D-1, the calculated wave heights can be used in expression D-2 to calculate the representative wave height.

First the representative wave height of class A2 at the outer bend will be calculated. The representative wave height can be calculated with use of the measured wave height in the following way:

$$H_{repr,outerbend,measured} = \sqrt{\frac{\sum_{j=1}^{n} H_{measured,j}^2}{n}} = \sqrt{\frac{0{,}25^2 + 0{,}37^2 + 0{,}23^2 + 0{,}50^2 + 0{,}10^2 + 0{,}08^2}{6}} = 0{,}294 \text{ m} \quad \text{(D-8)}$$

The ζ-values are determined iteratively, with the following expressions:

$$\sqrt{\frac{\sum_{j=1}^{n} H_{calc,j}^2}{n}} = H_{repr,calc} = H_{repr,measured}$$

$$H_{calc,j} = h_j \cdot \xi \cdot \left(\frac{s_j}{h_j}\right)^{\frac{1}{3}} \cdot Fr_j^4$$

$$h_j = \frac{A_c}{b} - 0{,}36 + h_{rod,j} \quad \text{(D-9)}$$

$$Fr_j = \frac{v_{s,w,j}}{\sqrt{g \cdot h_j}}$$

$v_{s,w,j} = v_{s,g,j} + v_{w,j}$ (v relative to water = v relative to the ground + flow velocity)

In which A_c=5460 m^2,b=435 m, following from the bathymetry data given in paragraph 2.3.1. and g=9,81 ms^{-2}. For simplicity it is assumed that the river flow is always 1 m/s. For upstream going vessels this means that the measured velocity is increased with 1 m/s and for downward going vessels this means that it is decreased with 1 m/s.

Nr.	h [m]	$v_{s,w}$ [m/s]	Fr [-]
5	15,09	6,61	0,543
18	14,52	2,09	0,175
53	14,33	4,87	0,410
80	14,21	6,72	0,570
81	14,19	3,35	0,284
82	14,17	2,89	0,245

Table D-7: Water depth, vessel velocity (r.t. water) and the Froude number of the class A2 vessels

After a few iterations it follows that ζ is 0,683

To check this value the calculated wave heights are given:

Nr.	H_{calc} [m]
5	0,455
18	0,005
53	0,138
80	0,540
81	0,031
82	0,018

Table D-8: Calculated wave heights with zeta=0,683

The resulting representative wave height is:

$$H_{repr,outerbend,calculated} = \sqrt{\frac{\sum_{j=1}^{n} H_{outerbend,calc,j}^2}{n}} = \sqrt{\frac{0,455^2 + 0,005^2 + 0,138^2 + 0,540^2 + 0,031^2 + 0,018^2}{6}} = 0,294 \text{ m}$$

(D-10)

So a ζ of 0,683 is the right value. It can be remarked that the calculated wave heights in Table D-8 do not correlate well with the measured wave heights in Table D-6. This can be explained by the fact that the chosen zeta value doesn't represent the mean wave height, but is a lower value, because the ships with a high speed (and therefore a theoretical height wave height) are more taken into account. This is done to be able to estimate the representative wave height at the inner bank and for straight river sections. If the objective was to represent each individual wave another approach should be applied.

Representative wave height

Above the representative wave height at the outer bank is determined with the measured wave heights (because the measurements took place at the outer bend). The representative wave heights at the inner bank and along straight sections are calculated with use of ζ.

$$H_{repr,innerbend,calc} = \sqrt{\frac{\sum_{j=1}^{n} H_{innerbend,calc,j}^2}{n}}$$

$$H_{innerbend,calc,j} = h_j \cdot \zeta \cdot \left(\frac{s_{innerbend,j}}{h_j} \right)^{\frac{1}{3}} \cdot Fr_j^4 \qquad \text{(D-11)}$$

$$s_{innerbend,j} = b - s_{outerbend,j}$$

The same approach is applied to calculate the representative wave height at the bank along a straight section. In this approach it is assumed that all the vessels travel through the middle of the river, so $s_{straight}$ Is b/2=217,5 m

Nr.	$s_{innerbend}$ [m]	$H_{innerbend,calc}$ [m]	$H_{straight,calc}$ [m]
5	315	0,325	0,368
18	315	0,003	0,004
53	315	0,099	0,112
80	335	0,356	0,411
81	315	0,023	0,025
82	315	0,013	0,014

Table D-9: Calculated values for inner bend and straight river section

$$H_{repr,innerbend,calc} = \sqrt{\frac{\sum_{j=1}^{n} H_{calc,j}^2}{n}} = \sqrt{\frac{0,325^2 + 0,003^2 + 0,099^2 + 0,356^2 + 0,023^2 + 0,013^2}{6}} = 0,201 \text{ m} \qquad \text{(D-12)}$$

$$H_{repr,straight,calc} = \sqrt{\frac{\sum_{j=1}^{n} H_{calc,j}^2}{n}} = \sqrt{\frac{0,368^2 + 0,004^2 + 0,112^2 + 0,411^2 + 0,025^2 + 0,014^2}{6}} = 0,230 \text{ m} \qquad \text{(D-13)}$$

Wave length and period

The wave length and period are calculated with the following expressions:

$$T = \cos(\theta) \cdot v_s \frac{2\pi}{g}$$

$$L = \frac{gT^2}{2\pi} \qquad \text{(D-14)}$$

In the report the mean values and the representative ones are calculated. The representative values are calculated in the following way:

Nr.	T [s]	L [m]	H^2 [m^2]
5	3,5	18,8	0,063
18	1,1	1,9	0,137
53	2,6	10,2	0,053
80	3,5	19,4	0,250
81	1,8	4,8	0,010
82	1,5	3,6	0,006
Mean	2,3	9,8	-

Table D-10: Calculated wave length and period and H^2

$$L_{repr} = \frac{\sum_{j=1}^{n} H^2_{measured,j} \cdot L_{calc,j}}{\sum_{j=1}^{n} H^2_{measured,j}} = \frac{0,063*18,8+0,137*1,9+0,053*10,2+0,25*19,4+0,01*4,8+0,006*3,6}{0,519} = 13,3 \text{ m}$$

(D-15)

$$T_{repr} = \frac{\sum_{j=1}^{n} H^2_{measured,j} \cdot T_{calc,j}}{\sum_{j=1}^{n} H^2_{measured,j}} = \frac{0,063*3,5+0,137*1,1+0,053*2,6+0,25*3,5+0,01*1,8+0,006*1,5}{0,519} = 2,7 \text{ s}$$

(D-16)

Erosion rate

The erosion rate is calculated with the BEM, as shown below:

$$dy = c_{\varepsilon} \cdot H^2 \cdot n \cdot T \cdot N \qquad \text{(D-17)}$$

As explained in paragraph 3.3.3. and appendix E all the parameters do have a standard deviation. The computation of the erosion rate is done with a Monte Carlo simulation. The erosion rate is 30.000 times calculated with different values for C_E, H, n, T and N. It leads to far to show the Monte Carlo simulation here, but an estimation can be made with the use of the mean values of C_E, H, n, T and N.

$$dy_{outerbend} = c_{\varepsilon} \cdot H^2 \cdot n \cdot T \cdot N = 1,233 \cdot 10^{-4} \cdot 0,294^2 \cdot 2 \cdot 2,7 \cdot 4457 = 0.257 \text{ m/year}$$
$$dy_{outerbend} = c_{\varepsilon} \cdot H^2 \cdot n \cdot T \cdot N = 1,233 \cdot 10^{-4} \cdot 0,201^2 \cdot 2 \cdot 2,7 \cdot 4457 = 0.120 \text{ m/year} \qquad \text{(D-18)}$$
$$dy_{outerbend} = c_{\varepsilon} \cdot H^2 \cdot n \cdot T \cdot N = 1,233 \cdot 10^{-4} \cdot 0,230^2 \cdot 2 \cdot 2,7 \cdot 4457 = 0.157 \text{ m/year}$$

The calculated values with use of the Monte Carlo simulation are a bit higher, this is mainly caused by the inaccuracy of H.

E. Sensitivity analysis BEM

This appendix describes the sensitivity analysis of the BEM model. The analysis is done with a Monte Carlo (full probabilistic method) and a FORM simulation (level II probabilistic method).
In section E.1 the input for both simulations is given and argued. Section E.2 gives the results of the probabilistic simulations.

E.1 Input

The erosion rate, caused by ship waves, is calculated according to a Monte Carlo simulation and a FORM simulation. In both simulations the probability distributions of all present parameters are used to calculate the erosion rate. The Monte Carlo simulation calculates the erosion rate for a 30.000 times, each time with random chosen variables. The advantage of a full probabilistic method is that it gives an idea of the reliability, the spreading, of the computation.
The FORM simulation is not a full probabilistic method, but can be used to obtain the relative importance of the different variables.

$$dy = c_{\varepsilon} \cdot H^2 \cdot n \cdot T \cdot N \qquad \text{(E-1)}$$

The simulations are based on expression E-1. The input for the simulation is given in Table E-1. The explanation for the chosen distributions and standard deviations will be discussed below.

Parameter	Distribution	Mean μ	Standard deviation σ	σ/ μ [%]
H	Normal	Varies	varies	10
n	Lognormal	2	0,5	25
T	Normal	varies	0,05 s	4
N	Normal	Varies	Varies	5
C_0	Normal	$1{,}85*10^4$	$0{,}5*10^4$	27
τ_c	Normal	1,5 Pa	0,25 Pa	17

Table E-1: Input for probabilistic simulations

Wave height
The mean values for the wave heights for different classes can be found in paragraph 3.3.3. For the probability distribution a normal distribution is assumed, because the wave height could as well be larger as smaller. The standard deviation is assumed to be 10%.

Number of waves per vessel

A wave train of secondary waves consists of a lot of waves with a varying height. During measurements the highest waves are measured. After visual observation it is assumed that each vessel will generate two of these representative waves, so n is taken as 2. A realistic variation for n is between 1,5 and 3. An n smaller than 1,5 is not realistic, because than the effect of smaller waves is ignored, which would underestimate the erosion. Higher than n = 3 is to large according to visual observations. For this parameter a lognormal distribution is taken, because this distribution has a steep front and a wider tail, which represents the variation between n = 1,5 and n = 3. The standard deviation is set to be 0,5 (25%).

Wave period

The values for the representative wave height can be found in paragraph 3.3.3. The values for the relative wave period is for all the classes around 2,5 s. Only class D shows some disorder, because of the small amount of wave period estimations. For the other classes the deviation from 2,5 s is maximum 0,2 s. Therefore a standard deviation of 0,1 s is chosen (4%).

Number of ship movements per year

The number of ship movements is based on a ship track of the coast guard over one month. Due to this the number of ship movements is quite reliable. A normal distribution with a standard deviation of 5% is assumed.

Constant C_0

According to Verheij [2001], the value of C_E is calculated with formula:

$$C_E = \frac{1{,}85 \cdot 10^{-4}}{\tau_{cr}} \qquad \text{(E-2)}$$

The constant, $1{,}85 \cdot 10^{-4}$, in this formula is named C_0 for simplicity. In Figure E-1 it can be seen that the exact fit could not be made. The difference between the fit in 2000 and in 2001 is assumed to be two times the standard deviation. So the standard deviation is $0{,}5 * 10^{-4}$ (27%).

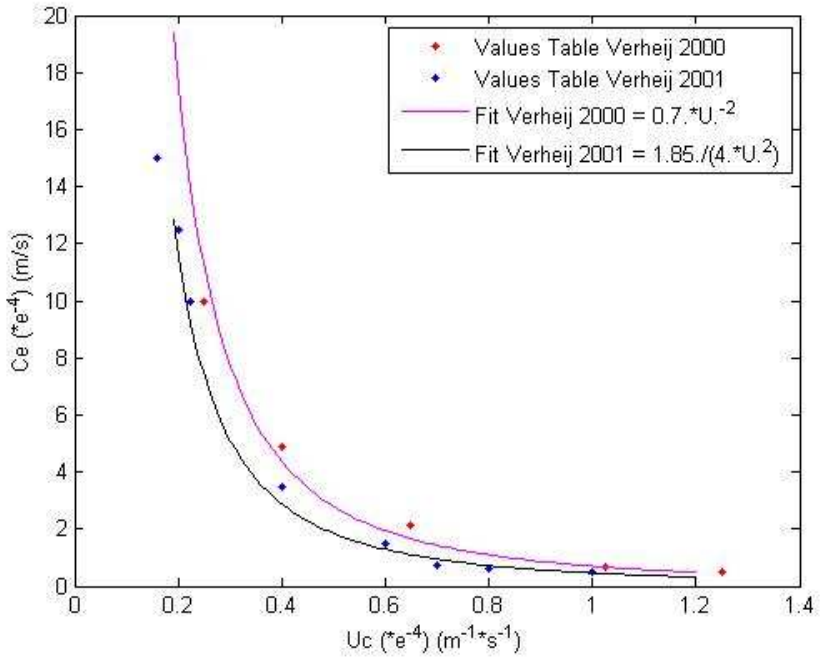


Figure E-1: Different methods to calculate C_E

Critical shear stress

According to Verheij [2001], the value of τ_c can be estimated with Table 2.10. The soil, as described in paragraph 2.4., can best be modelled as average clay. The corresponding value for τ_c is taken as 1,5 Pa. The upper limit for the critical shear stress is, according to this table, 2 Pa. The lower limit is 0,65 Pa. Because it could not be said if a higher or a lower value for τ_c is more likely, a normal distribution is assumed. The standard deviation is 0,25 Pa (17%).

*E.2 **Results***

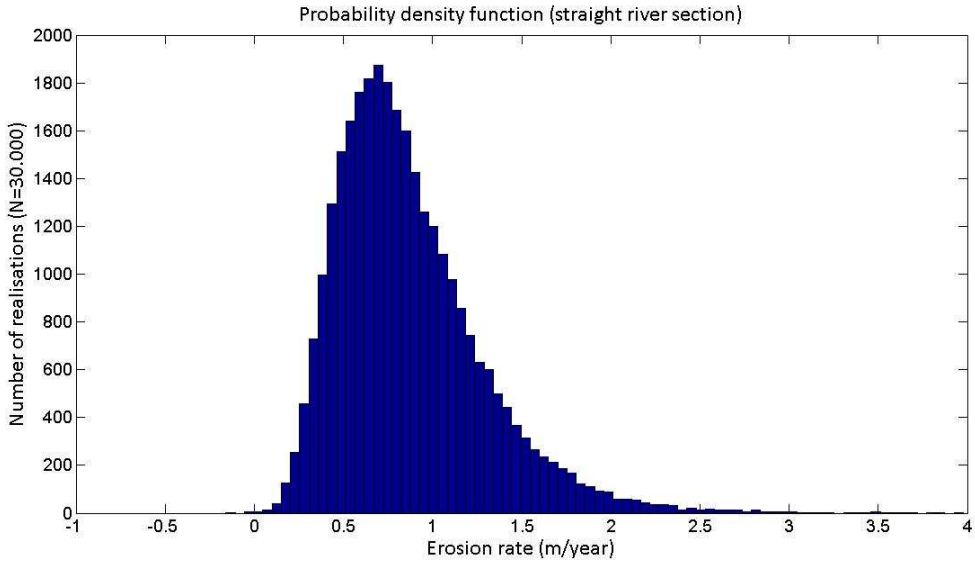


Figure E-2: Probability density function of the erosion rate at a straight river section

In Figure E-2 a histogram can be seen, which shows the results of the Monte Carlo simulation.

The mean erosion rate for a straight river section is 0,84 m/year. It can be seen that the erosion rate varies between 0 m/year and 2.5 m/year. The tail of this plot has a wider spreading than the front. The cumulative distribution function can be seen in Figure E-3. The y-axis can be regarded as the probability that the value of the erosion rate is lower than the value given by the x-axis. The cumulative distribution functions of the outer and inner bend can be seen in Figure E-4 and Figure E-5.

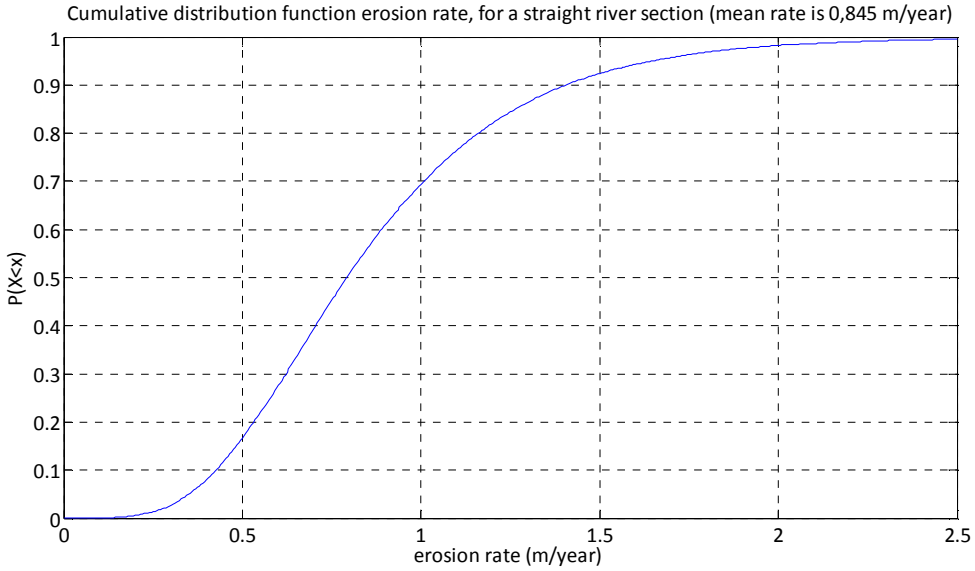


Figure E-3: Cumulative distribution erosion rate, straight river section

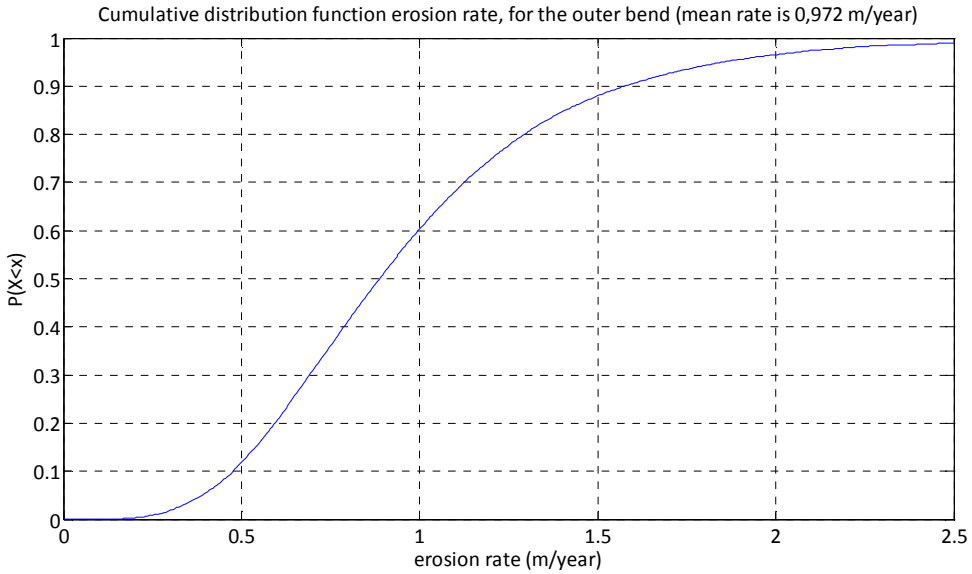


Figure E-4: Cumulative distribution erosion rate, outer bend

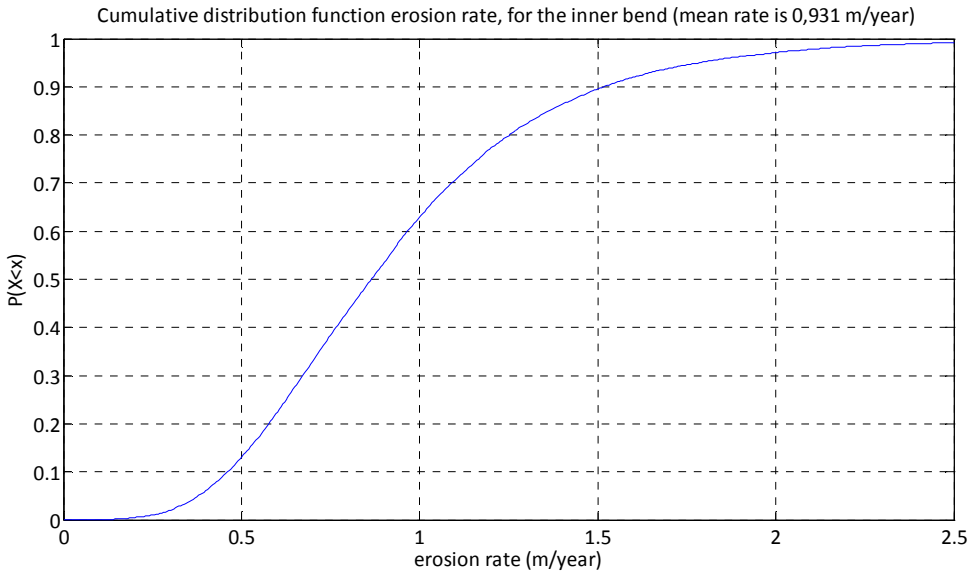


Figure E-5: Cumulative distribution erosion rate, inner bend

With the use of a FORM simulation (a level II probability method), the relative importance of the different variables is calculated. One of the results of a level II probability method are the α-values. For every variable an α-value is calculated, which can be seen as a indication for the influence of that specific parameter on the uncertainty of the desired event, in this case the erosion rate. The following expression explains the character of the α-value:

$$\alpha_i = \frac{\partial Z}{\partial x_i}\frac{\sigma_{x_i}}{\sigma_z} \qquad \text{(E-3)}$$

This calculation is only done for a straight river section, because the α-values are nearly the same for all other locations. In expression E-3 the Z represents the limit state function, but in our case formula 3-21 minus 0,869 (the mean erosion rate for a straight river section) is used for practical reasons. The alpha value depends on the influence of the parameter on the Z function and on the uncertainty of the variable.

Parameter	α-value	$(\alpha\text{-value})^2$
H	0,445	0,198
n	0,565	0,319
T	0,088	0,008
N	0,110	0,012
C_0	0,582	0,339
τ_c	0,353	0,125
		Σ=1,00

Table E-2: α-values

In Table E-2 it can be seen that the variation of C_0 and n are dominant on the variability of the erosion rate. For a better approximation of the erosion rate it is important to improve those parameters. The standard deviation of n can be decreased by a further analyzing of

the secondary wave train, coming from a vessel. It is harder to increase the reliability of C_0. It should be necessary to do laboratory experiments to get a better understanding of the relation between the critical velocity (or critical shear stress) and the C_E. The uncertainty of N and T hardly influence the uncertainty of the erosion rate.

F. Delft3D input

In this appendix, all the input of the Delft3D model is summarized in Table F-1 and Table F-2.

Domain	Latitude	-34,18°
	Orientation	0
	Number of layers	10
	Layer thickness	1: 20%
		2: 20%
		3: 15%
		4: 12%
		5: 10%
		6: 8%
		7: 6%
		8: 4%
		9: 3%
		10: 2%
Time frame	Reference date	01-09-2010
	Simulation start time	01-09-2010
	Simulation stop time	06-10-2010
	Time step	1 min
	Local time zone	0 +GMT
Processes	Sediments	
Initial conditions	Uniform values	
	Water levels	0,7 m
	Sediment mud concentration	0,2 kg/m^3
Boundary conditions	Upstream boundary	Total discharge (time-series, logarithmic)
		Thatcher-Harleman time lags: Surface 0 min, Bottom 0 min
	Downstream boundary	Water level (time-series)
		Thatcher-Harleman time lags: Surface -1 min, Bottom -1 min

Table F-1: First part of the Delft3D-FLOW input

Physical parameters	Gravity	9,81 m/s^2
	Water density	1.000 kg/m^3
	Roughness (Manning)	Uniform: U = 0,035 $sm^{-1/3}$, V = 0,035 $sm^{-1/3}$
	Slip condition	Free
	Viscosity (uniform)	Horizontal eddy viscosity = 1 m^2/s Horizontal eddy diffusivity = 10 m^2/s
		Vertical eddy viscosity = 0 m^2/s Vertical eddy diffusivity = 0 m^2/s Ozmidov length scale = 0 m
	Model for 3D turbulence	k-Epsilon
Sediment	Reference density for hindered settling	1.380 kg/m^3
	Specific density	2.650 kg/m^3
	Dry bed density	1.380 kg/m^3
	Settling velocity	0,864 mm/s
	Critical bed shear stress	Sedimentation: 1.000 N/m^2 Erosion: 1,5 N/m^2
	Erosion parameter (uniform)	0,0001 kg/m^2s
	Initial sediment layer thickness at bed	5 m
Morphology	Update bathymetry during FLOW simulation	
	Morphological scale factor	10
	Spin-up interval before morphological changes	720 min
	Minimum depth for sediment calculation	0,1 m
Numerical parameters	Default values	
Output – Storage	Start time	01-09-2010 00 00 00
	Stop time	06-10-2010 00 00 00
	Interval	60 min
	History interval	60 min

Table F-2: Second part of the Delft3D-FLOW input

Masterproject, CT4040
Faculty Civil Engineering and Geosciences
TU Delft